DISSERTATION

INVESTIGATION OF THE GROWTH MECHANISM OF HIGHLY BRANCHED SILICA NANOWIRES GROWN USING IN-SITU CU-CATALYST LOADING, AND THE DEVELOPMENT OF ELECTROCHEMICAL ANODIZATION SYNTHETIC METHODS SPECIFICALLY TARGETING SOLID IONICALLY CONDUCTING MATERIALS

Submitted by

Jacob Daniel Boissiere

Department of Chemistry

In partial fulfillment of the requirements

For the Degree of Doctor of Philosophy

Colorado State University

Fort Collins, Colorado

Summer 2023

Doctoral Committee:

Advisor: Amy Prieto

Richard Finke
Anthony Rappe
David Dandy

ABSTRACT

INVESTIGATION OF THE GROWTH MECHANISM OF HIGHLY BRANCHED SILICA NANOWIRES GROWN USING IN-SITU CU-CATALYST LOADING, AND THE DEVELOPMENT OF ELECTROCHEMICAL ANODIZATION SYNTHETIC METHODS SPECIFICALLY TARGETING SOLID IONICALLY CONDUCTING MATERIALS

Gaining a better understanding of the world around us is the fundamental objective of science, with chemistry looking to better understand the processes and applications that occur on a molecular and sub-molecular scale. Developing this better understanding has allowed us to create medicine and computers, begin exploring space and understanding the atom and is a never-ending process of asking questions and testing hypotheses as we work toward an increasingly objective answer. The best that I can hope for, not only in my time in graduate school, but as I move forward in life, is that I have moved this understanding, even in the slightest, in the correct direction. This may be a small impact, but much of the work presented in this dissertation will focus on small things. Two significant research directions will be presented along with work on device and process development for characterization. The first major system that will be discussed is the chemical vapor deposition of highly branched silica nanowires that were grown in a single synthetic step as a result of *in-situ* Cu-catalyst loading. The second research direction involves the investigation into using electrochemical anodization synthesis as a way to target the formation and discovery of ionically conducting materials.

The overall link between these research topics involves the focus on solid inorganic materials, with a broad direction of understanding materials systems, process development and

optimization, careful characterization, hypothesis generation, and considerations of potential applications and future directions of the materials and techniques being investigated. Systems of interest could loosely be classified as energy related materials. Both systems provided unique and challenging aspects to understanding the synthetic processes involved as products were formed under highly dynamic environments. Additionally, device and process developments were perused to address systematic variables such as instability of products and improve overall reaction design and therefore reproducibility and significance of results.

The first system investigated involved the chemical vapor deposition of silicon-based nanowire products. The initial objective of the project was to investigate the unique structures of highly branched nanowires that were grown through *in-situ* doping of Cu, and investigate their properties and performance as a potential anode material for use in Li-ion battery devices. The synthetic method used, and the unique structures observed were previously reported by the Prieto research group. The hypothesis was that these products were grown as crystalline Si and being catalytically oxidized due to the presence of Cu and Cu_3Si post synthesis. The work presented here disproves this hypothesis, instead proposing that the product is grown as the oxide. Due to this new conclusion, the battery application study was no longer pursued, and investigation instead focused on developing and proposing a new growth hypothesis. This new hypothesis involves the formation of a multi-wire backbone, which is believed to be the first report to directly investigate and explain this phenomenon.

The second research direction outlines the motivation, theory, and initial outcomes of attempting to develop a new synthetic methodology for ionically conducting materials through electrochemical anodization. While anodization is itself far from a new synthetic method, it has never been used to synthesize the targeted material systems, nor has it been used to pursue the

synthesis of ionically conducting materials generally. Much of the discussion will revolve around the background, motivation, and hypotheses relating to this project. This focus is partially due to the limited success of certain research objectives, but the intention is to hopefully highlight the intrinsic value of the synthetic concept and theory behind it, as well as direct future potential research based on what has been learned. The synthetic results and discussion focus on the anodization synthesis of AgI, the morphologies and crystallographic properties of the materials formed, and insights into the synthetic process. The related systems of CuI and Cu_xS will also be touched upon, as well as attempts to pursue the synthesis of Na_3PS_4.

Throughout these investigations, a variety of side project and collaborations were worked on, but the one of significance that will be included in the final chapter relates to the development of an air-free sample transfer holder. This was developed to allow the air-free transfer of a surface sensitive material between a glove-box and an X-ray photoelectron spectroscopy instrument. This enables more accurate and meaning data to be collected on samples that could otherwise be modified or compromised through exposure to ambient air before analysis.

ACKNOWLEDGEMENTS

My greatest thanks is to my wife, Sarah. Without you this would have neither happened nor mattered. You are my best friend, and I am grateful to have you in my life every day.

Thank you to Dr. Prieto, your wisdom, support, patience, and guidance were ever-present and unwavering, and for that I am both indebted to you and eternally grateful to have had you as an educator, boss, and even friend.

To my family, thank you for your support and encouragement.

To Dr. Jeffrey Ma and Dr. Dan Agocs, you guys made research enjoyable. Without our talks, whether about science or otherwise, I would have surely been lacking in my education and insight during my time at CSU. Particularly Jeff, you have been much more than a colleague, but a true friend.

A special thanks to all those at CSU that helped me in so many ways, as a PhD is like a child, it takes a village. Specifically, Dr. McCurdy and Dr. Geiss, you helped me see things more clearly, Dr. Shissler, you set me on a path and led by example, and to Kathy Lucas and Dezirae Todd, who I believe actually keep the department running.

TABLE OF CONTENTS

I. INTRODUCTION[i]

1.1 Overview of dissertation formatting and content

Chapter 1 will act as a general overview of the contents of the dissertation and provide background information relevant to the following chapters including pertinent literature and historical perspective to provide contextual understanding and motivation for the following chapters. This chapter has not been prepared for journal submission and is formatted according to dissertation guidelines, with individual sections relevant to the following chapters. Chapters 2 and 4 will follow a "journal's format" where these chapters have been prepared for, and submitted or accepted for publication, in a peer-reviewed scientific journal and therefore follow the formatting guidelines of the respective journals. The Supporting Information for each of these manuscripts is added at the end of the respective chapters, with minor changes to overall formatting to allow for better integration into the dissertation. Chapter 3 has not been prepared for a manuscript and will be formatted according to dissertation guidelines.

Chapter 2 describes the work done on the synthesis and characterization of highly branched silica wires, and how a greater understanding of the synthetic mechanisms that lead to these products was developed, resulting in a multi-wire backbone hypothesis being proposed. This chapter was formatted for the journal *Chemistry of Materials*.[1] The authors Shissler, Johnson, and Prieto contributed to the background and synthetic development for the work presented in the chapter, but nearly all writing, presented data, data analysis, and the entire multi-wire hypothesis is the work of the dissertation author. The one exception to this is the EELS analysis in this chapter,

[i] This chapter has not been prepared for journal submission and is formatted according to dissertation guidelines, with individual sections relevant to the following chapters. All information, data, and figures in this chapter have been written, collected, and formatted by Jacob Boissiere for this dissertation except where cited.

which was conducted by Prof. Beth Guiton, who also contributed to the data analysis and writing of that specific section. Additional previous work on this system can be found in Dr. Shissler's dissertation.[2]

Chapter 3 introduces the concept of developing a method of electrochemical corrosion synthesis for targeting ionically conducting solid materials. The majority of quantitative results for this chapter come from investigating the AgI system. Additional discussion revolves around related systems, targeting alternative materials such as Na_3PS_4 and related compositions, and the understanding and insights that have been gained from these studies. Due to the nature of the results, few definitive conclusions have been drawn, so the objective of this discussion is to determine the merit of the initial proposal, and direct subsequent work through consideration of the work completed and presented. This initial concept of using electrochemical corrosion for synthesis in such a unique way, and the background for the fundamental science and research targets, came from Dr. Amy Prieto and Dr. Jamie Neilson, but all work, results, and proposed directions presented in this chapter are solely that of the author.

Chapter 4 presents a device that was developed to allow air-free sample transfer from a glovebox into the X-ray photoelectron spectrometer instrument at CSU. This work was published in *Chemistry of Materials.*[3] The development of this device is tangentially related to attempting to prevent air exposure to the branched wire system and surface analysis of electrochemical products from the previous chapter, but was primarily motivated by general discussion with colleagues about improving analytical capabilities and systemic limitations to research and collaborations analyzing Li and Na ion battery materials. Collaborating author Dr. Agocs conducted the XPS analysis and contributed to a portion of XPS data analysis, but all holder design, optimization, test system development, and the rest of writing are the work of the author. The production and testing

of the sample transfer holder has allowed the author to collaborated with multiple group members resulting in additional publications.[4,5] Additional holders have been produced and instructions provided for general use in the CSU chemistry department and ARC facilities.

1.2 Introduction

1.2.1 Developing and testing meaningful hypotheses on the synthesis and products of challenging solid inorganic materials systems

Our ability to gather results and accurate data on chemical systems has been improved drastically through modern techniques and instrumentation, advances in theory and computation, and, most importantly, the ability to review literature and continually build on the expanding knowledge of our fields. Despite this, gaining truly valuable insights into most chemical systems remains difficult, as every field, topic, and project has its own unique complicating factors. Therefore, what is meant by "challenging solid inorganic materials systems?" The two primary materials systems that will be discussed herein are the vapor deposited highly branched silica nanowire system and the electrochemical corrosion system. Each of these cases present individual, but related challenges that will be discussed in greater specific detail in their respective sections. The holder project is related to the overall discussion of gathering meaningful data from systems that pose unique challenges, as its development arose from investigating and considering how to best go about collecting accurate information generally. However, it will not be a focus of the following section, as the holder is itself an attempted solution to the problem of analyzing highly reactive surfaces accurately, instead of a materials research project which presents new or distinct challenges. Additionally, while specific systematic developments occurred while studying these materials systems, those process improvements are included as a subset of the research outcomes instead of a standalone project, as is the case of the XPS transfer holder.

1.2.2 Considerations for studying materials synthesis, analyzing results, and proposing hypotheses

For both the chemical vapor deposition (CVD) reaction system and the electrochemical anodization (E-chem) system, the syntheses involve highly dynamic processes resulting in solid inorganic products that form on a substrate interface from non-solid precursors under relatively harsh conditions. Such reaction conditions can be difficult, if not impossible, to link directly to, or recreate in, an analytical instrument. As a result, it is impractical to gain direct insight into the synthetic processes through in-situ analysis. Because of this limitation, it is difficult to determine if the product formed at the reaction conditions is representative of what is observed once it is removed from the reaction conditions such as the higher temperature or applied potential. Furthermore, if the product changes or decomposes over time or due to general instability or atmospheric exposure, appreciable alterations can occur to the material before analysis can be conducted. Additionally, as these are solid inorganic systems, with intermediate reactions and precursors forming over small time and spatial ranges, isolating such intermediates, or designing traps or side reactions to identify potential candidates requires careful considerations. Due to these factors, much of the insight into synthetic processes is based on the careful analysis of the post-synthetic stable products upon numerous repeated syntheses with minor variable modification.

For the chemical vapor deposition (CVD) growth of the branched silica nanowires, no directly relevant growth mechanism currently exists in literature outside of this research group. While the study of nanowires,[6–9] the interaction of Cu in Si,[10–12] CVD methods,[13–16] and most other individual components of the project exist in well-established fields, this synthetic system employs a unique combination of variables from all of these fields, and this combination in turn yielded the branched nanowire product of interest. As a result, investigating the synthetic processes of these products balances the combined knowledge of individual fields and numerous investigations

against the logical conclusions that can be drawn from a single system. This is fundamentally not unique, and similar statements can be made for any synthesis of a new material or structure, but the complexity and variability of these highly branched silica nanowire products does make this consideration note-worthy. Additionally, looking at defining the synthetic steps of such a product may also differ from the fundamental and rigorous investigation of molecular or other more established synthetic mechanisms, as the ultimate goal of this project is to propose essentially new hypothetical steps to support an unreported growth mechanism, as compared to the continuing development of established hypotheses through refuting or responding to previously published work on a directly related project.

Electrochemical synthetic techniques are well established in academic and commercial fields, and anodization is a fundamental step to any electrochemical process or redox reaction. Anodization, also referred to as corrosion or oxidation, is a significant field due to the impact this process has on infrastructure, commercial products, and much more.[17–19] In the case of corrosion however, the majority of research has been conducted on *preventing* corrosion, not using *corrosion* for beneficial or synthetic processes. There are still numerous instances where corrosion is used as a beneficial process. For commercial applications there are most notably three examples of metal anodization in acidic media to produce consistent and robust oxide coatings, and these and other related processes can be controlled electrostatically or galvanostatically. Similarly, electrochemical anodization can be used for the formation of patterned anodic films, porous coatings, or the formation of nanostructures products, but again, these are almost exclusively oxides.[19–24] There are a limited number of exceptions to the formation of oxides using electrochemically controlled oxidation which will be outlined in Chapter 3. While the products of these processes display a range of morphologies and functions, anodization has never been used

with the intention of synthesizing ionically conducting materials to the best of the author's knowledge, and extremely few anodization syntheses result in products with any significant ionic mobility. Because of this, while anodization literature is an invaluable resource to designing reactions and considering synthetic processes, there is practically no literature to directly build on. As a result, gaining insight and support behind the analysis of synthesized materials and proposing hypotheses surrounding product formation is again an amalgamation of multiple fields of study, reports related to specific system variables, and the careful consideration of any results, observations, and systematic testing of hypotheses.

In order to overcome analytical barriers and resource limitations, proper systematic analysis must be done to yield meaningful results. This is fundamentally a restatement of any good scientific investigation, but designing controls carefully, consideration of system variables to identify or disprove possible intermediates or alternative reaction pathways, and methodical variation of reaction conditions can provide a wide range of data and information about individual aspects of the system, but only when looked at holistically. When done properly, approaching the study of such materials system in this manner can yield significant conclusions regardless of any specific piece of instrumentation or analytical technique employed, or an individual's background or skillset. Consequently, the individual pieces of data presented here are rarely adequate for disproof of any hypothesis, but rather the data needs to be taken as a whole to identify which hypothesis is able to most satisfactorily address *all* observations, as well as what is consistent with literature and any other information or insight available to the researcher.

The hope then is that the conclusions presented follow this logic and best research practices, while acknowledging the limitations of the data and researcher. The intention is to convince the reader that the conclusions being drawn, or rather hypotheses being proposed, are

much closer to the truth than the hypotheses outlined in this introduction. As most of the data has come from analyzing products that may be multiple chemically significant steps away from the as-synthesized product, there is a non-zero potential that the proposed hypotheses are still steps away from being chemically accurate or "true." Despite that, a sincere best effort was given to make the hypotheses meaningful, provide context for relevance to the field, and ensure accuracy to the full extent of data collected. Additionally, future directions will be proposed where the author feels continued research and expenditure of resources is warranted.

1.3 Project introduction: Chemical Vapor Deposition of Si-Based Nanowires

1.3.1 A Brief Introduction, History, and Background Literature for the vapor synthesis of Silicon-Based Nanowires

Small metallic wires and ribbons are some of the oldest examples of nanomaterials, or at least nearly nanomaterials due to their macroscopic analysis capabilities, which were studied academically dating back to "filamentary crystals" in the 18th century, which were often called "nanowhisker" studies in the 19th and early 20th century.[8,25–28] Many of these materials were formed via high temperature reactions with the whiskers or needles growing through axial dislocation or initialized through defects caused by impurities such as sulfides and oxides. The earliest example of crystalline silicon whiskers being described is often attributed to Treuting and Arnold in 1957 who reported the identification of the (111) growth direction of silicon products being grown by their colleagues at Bell Laboratories. Potentially the most significant advancement in the field came several years later, when Wagner and Ellis, also of Bell Labs, determined that silicon whisker growth could be initiated and controlled through the use of a metal catalyst and defined the vapor-liquid-solid (VLS) mechanism of growth.[29] Through studying Si, Ge, Sn, and related systems, it was determined that catalyst materials for crystalline wire growth could be

rationally identified through the use of equilibrium phase diagrams such as that of Au-Si seen in Figure 1.1. It is this type of synthetic insight and understanding of fundamental growth processes which has allowed for continued optimization and modification of nanowire systems to this day.

The VLS mechanism identified by these studies involves heating the metal catalyst (for this example Au) past the Au-Si eutectic (363 °C minimum[30] as seen in Figure 1.1), and then flowing a reactive Si precursor gas such as silane (SiH_4) over the substrate.[27,31] Silane reacts with the Au, producing hydrogen gas and dissolves Si in the gold droplet. As the atomic percent Si increases, a solubility limit is reached, and solid Si is precipitated out of the liquid droplet onto the substrate below. As Si continues to be dissolved and deposited, a nanowire is grown.[2,27,31–34]

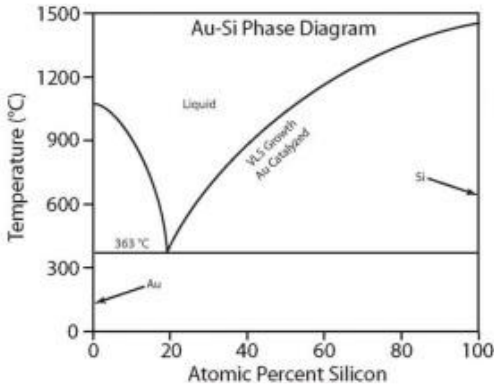

Figure 1.1: Au-Si phase diagram showing the lowest eutectic melting point at 363 °C at 18.6% Si. The curve on the right represents the saturation limit were VLS growth occurs.

As the practical use and study of nanotechnologies has become increasing viable, and techniques to analyze nanomaterials have improved, silicon-based nanowires (SiNWs) have continued to be studied for a wide range of applications. Numerous methods to synthesize these products have been developed in addition to metal catalyzed CVD including plasma enhanced CVD (PECVD), laser ablation, molecular beam epitaxy (MBE), evaporative or physical vapor deposition (PVD), simple annealing, as well as solution-based syntheses.[27,35–37] Despite this, metal catalyzed growth has remained at the forefront, with various adaptations and iterations to the fundamental growth mechanism resulting in structures of unique morphologies and composition. Through developing metal nanoparticle catalyst synthesis, optimizing deposition procedures, and

manipulating growth conditions, SiNWs can controllably and reproducibly be synthesized through metal catalyzed CVD, typically utilizing gaseous Si precursors on a variety of substrates and surfaces. These synthetic techniques allow for relatively good control over wire size, length, and density on a substrate, as well as doping, surface modification, post-synthetic coatings, or other modifications.

One common modification to the metal catalyzed growth method that can have a variety of impacts is utilizing non-Au catalysts, such as Cu. Using a Cu catalyst allows for an alternative growth method vapor-solid-solid (VSS) growth, where the wire catalyst is a solid silicide. The VSS mechanism is similar to the VLS mechanism but depends on the ability of the metal catalyst to readily form a series of solid silicides at temperatures below any eutectic points for that system, as highlighted in Figure 1.2. Again, as the atomic percent of Si increases across this series, a solubility limit is reached and Si precipitates out of the silicide, forming a crystalline Si 2-D nanostructure. The primary difference between the VLS and VSS growth mechanism, is that in VSS growth, the crystallinity of the catalyst and its orientation relative to the growth substrate have an impact on the growth direction and shape of the grown wires. As the SiNWs grow "down" from the catalyst, different catalyst structural properties produce faceting of wire surfaces, influence what internal

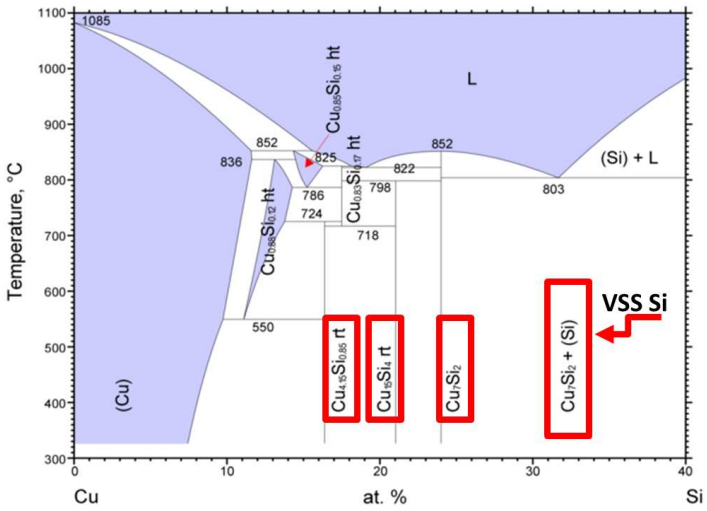

Figure 1.2: Cu-Si phase diagram showing the lowest eutectic melting point at 803 °C. The room temperature silicides are highlighted in the red boxes. As silicon is added into these solid silicide systems it is precipitated out as indicated by the box and arrow on the right. © ASM International 2012. Diagram No. 104105

defects will be present, and determine if SiNWs will grow epitaxially to the deposition surface.[12,38,39] Additionally, VSS catalyzed growth rates are generally lower than VLS catalyzed growth rates.[2,32,39]

Utilizing either VLS or VSS growth, CVD remains at the forefront of SiNW synthesis due to the numerous parameters that can be adjusted to manipulate product properties. Being able to control and manipulate product properties is valuable for optimizing products for specific applications such as sensing, energy conversion, catalysis, nano-electronics, and more, but the application of interest that motivated the work reported herein was that of energy storage.

1.3.2 Original Motivation and Application of interest for Si-Based Nanowires

While silicon nanowires are of interest for multiple applications in current materials chemistry, and they are of particular interest for use as a Li-ion battery anode. Current research motivation is due to crystalline Si having the highest volumetric capacity (2194 Ah L^{-1}) and, more significantly, the highest gravimetric capacity (3579 mAh g^{-1}) out of any alloying or intercalating anode materials.[31,40–42] As seen in Figure 1.3, Silicon's volumetric capacity is almost three times that of graphite (719 Ah L^{-1}), and the gravimetric capacity of Si is over ten times that of graphite (350 mAh g^{-1}). Graphite is used as a reference due to its broad commercial use.[6,40]

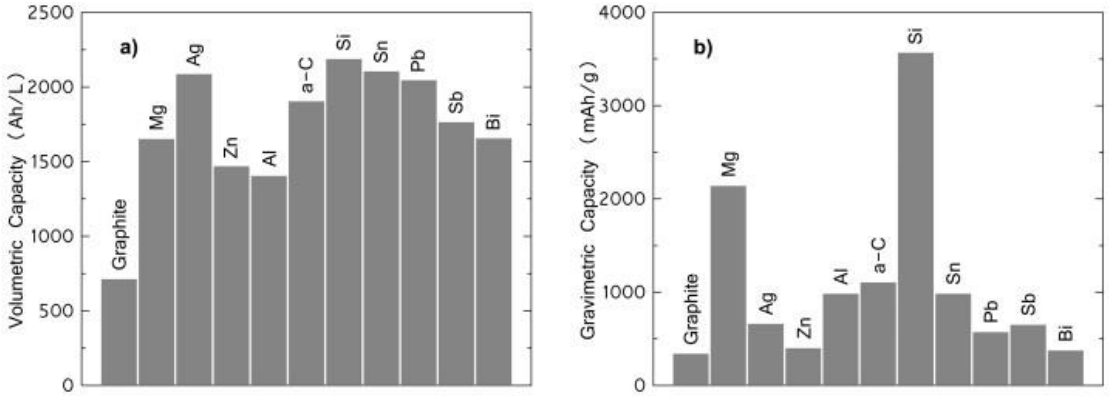

Figure 1.3. Volumetric (a) and gravimetric (b) capacities for various single-component alloying Li-ion battery anode materials, with graphite (an intercalation anode) included for comparison as it the most widely used commercial material at this time. Figure reproduced from Obrovac and Chevrier.[40]

Battery materials with higher energy densities are important to the advancement of rechargeable energy storage, especially for application in electric vehicles, as the size and weight of current batteries is one aspect inhibiting technological progress. Despite this potential for Si to be used in high-energy density rechargeable batteries, there are several issues that need to be addressed before Si can be used as the primary anode material. One major issue facing Si anodes is that upon full lithiation to the $Li_{15}Si_4$ phase, the material undergoes a 300-400 % volumetric expansion.[31,40,41] This expansion, and subsequent contraction upon delithiation, leads to high internal strain in the material. Repeated cycling causes Si to fracture and break, which leads to rapid capacity loss over only a few cycles as is depicted in part A of Figure 1.4. This pulverization of the anode is one common failure mechanism for most alloying materials, and one solution to mitigate this issue has been to synthesize these materials on the nanoscale.[40,43,44] Through synthesizing electrode materials below their "critical size," the material can handle the internal physical strains of expansion and contraction without fracturing into smaller pieces. For 1 dimensional silicon, this critical size has been found to be around 300 nm and a representation of this effect is seen in part B of Figure 1.4.[40]

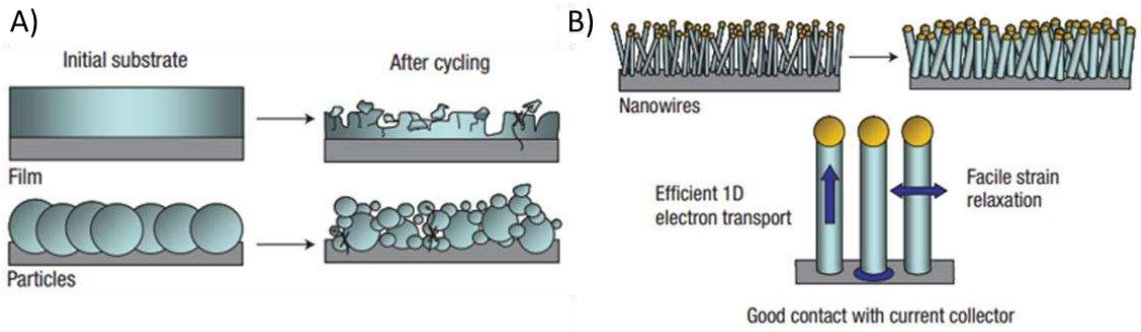

Figure 1.4. A) Thin films and small particles of Si and other alloying anodes degrade through fracturing upon battery cycling. B) SiNWs with diameters less than 300 nm do not as readily degrade. Figure reproduced from Chan.[31]

Silicon deposited through CVD methods has the potential to be very pure, which is desirable for the computer technology and photovoltaic industries, but pure, crystalline Si has

relatively high resistivity (~10 Ω cm),[33] which leads to low cycling rates when used in Li-ion batteries. Therefore, in order to increase conductivity throughout the material, changes such as conductive coatings or material doping are commonly used.[45,46] Copper silicides have been incorporated in various capacities in Li-ion battery materials,[42,47–49] but this has not previously been implemented for nanowire based anode materials. Being able to dope SiNWs with Cu *in-situ* could allow for simple, single step synthesis of more highly conductive wires, with synthetic control over the degree of doping and therefore cycle-rate capabilities.[33] One added benefit to incorporating Cu into SiNWs that was hypothesized was an increase in mechanical stability. Using nanowires vastly improves the cycle-life of Si as mentioned previously, but Cu_3Si is inactive toward lithiation, resulting in small regions dispersed throughout the wire that will not undergo expansion and contraction upon cycling. This would lead to a decrease in overall capacity, but given the fact that Si has a gravimetric capacity 10× greater than graphite, some capacity can be forfeited in order to achieve comparable cycle rates and extend material lifetime.

1.3.3 Foundation of Individual Research: Previous Group Work and Proposed Growth Mechanism Hypothesis

The current research on Cu-doped Si nanowire structures is a continuation of a long-term project in the Prieto group. This project was started by Dr. Derek Johnson and continued by Dr. Dan Shissler.[2] Johnson's first paper on the topic describes the synthetic process of forming Cu-doped Si nanowires through chemical vapor deposition and demonstrates that the doping results in decreased resistivity of the wires.[33] Not reported in this original paper was the observation of highly branched nanowires that were formed as a byproduct of this growth. This was believed to be the first observation of a single step synthesis of highly branched silicon wires. To investigate these unique products further, the system was modified and studied by Dr. Shissler and described

in his PhD dissertation.[2] The highly branched structure is also of interest for the battery anode application mentioned previously as it increases the net capacity of the product and has the potential to result in a more integrated network of wire products. If the conductivity of the wires is high enough, and there is significant contact between wires, this could help retain electrical contact throughout the anode even if induvial wires lose contact with the current collector. This would help to further mitigate the impact of material fracturing and loss of contact, allowing reduced capacity loss, and therefore greater lifetime of the material.

The growth mechanism proposed by Johnson and Shissler states that branched wires are a result of simultaneous VLS and VSS catalyzed growth. A general depiction of this process for a single branched wire is seen in Figure 1.5. In this mechanism, the primary "backbone" wire growth is through Au catalyzed VLS growth. The liquid Au catalyst droplet swells as gas-phase Si and Cu dissolve. Si deposits out at relatively low concentration, and some degree of Cu_3Si is also deposited with appreciable amount of Cu in the catalyst droplet. It is believed that Si has a higher partial pressure than Cu near the growth substrate surface due to wires being primarily Si. As Cu continues to dissolve in the catalyst head, a Cu_3Si rich core deposits in the wire. This Cu_3Si beads in the wire and diffuses to the surface, where it acts as a VSS growth catalyst for the branches.

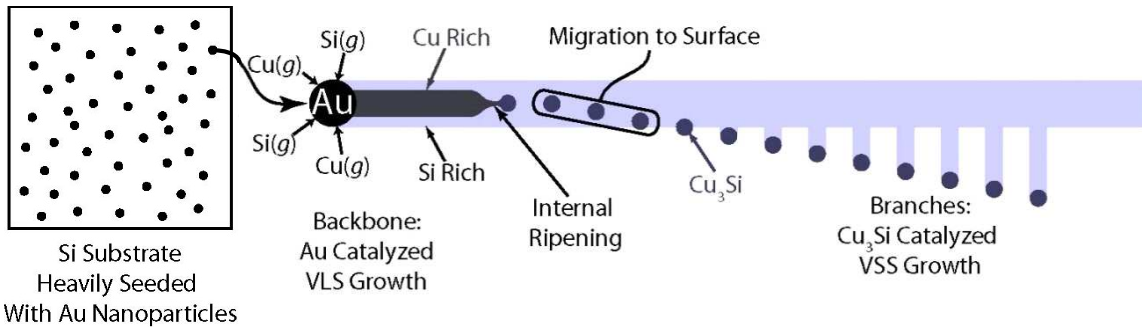

Figure 1.5. Growth mechanism for highly branched SiNWs proposed by Johnson and Shissler.[32] Growth is initiated using AuNP primary catalysts. Secondary growth is hypothesized to be the result of a Cu-rich core in a crystalline Si backbone, which forms secondary copper silicide catalyts which migrate to the surface and initiate growth of branches through a VSS mechanism.

Following the work done by Johnson, Shissler focused on further developing the hypothesis behind the growth mechanism and exerting improved control over system variables. In doing so the procedure was modified to first deposit Cu onto the Si (100) surface to act as a catalyst before initiating wire growth. This allowed for the Cu to function as the catalyst for both the wire backbone and branches. The new procedure eliminated the use of gold and removed the process of pre-seeding the substrate but required careful surface modification to achieve relatively consistent Cu deposition. The modified procedure includes several other changes compared to the Johnson synthesis, and the specific modifications tested and the rationale for these changes are explained in Shissler's dissertation.[2] Both syntheses contribute to the data presented in Chapter 2, and additional details regarding the synthetic processes and variables used can be found in Chapter 2 Section 2.6.

Several mechanistic insights were provided to support the previously proposed hypothesis. One observation to support the crystalline growth hypothesis is an ordered, three-fold symmetry of branches, as seen in Figure 1.6 A, which is common in highly branched samples. The hypothesis was that Cu preferentially diffuses out of the SiNW along certain crystalline lattices or decorates

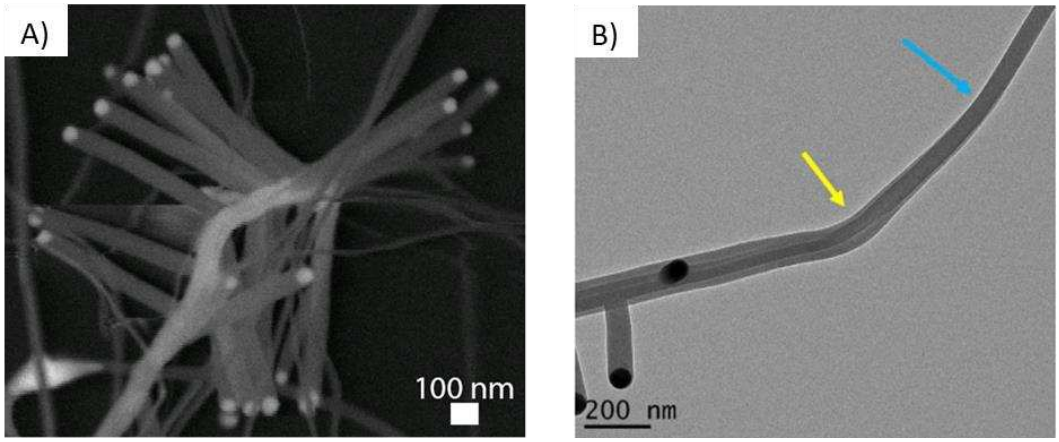

Figure 1.6: A) The three-fold symmetry of branching is a good example of an indirect observation used to infer crystalline wire growth. B) Blue and Yellow arrows point to the observed kinks that often occur near the onset of wire growth. The development of contrast lines is in this region is suggested to be due to crystalline defects.

specific facets upon diffusion to the surface. The most interesting mechanistic insight came from the observation of two distinct kinks in the wire, which were often observed just prior to the onset of branched growth. The blue and yellow arrows in Figure 1.6 B indicate the two observed kinks previous to branching and indicates that these kinks seem to correspond to the development of contrast lines within the wire.

The hypothesis behind the growth mechanism is rooted in key assumptions relating to the solid and gas phase precursors. Further detail relating to the design of the reaction can be found in previous publications and Chapter 2. Generally the copper precursor consists of a mixture of Cu_2O and graphite, and the silicon precursor comes from crushed Si-wafer upstream, as well as the deposition substrate itself. The reaction is done under a flowing mixture of H_2 and Ar, and it is understood that at high temperatures (1050° C) and lower pressures (50 torr), these species will decompose into volatile species, leading to the observed growth. The reactions that were assumed to be taking place previously were influenced by the belief that the reaction was producing a crystalline product which was being oxidized post-synthesis. Relevant reactions to the individual precursors and growth processes are included below.

The Cu_2O and graphitic carbon precursor was assumed to undergo carbothermal reduction, which is a well established procedure in literature at comparable and lower temperatures. The hypothesis was then that Cu^0 would be produced and evaporated in the process along with CO_2 as shown in Reaction 1.1.

$$Cu_2O_{(s)} + C_{graphitic} \xrightarrow{\Delta} Cu_{(g)} + CO_{2(g)} \qquad \text{Reaction 1.1}$$

The solid silicon precursor was kept close to the deposition substrate, and therefore only assumed to be evaporating and re-depositing over a short distance, simply through thermal

decomposition as shown in Reaction 1.2. Another possibility hypothesized was the reaction between H_2 gas and Si, producing the volatile species SiH_4 as shown in reaction 1.3

$$Si_{(s)} \xrightarrow{\Delta} Si_{(g)} \qquad \text{Reaction 1.2}$$

$$Si_{(s)} + 2H_{2(g)} \xrightarrow{\Delta} SiH_{4(g)} \qquad \text{Reaction 1.3}$$

For both the Cu and Si precursors additional considerations contributed to the hypotheses behind the formation of the observed products, but this will be explored in additional detail in Chapter 2.

In order to initiate the growth of the nanowires through the VLS mechanism, both the Cu and Si vapor phase precursors can react with each other as they reach the lower temperature growth regime (approximately 850° C - 950° C) as shown in Reactions 1.4 and 1.5, as well as the Cu precursor can react with substrate during the temperature ramp and catalyst formation component of the reaction as shown in Reaction 1.6. No specific stoichiometry is given as the product formed is a liquid drop with varying composition that corresponds to the continuous liquid solution composition that can be achieved at these temperatures as shown in the Cu-Si phase diagram found in Figure 1.2.

$$xCu_{(g)} + Si_{(g)} \xrightarrow{\Delta} Cu_xSi_{(l)} \qquad \text{Reaction 1.4}$$

$$xCu_{(g)} + SiH_{4(g)} \xrightarrow{\Delta} Cu_xSi_{(l)} + 2H_{2(g)} \qquad \text{Reaction 1.5}$$

$$xCu_{(g)} + Si_{(s)substrate} \xrightarrow{\Delta} Cu_xSi_{(l)} \qquad \text{Reaction 1.6}$$

No specific stoichiometry is given as the product formed is a liquid drop with varying composition that corresponds to the continuous liquid solution composition that can be achieved at these temperatures as shown in the Cu-Si phase diagram found in Figure 1.2. As Si continues to deposit out of the gas phase as it reacts with the liquid catalyst, the solubility limit of Si in the

catalyst droplet is reached, resulting in the deposition of solid Si at the catalyst head/substrate or catalyst head/nanowire interface, resulting in the upward growth of the product (Reaction 1.7)

$$Cu_xSi_{(l)} + ySi_{(g)} \xrightarrow{\Delta} Cu_xSi_{(l)} + ySi_{(s)solid\ nanowire} \qquad \text{Reaction 1.7}$$

Shissler completed a careful analysis of the diameter of the wire before, between, and after kinking as well as after the first instance of branching. The wire diameter increases as the catalyst head continues to dissolve Cu and Si, and the kinking was interpreted as an indication of a change in growth direction due to the change in catalyst size. Growth direction has been shown to depend on catalyst size for other systems, but there have not been reports relating to a system with a dynamic catalyst such as this. For diameters and hypothesized corresponding crystal lattices and defects see ref. (2). The primary limitation to finding support or disproof of this hypothesis was the products studied were completely oxidized. It is well understood in literature that the presence of Cu and Cu_3Si catalyzes the rapid oxidation of Si.[10,11,50–52] Having fully oxidized nanowire products (SiO_2) prevented the direct investigation of crystallographic information, as well as limited the interest in use as a battery anode. Generally, SiO_2 is not as relevant an anode material as crystalline Si, with SiO_2 having increased Li consumption, reduced capacity, and decreased conductivity and rate capabilities. Therefore, in order to continue investigating this system for both greater mechanistic insight, and for incorporation into battery devices, the initial objectives of the work was to 1) prevent oxidation, 2) continue characterizing products, 3) optimize synthesis for increased yield, and 4) develop methods for device incorporation.

1.3.4 Disproof of the previous growth hypothesis and new proposed mechanism

As previously stated, in order to progress the work done on this system the primary initial objective was to prevent oxidation. To achieve this, various modifications to the reaction system and materials handling and characterization procedures were investigated. Attempts to prevent

oxidation post synthesis included modifying the reaction vessel so it could be disconnected from the CVD system and transferred into a glovebox without opening the reaction chamber to atmosphere, dumping the substrate and nanowire product directly from the reaction environment into liquid nitrogen under flowing Ar for transfer to analysis instrumentation, and depositing a carbon coating. None of these processes worked, to prevent oxidation, and during this process it was determined that the product was growing as an oxide instead of a crystalline Si product that was being oxidized post-synthesis due to the presence of Cu. While the modifications to the reaction vessel and liquid nitrogen transfer were subsequently abandoned, the carbon coating provided additional benefits to characterization and greater synthetic insight.

While working to prevent oxidation through these methods, reaction variables were continuing to be tested and products analyzed to better understand and optimize the system, with the intention of still investigating these products for their electrochemical properties and integration into a Li-ion battery cell for testing as an anode material. As a result, improved synthetic methods were developed allowing for deposition onto multiple substrates simultaneously and the yield of the branched products of interest was increased, resulting in a more efficient production of product for analysis. Other systematic improvements included developing an improved wire transfer method, which was referred to as the "solvent chip" method and is briefly mentioned in Chapter 2 Section 2.3.3, as well as growing some product directly onto Mo grids. The outcomes of these methods allowed for product integrity to be better retained and a higher rate of analysis, resulting in the collection of more, higher quality data, some of which can be found in Chapter 2. The last significant change to the analytical approach was to broaden the scope of the investigation away from focusing on the branched wire products, and instead investigating all

reaction products across the various growth regions. The explanation of the various regions and results are explained in Chapter 2, section 2.4.1 as well as the Supporting Information.

The ultimate result of all of these methodological changes, process improvements, and expanded scope of investigation was determining that the nanowire products being investigated were being grown as an oxide product. This refuted any previously held hypothesis, and therefore determining a new growth mechanism corresponding to this new information became the objective of this study. This new synthetic hypothesis, as well as the data and background that support it is presented in the following chapter. The insights into the growth of this unique branched nanowire product contributes to the fundamental understanding of silica wire growth processes and can potentially contribute to understanding "nanopeapodded" systems, which at times seem to have related structures and properties.[53–59] Hopefully this proposed growth hypothesis and branched silica nanostructure can contribute to the overall field of silica nanostructures, as there are a variety of applications and interests in these materials that have emerged alongside nanotechnologies. Most notably nanosilica materials have been investigated for advanced sensor technologies, but that research direction was not of interest for this report. As such, the project is considered to be essentially complete with respect to the preliminary motivation behind the investigation of these materials and the research objectives initially defined.

1.4 Project Introduction: Targeting inorganic solid ionic conducting materials through electrochemical anodization.

1.4.1 Electrochemical anodization as a synthetic technique

For the purposes of this report the term "electrochemical anodization," or simply "anodization," refers to the electrochemically driven oxidation of an electrode through an applied potential (electrostatic cell process). Other terms that may be used, and can mostly be considered

synonymous herein, include “corrosion” and “oxidation.” All three of these terms have more general meanings, broadly referring to the loss of electrons or increase in oxidation state, but rather than stating “electrochemically regulated anodization synthesis” or similarly convoluted language, the shortened terminology will often be used unless “electrochemical” or “controlled” are used for emphasis or specificity. The alternative to electrostatic, or potentially regulated, oxidation is galvanostatic oxidation commonly referred to as spontaneous corrosion, which occurs due to chemical potentials driving the reaction at ambient conditions. This is a significant distinction as an important initial step when designing reactions for anodization synthesis is that the electrodes and precursor electrolyte solutions need to be relatively stable, at least enough to be able to be electrochemically regulated. If reactants are combined and the electrolyte constituents begin to spontaneously react with each other or the electrode surface, that limits the ability to drive new reactions and pursue innovative syntheses and materials, compared to common solution-based precipitation or other such synthetic methods.

Electrochemistry in general is considered lower cost than many thermal and vapor synthetic techniques. Control over variables such as potential applied (rate of reaction), total current passed (extent of reaction/film thickness), solution additives (surface modification, reactant solubility and environment), concentration (diffusion rate), and many other synthetic handles. Understanding corrosion is an important commercial and academic field, with billions of dollars spent on processes relating to corrosion annually, but almost all that goes into corrosion prevention. Surface modifications such as paints, galvanizing metal films, polymeric coatings, anodized surfaces and more are used to prevent uncontrolled oxidation and corrosion, and metal alloys are specially designed with a wide variety of compositions and additives to increase corrosion resistance for applications from cutlery to ship-building. Despite all of this work on

corrosion, relatively little goes into investigating electrochemically controlling these anodic processes for synthetic purposes. While redox chemistry is fundamental to chemical reactions, and the oxidative potential or anodic constituent of a reaction is taught in general chemistry courses if not before, the focus on isolating oxidative processes electrochemical as a synthetic method has been utilized in a relatively narrow scope.

Almost all work done on electrochemical anodization synthesis has to this point been focused on the formation of oxides of varying morphologies. The metals used in these processes include most notably Ti, Al, Fe, Cu, Nb, W, and Sn, but there are many more examples of other metals oxides formed through anodization both commercially and in academic literature.[19,20,64,21–24,60–63] The applications for these materials vary from incorporation in biological implants, to catalytic surfaces, to nanostructured materials for energy applications. While there is a lot to be learned from these systems, the resulting products being almost exclusively binary oxides inherently limits both the applications of the products, as well as the scope systems where anodization synthesis has been used.

The most relevant literature that could be found pertaining to the investigation of synthesizing non-oxide inorganic materials through anodization are reports on the synthesis of mixed ZnO/ZnS,[60] thin films of Cu_2S,[65,66] nanostructured Cu_2S and CuS,[67] and faceted CuI thin films.[68,69] While there are undoubtedly other reports of anodization synthesis of materials in classic electrochemical research or systems that did not arise during research (or that arose but could not be accessed because only a title pertaining to anodization of binary sulfide materials could be found from the late 80's "Soviet Materials Science" journal), it seems evident that the depth of information and the scope of use of anodization synthesis outside of oxide products is very limited.

Despite this, it is hypothesized that this method may hold unique applicability to research relating to ionically conducting materials.

1.4.2 Introduction and background literature for solid ion conductors and their applications.

Solid Ionic conductors are a class of materials of interest for a wide variety of applications, most notably as solid state electrolytes (SSEs) in energy storage systems such as Li-ion batteries (LIBs), or as ion-exchange membranes for applications such as water desalinization. Switching from the current state of liquid carbonate electrolytes for LIBs to SSEs has multiple proposed benefits. The benefits of incorporating solid electrolytes into secondary batteries for consumer electronics and electric transportation include increasing the overall energy density of secondary battery devices, increasing lifetime through reduction of electrolyte decomposition and increasing mechanical stability, and greatly improving safety due to the lack of flammable organic electrolyte.[70–76] Solid electrolytes have the potential to act as a physical separator in addition to the primary function of acting as an electrolyte, meaning no volume is required by a completely inert and inactive separator material, minimizing the overall volume of the cell and increasing energy density, allowing cars to travel further, and electronic devices to last longer.

Reducing the number of charge discharge cycles may extend the in-use lifetime of cells, because even if failure rate / number of cycles is consistent, extending the length of cycle extends usable lifetime. Researchers also hope that solid electrolytes will be able to form stable interfaces with metal anode electrodes such as Li and Na, allowing for the use of pure metal anodes instead of intercalation anodes which or alloying electrodes. Studies also suggest that depending on the material properties of the electrolyte used, such as the crystalline structure, hardness, and interfacial properties, solid electrolytes can inhibit the growth of dendrites, preventing shorting.

The formation of dendrites in current liquid electrolytes can cause shorts that result in thermal runaway, resulting in electrolyte decomposition and destructive device failure.

Utilizing the plating and stripping of a pure metal anode for a Li-ion or Na-ion battery significantly increases energy density of the anode electrode compared to the most common Li/C integration electrode, and even surpasses next generation alloying electrodes such as Si, while also lowering the potential of the anode, in turn increasing the overall voltage and power of the full battery cell. Defining the safety of a battery is largely dependent on the industries and applications that are evaluating and using the device in question, but across the board safety is still one of the biggest motivations for moving to SSEs. The flammable component of current LIBs is the liquid electrolyte, and moving to solid electrolytes eliminates the threat of flammability and minimizes hazards related to certain dangerous gaseous byproducts of liquid electrolyte decomposition, as well as concerns over the presence of HF which forms when common fluorine containing additives are exposed to moisture.[71,77–81] In the case of battery failure thermal runaway could still occur but is less likely to cause a fire due to the lack of fuel given many SSEs compositions consisting of inorganic materials with oxidized metal constituents and a lack of available carbon. This does not necessarily relate to polymer or hybrid/hierarchical systems which utilize polymer electrolytes or saturated/gelled electrolyte systems, but the focus for this discussion is on solid inorganic materials. There are many additional proposed benefits, such as the use of sulfur based cathodes, which current electrolytes suffer from sulfur decomposition and dissolution and S cluster transport to the anode that will not be discussed. For the research conducted relating to developing a synthetic approach toward targeting ionically conducting solid inorganic materials, we will be focused on applying an oxidative potential to the anode and investigating the resulting materials and proposed benefits of such a synthetic system.

1.4.3 Defining ionically conducting materials: classification and ionic mobility

The study of ionic conductivity in the solid state is an interdisciplinary field being explored by chemists, physicists, materials scientists, engineers, and more, seeking to gain fundamental insights into relevant materials and mechanisms, develop new and interesting compounds, and practically utilize ionically conducting materials for a variety of applications. Ionic conductivity within a solid inorganic material occurs through the net motion of ions when an electric potential or bias is applied to the system. For solid inorganic systems, these mobile ions typically move through a network of polyhedra consisting of metal and non-metal ions which is possibly due to defects including vacancies, interstitials, or partial occupancy of ions on certain lattice sites. The regular presence of these defects distributed throughout the solid electrolyte in sufficiently high concentration allows for ions to move between adjacent sites with sufficiently low activation energy or resistance to "hopping". The exact mechanisms behind the movement of ions are still being investigated with researchers focusing on collecting more accurate data and combining advanced computational methods with experimentally determined values and observations in order to model and gain mechanistic insight into these systems. While certain methods are able to achieve high consistency between experimental and theoretical results, these are often specific to individual systems and pertain to the localized movement of an ion within a readily defined structure and therefore calculatable energy landscape. Applying these models to the long-range mobility of either an individual ion or the net transfer of charge via the concerted ionic movement throughout a complex environment (for example the non-uniform structure of an amorphous glass) has not been regularly achieved to the best of the author's knowledge.

The concentration of these defects is an important factor influencing the rate of ionic conductivity, and the label or classification typically assigned to ionically conducting materials

corresponds to these differences in conductivity. Generally anything with an ionic conductivity below 10^{-6} $\Omega^{-1}cm^{-1}$ is considered ionically insulating. From ~10^{-6} $\Omega^{-1}cm^{-1}$ to ~10^{-2} $\Omega^{-1}cm^{-1}$ near room temperature are considered "standard" ionic conductors, and materials with conductivities above 10^{-2} $\Omega^{-1}cm^{-1}$ being considered "fast" ionic conductors. Additional breakdowns or titles are common in literature, with materials exhibiting ionic conductivities approximately 10^{-1} $\Omega^{-1}cm^{-1}$ or above being called "super ionic conductors" or SICs, as these rates are comparable to certain liquid electrolytes and molten salts. Terms such as "advanced superionic conductors" or "ultra ionic conductors" have also been used to describe materials with notably high ionic conductivities, particularly at lower temperature, but for this investigation, the term "ionic conductor" will often be used ubiquitously for all materials with a sufficiently high ionic conductivity, and the terms "fast" and "super" will be used interchangeably. The electronic conductivities of these materials will also largely be ignored, but the ratio of ionic to electronic conductivity determines if a material with be an electrolyte (capable of preventing current leakage through electron movement through the material, allowing charge transfer only through ionic mobility) or a mixed ion-electron conductor if the electronic conductivity is sufficiently high (greater than ~ 10^{-12} $\Omega^{-1}cm^{-1}$ to 10^{-10} $\Omega^{-1}cm^{-1}$) depending on the application, ionic conductivity, and who is defining the material.

The explanation and corresponding modeling of the diffusion of ionic species in crystalline solids focusses on the requirement of this mobile ion to pass through periodic energetic barriers that separate the local minima (typically crystallographic defect sites as defined previously) along some energy pathway. It is these periodic bottlenecks that ions must readily overcome to allow for migration of the ion throughout the structure, and this motional energy greatly influences the overall ionic conduction properties of a material. When considering modifications to, or synthesis of, any solid electrolyte then, the primary focus of discussion pertains to the minimization of this

migrational energy barrier. In order to achieve this, it is beneficial to focus on increasing the overall concentration of these defect sites through reducing the defect formation energy. This is achieved through incorporation of dopants, stoichiometric substitution of lattice constituents, introduction of lattice strain or long-range disorder, or incorporation of mixed oxidation ions, in order to maximize the defect concentration and minimize the corresponding number of noninteracting mobile ion species. While there are numerous iterations of demonstrating and applying this knowledge to model and better understand various solid ionic conductors, there are still major shortcomings to these practices.

While the explanations of the fundamental science and understanding behind these systems has thus far been explained generally, there is an apparent lack of true generalizability to the computational and theoretical models widely utilized. Most current systems cannot model both ion conductivity pathways intrinsic to a material, and incorporate transport through things like grain boundaries with a structure, or interfacial ion transfer between solid electrodes and electrolytes or electrolyte/electrolyte interfaces. Additionally, for highly disordered glasses or other amorphous products exhibiting no long-range order, while modeling can be done accurately for these materials through identification of the local minima pathways that most greatly contribute to the net electrolytic pathways, predictive modeling capabilities are as of now insufficient for driving the discovery of new materials in this phase-space. Current "predictive" methods have proven most capable when employed to determine specific dopants or stoichiometric modifications to known and characterized systems. While this is functionally beneficial in order to achieve optimized performance of existing materials systems, a slew of issues prevents the widespread incorporation of solid state electrolytes into practical and commercially relevant devices. The property of ionic conductivity in SSEs is already sufficiently high for use in modern energy storage devices, as solid

ion conductivities that meet or exceed those found in comparable liquid organic or molten salt electrolytes have been achieved for multiple instances of materials. It is because of this that the objective of developing a new methodological approach to synthesizing ionic conductors is of interest. The hypothesis driving this project is that through establishing a synthetic paradigm where *only* materials that have the desired property of ionic conductivity can form under the designated reaction conditions will allow for the "natural selection" of these materials. If such a synthetic methodology can selectively limit the throughput of products, yielding only results that display intended properties, this could function to amplify and accelerate the discovery of solid inorganic ion conducting materials, without focusing strictly on the modification of existing materials or the serendipitous observation of ionic conductivity in some amorphous or glassy product.

Given the motivation and design of the electrochemical anodization research project, which will be discussed in greater detail later, the terms ionic conducting material and electrolyte may be used interchangeably at times. Using the proposed reaction design, the solid inorganic materials being synthesized through anodization should be in contact with another (liquid) electrolyte at the reactive interface, so electronic conductivity will not short the system or inhibit the utility of this reaction. Therefore, it is important to understand the implications for the electronic conductivities of any products synthesized for application purposes, but that should not play a significant role in the development of the electrochemical synthetic methodologies.

1.4.4 Addressing limitations and considerations for the incorporation of current materials

As stated previously, solid ionic conductivities already meet or exceed the rate requirements for current technological applications. Despite this, limited practical incorporation of these materials has been achieved due to a variety of limitations to these materials extrinsic to the single property of ionic conductivity. It is therefore valuable to consider the wide range of

challenges that face the field when setting off to design a new synthetic paradigm with the hopes of discovering new chemical systems and target the discovery of functionally relevant materials.

Instead of focusing on any given system, an overview is provided on individual challenges, or systemic considerations, which regulate the practical incorporation of solid electrolytes into devices. No single material can necessarily be considered as either sufficient of insufficient in all of these categories, as individual requirements or expectations for any given consideration will be predicated on the discrete needs of the unique system in which the ionically conducting material is being utilized. It is the intention of introducing this list of desirable features and/or barriers to help isolate the key general parameters to be targeted through the proposed electrochemical anodization method. Considerations are not given in an order to suggest value or merit.

The first and most obvious consideration when targeting the production of new solid electrolytes is the mobile ion in question. This is determined by the intended application. If the goal is to incorporate the material into a Li-ion battery, then Li^+ needs to be the mobile ion. If a researcher is attempting to discover a material relevant to desalination, conductivity of Na^+ or Cl^- may satisfy the system requirements. The design of the anodization project satisfies this consideration by beginning with an electrode consisting of the intended mobile ion. This electrode will be electrochemically oxidized in order to generate the metal cation of interest.

The dimensionality of ionic conduction is an important practical consideration. The more restricted the movement of the ion through a material is, the more likely there will be greater design complexity or hinderances to incorporating this material. Examples exist for fast ionic conductors that display 1-dimensional conductivity through specific channels such as hollandite electrolytes, 2-dimensional conductivity along planes or cross-sectional lattices such as β-alumina, and 3-dimensional conductivity throughout an open solid framework such as that displayed by the

NaSICon class of materials. Greater dimensionality allows for more straightforward incorporation of solid electrolytes into practical devices, as 1- and 2-dimension conductors require alignment of conductive channels or planes between electrodes. Compressed pellets of such materials do not directly align these pathways, and net ionic mobility requires the ability to transfer between adjacent particles with the direction of motion dictated by structure, resulting in indirect and meandering pathways of least resistance between electrodes, effectively increasing the practical distance an ion must travel, thereby limiting rate and performance capabilities.

Thermal considerations are extremely important but also highly variable depending on target system. The first temperature consideration is intended operating range, for example consumer products / mobile storage are required to operate under the range of conditions that can exist for those applications such as driving in the Canadian winter vs an Arizona summer. This range could be less important for commercial or industrial applications such as grid storage, where thermal controls and regulation could be implemented for large, static devices if there is enough utility to warrant the energy cost. Additionally, materials are needed for use in extreme environments such as molten salt reactors, so near ambient ionic conductivity is not the only objective for the goal. Additional thermal considerations for certain materials involve drastic changes to properties depending on operating temperature due to potentially undergoing order-disorder phase change, as is the case for AgI. The last, and very important consideration is the overall thermal stability. If a material has good properties at operating conditions, but readily fails and decomposes outside of that range, that can greatly hinder the practical utility of that material.

Related to the dimensionality parameter previously discussed is the crystallographic information of targeted materials. To reiterate earlier discussion, the impact of defect concentration, increased local disorder through the incorporation of dopants and strain, and

minimization of activation energy between interstitial sites is of key importance to the fundamental property of ionic mobility. Therefore, designing a system which not only rewards the incorporation of defects and minimization of this energy landscape, but also promotes the discovery of non-crystalline products and the formation of non-thermodynamically favorable systems through driving the reaction via kinetic pathways is an exciting concept for the discovery of material systems that would be otherwise difficult to predict or model.

For the application of SSEs, balancing ionic and electronic conductivities is necessary to adequately separate stored charge and prevent current leak and self-discharge. Even if sufficiently high ionic conduction is achieved in a material, if the electronic conductivity is too high the material can act as a mixed conductor, which may still have practical utility as an ionic membrane, catalytic surface, or in other applications, but will not be viable for practical use in an energy storage device such as a secondary battery or ionic capacitor.

A key motivator for targeting an electrochemical synthetic methodology is practicality. The ability to process given materials and incorporate it into a device is greatly influenced by the synthetic method cost and ability to scale. Ideally the synthesis is reproducible, scalable, and synthetically "forgiving," as implementing a material synthesis on the scale of commercial production can lose certain aspects of rigorous quality control and consistency between operators compared to small-scale bench-top experiments. This is not necessarily the case, as certain instances benefit from large scale operations which allow for reduction of impact of slight inconsistencies, as a small discrepancy on a small scale can yield a greater impact than a moderate discrepancy on a very large scale. Additional considerations include material composition, which corresponds to the abundance and cost of precursors, safety pertaining to the synthetic methods,

product handling, waste generation and disposal, and processing and modification limitations which can impact the ability of a material to be incorporated in new or diverse applications.

Related to the practicality of material production, is the property of mechanical and chemical stability. If a SSE is discovered which exhibits extraordinary properties, but readily decomposes, or only exhibits these properties as synthesized in a metastable state but readily relaxes to a non-ionic conducting phase, then it is not functionally practical. This stability does not only relate to the product being stable intrinsically at ambient conditions, but also requires stability when incorporated into a device, and over the range of operating conditions. For example, if a Li-ion conducting material is reduced and decomposes upon exposure to Li-metal or has a stable electrochemical window of only 1 V and is otherwise electrochemically oxidized or reduced, then its realistic applications are subsequently limited.

These are the most significant general considerations surrounding the practical production and functionality of solid ionically conducting materials, and this list only grows when investigating specific applications. While this may seem like a daunting list of considerations and restrictions, balancing these objectives is functionally the reason why SSEs are not in widespread use currently. Therefore, the objective was not to address every single potentiality when deciding what synthetic methodology to pursue, but rather to identify the most fundamentally important aspects or instances where current methods and understanding fall short. The outcome of reviewing the state of the field and the greatest challenges facing materials discovery allowed us to focus on those most critic facets, with the ultimate goal of developing an explorative methodology to approach material's discovery in a new and unique way. This resulted in the proposal to use electrochemical anodization as a means to drive synthesis through the ionic conductivity of relevant metal cations. Additional details outlining the specific hypotheses behind

this synthetic methodology are further explained in Chapter 3. Beyond the requirement of ionic conductivity, the ability of electrochemical anodization to address the listed considerations for ionically conducting systems will be addressed.

Given the proposed synthetic method of using electrochemical anodization, the transfer of ions across the electrode-electrolyte interface must be sufficiently rapid, otherwise the reaction will not progress. Electrochemical syntheses are industrially relevant and generally considered low cost meaning the methodology is practical in that regard, but additional considerations would be needed for individual reactions depending on materials used in terms of safety, overall cost, and scalability. Electrochemical anodization is proposed to be a highly tunable strategy as a wide variety of system modifications are available and electrolyte additives and dopants are abundant. As the goal is to target materials relevant to energy storage, operating temperature near ambient is desired. This is built into the synthetic method, as ionic conductivity is hypothesized to be required for synthesis. Therefore, if the synthesis is conducted at the expected operating temperate of a material, and the synthesis requires ionic conductivity, then that material should inherently display ionic conductivity unless it is an unstable product and decomposes post-synthesis.

While any chemical reaction inherently has significant kinetic considerations, electrochemically driven reactions have the opportunity to manipulate rates through modifying the applied potentials, use of alternating potentials and currents, and the incorporation of other variable electrochemical techniques. Utilizing the kinetic features available to this synthetic methodology minimizes the need to focus on certain thermodynamic concerns or individual crystallographic or compositional targets. Hypothetically, any product that can be formed under the given reaction conditions that minimizes the resistance for the reaction to proceed should ideally be the majority product formed. If the product formed does not meet this requirement, then the reaction ceases,

and modifications to the reaction design are needed. This allows for the potential to produce amorphous, highly defected, metastable, and otherwise non-standard materials compared to those predicted by modelling or alterations to known crystallographic systems.

At the end of such a synthesis, the final product would essentially be 2/3 of an energy storage device, in which ionic conductivity has already been demonstrated moving across the deposited material away from the metal anode, along with requiring sufficiently low interfacial impedance between the anode surface and formed electrolyte.

1.5 Project Introduction: Development of an air-free XPS sample transfer holder.

This project shows the development, design, and testing of a sample transfer holder that allows for the air-free transfer of samples from a glovebox to the entrance antechamber of an X-ray photoelectron spectrometer (XPS) instrument. The development of this holder came about through collaborating and interacting with other group members, most notably those working on anode materials for Li-ion and Na-ion battery applications. For systems that employ standard carbonate electrolytes, electrolyte decomposition results in what is called the "solid electrolyte interface," or SEI. The properties of the SEI that is deposited on the battery electrode is fundamentally important to the overall performance and lifetime of a device, and therefore the ability to understand and regulate how this SEI is formed and the resulting properties of the deposited film is necessary to be able to produce functional battery cells and incorporate new or modified electrode materials.[79,82–86] The formation of the SEI is highly dependent on the electrode (in this case the anode), the electrolyte solvent composition, the Li or Na salt used, the supporting electrolytes or additives dissolved, and the concentrations and ratios of all of these constituents. A complex mixture of byproducts is formed throughout cycling, and while the composition can vary greatly depending on each system variable, generally the SEI of Li-ion batteries using carbonate

electrolytes includes inorganic components such as lithium oxides and fluorides, lithium carbonates, trapped salts, oligomer, and polymeric byproducts.

The investigation of the SEI following cycling is an important and challenging undertaking due to the complexity of the system, and XPS is one valuable component in the overall characterization of these various products that can lead to vital chemical insights into the decomposition processes and potential failure mechanisms or opportunities to improve electrolyte formulations. One complicating factor is that many of the SEI components are unstable and susceptible to reaction upon exposure to air. This led to the development of the holder presented in Chapter 4, which allows for the air-free transfer of samples for XPS analysis. The holder is shown to be robust, maintaining sample integrity for extended periods of time, readily produced at a low cost, and capable of not only transferring samples to the instrument for analysis, but the holder can be resealed, allowing for transfer back to the glove-box environment, allowing for further use or characterization of the product following XPS analysis.

This work has resulted in collaborations and additional publications on the study of SEI.[4,5] While that has been the primary use of the holder, it is in no way limited to that application, as previous researchers could have benefited from it, including the collaborating author Dr. Agocs, who underwent a complete time oxidation study of Cu-Sb-Se nanoparticles due to observations in changes to photoelectrochemical properties and surface sight bonding environments over time due to oxidation under ambient conditions. Preventing air exposure is beneficial whenever trying to understand the surface properties of a reactive material, and for a technique as surface sensitive as XPS, being able to transfer and analyze samples while maintaining characteristics as close to the as-synthesized is necessary for meaningful characterization.[87–89]

REFERENCES

(1) Boissiere, J. D.; Shissler, D. J.; Johnson, D. C.; Guiton, B. S.; Prieto, A. L. Single Step Chemical Vapor Deposition Synthesis of Highly Branched SiO 2 Nanowires from a Multi-Wire Backbone : Initiat- Ing and Controlling Branching via In Situ Cu-Catalyst Loading. *Chem. Mater.* **2021**, *Submitted*.

(2) Shissler, D. J. Part I: Synthesis and Characterization of Titania and Magnesium Nanoparticles for Hydrogen Production and Storage. Part II: Characterization and Growth of Branched Silicon Nanowires Grown Via a Simultaneous Vapor-Liquid-Solid and Vapor-Solid-Solid Mechani, Colorado State University, 2015.

(3) Schneider, J. D.; Agocs, D. B.; Prieto, A. L. Design of a Sample Transfer Holder to Enable Air-Free X-Ray Photoelectron Spectroscopy. *Chem. Mater.* **2020**, *32* (19), 8091–8096. https://doi.org/10.1021/ACS.CHEMMATER.0C01895.

(4) Kraynak, L. A.; Schneider, J. D.; Prieto, A. L. Exploring the Role of Vinylene Carbonate in the Passivation and Capacity Retention of Cu2Sb Thin Film Anodes. *J. Phys. Chem. C* **2020**, *124* (48), 26083–26093. https://doi.org/10.1021/ACS.JPCC.0C04064.

(5) Gimble, N. J.; Kraynak, L. A.; Schneider, J. D.; Schulze, M. C.; Prieto, A. L. X-Ray Photoelectron Spectroscopy as a Probe for Understanding the Potential-Dependent Impact of Fluoroethylene Carbonate on the Solid Electrolyte Interface Formation in Na/Cu2Sb Batteries. *J. Power Sources* **2021**, *489*, 229171. https://doi.org/10.1016/J.JPOWSOUR.2020.229171.

(6) Wu, H.; Cui, Y. Designing Nanostructured Si Anodes for High Energy Lithium Ion Batteries. *Nano Today* **2012**, *7*, 414–429. https://doi.org/10.1016/j.nantod.2012.08.004.

(7) Rey, B. M.; Elnathan, R.; Ditcovski, R.; Geisel, K.; Zanini, M.; Fernandez-Rodriguez, M.-A.; Naik, V. V; Frutiger, A.; Richtering, W.; Ellenbogen, T.; Voelcker, N. H.; Isa, L. Fully Tunable Silicon Nanowire Arrays Fabricated by Soft Nanoparticle Templating. *Nano Lett.* **2015**. https://doi.org/10.1021/acs.nanolett.5b03414.

(8) Wang, J. .; Zhan, C. .; Li, F. . The Synthesis of Silica Nanowire Arrays. *Solid State Commun.* **2003**, *125* (11), 629–631. https://doi.org/10.1016/S0038-1098(03)00034-6.

(9) Yoon, J.-H. Alternative Vapor–Liquid–Solid Process in Au-Assisted Growth of Silica Nanowires. *Mater. Lett.* **2014**, *123*, 131–134. https://doi.org/10.1016/j.matlet.2014.03.005.

(10) Krylyuk, S.; Davydov, A. V.; Levin, I.; Motayed, A.; Vaudin, M. D. Rapid Thermal Oxidation of Silicon Nanowires. *Appl. Phys. Lett.* **2009**, *94* (6), 063113. https://doi.org/10.1063/1.3079395.

(11) Stolt, L. Formation of Cu3Si and Its Catalytic Effect on Silicon Oxidation at Room Temperature. *J. Vac. Sci. Technol. A Vacuum, Surfaces, Film.* **1991**, *9* (3), 1501. https://doi.org/10.1116/1.577653.

(12) Wen, C.-Y.; Reuter, M. C.; Tersoff, J.; Stach, E. A.; Ross, F. M. Structure, Growth Kinetics, and Ledge Flow during Vapor−Solid−Solid Growth of Copper-Catalyzed Silicon Nanowires. *Nano Lett.* **2010**, *10* (2), 514–519. https://doi.org/10.1021/nl903362y.

(13) Dobkin, D. M. *Principles of Chemical Vapor Deposition*; Zuraw, M. K., Ed.; Kluwer Academic Publishers: Dordrecht ; Boston, 2003.

(14) Pierson, H. O. *Handbook of Chemical Vapor Deposition Principles, Technology, and Applications*; Materials science and process technology series Electronic materials and process technology; Noyes Publications: Norwich, N.Y., 1999.

(15) Johnson, D. C.; Morris, W. D.; Prieto, A. L. Effects of Transport Gradients in a Chemical

Vapor Deposition Reactor Employing Vapor-Liquid-Solid Growth of Ternary Chalcogenide Phase-Change Materials. *Nanotechnology* **2010**, *21*, 165604. https://doi.org/10.1088/0957-4484/21/16/165604.

(16) Khmel, S. Y.; Baranov, E. A.; Zaikovskii, A. V.; Zamchiy, A. O.; Maximovskiy, E. A.; Gulyaev, D. V.; Zhuravlev, K. S. Synthesis of Silicon Oxide Nanowires by the GJ EBP CVD Method Using Different Diluent Gases. *Phys. status solidi* **2016**, n/a-n/a. https://doi.org/10.1002/pssa.201532955.

(17) Yanson, A. I.; Rodriguez, P.; Garcia-Araez, N.; Mom, R. V.; Tichelaar, F. D.; Koper, M. T. M. Cathodic Corrosion: A Quick, Clean, and Versatile Method for the Synthesis of Metallic Nanoparticles. *Angew. Chemie Int. Ed.* **2011**, *50* (28), 6346–6350. https://doi.org/10.1002/anie.201100471.

(18) Vishwanath, R. S.; Kandaiah, S. Electrochemical Preparation of Crystalline γ-CuI Thin Films through Potential-Controlled Anodization of Copper and Its Photoelectrochemical Investigations. *J. Solid State Electrochem.* **2016**, *20* (7), 2093–2102. https://doi.org/10.1007/s10008-016-3218-3.

(19) Su, Z.; Zhou, W.; Jiang, F.; Hong, M. Anodic Formation of Nanoporous and Nanotubular Metal Oxides. *J. Mater. Chem.* **2012**, *22* (2), 535–544. https://doi.org/10.1039/C1JM13338A.

(20) Mor, G. K.; Varghese, O. K.; Paulose, M.; Shankar, K.; Grimes, C. A. A Review on Highly Ordered, Vertically Oriented TiO2 Nanotube Arrays: Fabrication, Material Properties, and Solar Energy Applications. *Sol. Energy Mater. Sol. Cells* **2006**, *90* (14), 2011–2075. https://doi.org/10.1016/j.solmat.2006.04.007.

(21) Kar, P.; El-Tahlawy, M. K.; Zhang, Y.; Yassin, M.; Mahdi, N.; Kisslinger, R.; Thakur, U.

K.; Askar, A. M.; Fedosejevs, R.; Shankar, K. Anodic Copper Oxide Nanowire and Nanopore Arrays with Mixed Phase Content: Synthesis, Characterization and Optical Limiting Response. *J. Phys. Commun.* **2017**, *1* (4), 045012. https://doi.org/10.1088/2399-6528/AA93A4.

(22) Zhang, M.-M.; Chen, J.-Y.; Li, H.; Wang, C.-R. Recent Progress in Li-Ion Batteries with TiO2 Nanotube Anodes Grown by Electrochemical Anodization. *Rare Met. 2020 402* **2020**, *40* (2), 249–271. https://doi.org/10.1007/S12598-020-01499-X.

(23) Stepniowski, W. J.; Misiolek, W. Z. Review of Fabrication Methods, Physical Properties, and Applications of Nanostructured Copper Oxides Formed via Electrochemical Oxidation. *Nanomater. 2018, Vol. 8, Page 379* **2018**, *8* (6), 379. https://doi.org/10.3390/NANO8060379.

(24) Liu, S.; Tian, J.; Zhang, W. Fabrication and Application of Nanoporous Anodic Aluminum Oxide: A Review. *Nanotechnology* **2021**, *32* (22), 222001. https://doi.org/10.1088/1361-6528/ABE25F.

(25) Morales, A. M.; Lieber, C. M. A Laser Ablation Method for the Synthesis of Crystalline Semiconductor Nanowires. *Science (80-.).* **1998**, *279* (5348).

(26) Agarwal, R.; Lieber, C. M. Semiconductor Nanowires: Optics and Optoelectronics. *Appl. Phys. A* **2006**, *85* (3), 209–215. https://doi.org/10.1007/s00339-006-3720-z.

(27) Schmidt, V.; Wittemann, J. V.; Senz, S.; Gósele, U. Silicon Nanowires: A Review on Aspects of Their Growth and Their Electrical Properties. *Adv. Mater.* **2009**, *21*, 2681–2702. https://doi.org/10.1002/adma.200803754.

(28) Wang, N.; Cai, Y.; Zhang, R. Q. Growth of Nanowires. *Mater. Sci. Eng. R Reports* **2008**, *60* (1–6), 1–51. https://doi.org/10.1016/j.mser.2008.01.001.

(29) Wagner, R. S.; Ellis, W. C. VAPOR-LIQUID-SOLID MECHANISM OF SINGLE CRYSTAL GROWTH. *Appl. Phys. Lett.* **1964**, *4* (5), 89. https://doi.org/10.1063/1.1753975.

(30) Hansen, M. 1901-. *Constitution of Binary Alloys*; Anderko, K., Ed.; Metallurgy and metallurgical engineering series; McGraw-Hill: New York, 1958.

(31) Chan, C. K.; Peng, H.; Liu, G.; McIlwrath, K.; Zhang, X. F.; Huggins, R. a; Cui, Y. High-Performance Lithium Battery Anodes Using Silicon Nanowires. *Nat. Nanotechnol.* **2008**, *3*, 31–35. https://doi.org/10.1038/nnano.2007.411.

(32) Johnson, D. C.; Guiton, B. S.; Shissler, D. J.; Prieto, A. L. *Nanowire Synthesis with Controllable Three Dimensional Branching: Simultaneous Incorporation of Vapor-Liquid-Solid and Vapor-Solid-Solid Growth*; Fort Collins, CO, 2015.

(33) Johnson, D. C.; Mosby, J. M.; Riha, S. C.; Prieto, A. L. Synthesis of Copper Silicide Nanocrystallites Embedded in Silicon Nanowires for Enhanced Transport Properties. *J. Mater. Chem.* **2010**, *20*, 1993. https://doi.org/10.1039/b919281f.

(34) Kolb, F. M.; Hofmeister, H.; Scholz, R.; Zacharias, M.; Gösele, U.; Ma, D. D.; Lee, S.-T. Analysis of Silicon Nanowires Grown by Combining SiO Evaporation with the VLS Mechanism. *J. Electrochem. Soc.* **2004**, *151* (7), G472–G475. https://doi.org/10.1149/1.1759365.

(35) Tu, J.; Yuan, Y.; Zhan, P.; Jiao, H.; Wang, X.; Zhu, H.; Jiao, S. Straightforward Approach toward SiO 2 Nanospheres and Their Superior Lithium Storage Performance. *J. Phys. Chem. C* **2014**, *118*, 7357–7362. https://doi.org/10.1021/jp5011023.

(36) Pan, Z. W.; Dai, Z. R.; Xu, L.; Lee, S. T.; Wang, Z. L. Temperature-Controlled Growth of Silicon-Based Nanostructures by Thermal Evaporation of SiO Powders. *J. Phys. Chem. B*

2001, *105* (13), 2507–2514. https://doi.org/10.1021/jp004253q.

(37) Wang, F.; Dong, A.; Sun, J.; Tang, R.; Yu, H.; Buhro, W. E. Solution-Liquid-Solid Growth of Semiconductor Nanowires. *Inorg. Chem.* **2006**, *45* (19), 7511–7521. https://doi.org/10.1021/ic060498r.

(38) Morral, J. A. and B. K. and P. R. i C. and J. R. M. and A. F. i. Influence of Cu as a Catalyst on the Properties of Silicon Nanowires Synthesized by the Vapour–Solid–Solid Mechanism. *Nanotechnology* **2007**, *18* (30), 305606.

(39) Kolasinski, K. W. Catalytic Growth of Nanowires: Vapor-Liquid-Solid, Vapor-Solid-Solid, Solution-Liquid-Solid and Solid-Liquid-Solid Growth. *Curr. Opin. Solid State Mater. Sci.* **2006**, *10* (2006), 182–191. https://doi.org/10.1016/j.cossms.2007.03.002.

(40) Obrovac, M. N.; Chevrier, V. L. Alloy Negative Electrodes for Li-Ion Batteries. *Chem. Rev.* **2014**, *114* (23), 11444–11502. https://doi.org/10.1021/cr500207g.

(41) Liu, X. H.; Zhang, L. Q.; Zhong, L.; Liu, Y.; Zheng, H.; Wang, J. W.; Cho, J. H.; Dayeh, S. a.; Picraux, S. T.; Sullivan, J. P.; Mao, S. X.; Ye, Z. Z.; Huang, J. Y. Ultrafast Electrochemical Lithiation of Individual Si Nanowire Anodes. *Nano Lett.* **2011**, *11*, 2251–2258. https://doi.org/10.1021/nl200412p.

(42) Huang, R.; Fan, X.; Shen, W.; Zhu, J. Carbon-Coated Silicon Nanowire Array Films for High-Performance Lithium-Ion Battery Anodes. *Appl. Phys. Lett.* **2009**, *95* (2009), 93–96. https://doi.org/10.1063/1.3238572.

(43) Mortazavi, M.; Ye, Q.; Birbilis, N.; Medhekar, N. V. High Capacity Group-15 Alloy Anodes for Na-Ion Batteries : Electrochemical and Mechanical Insights. **2015**, *285*.

(44) Li, Z.; Ding, J.; Mitlin, D. Tin and Tin Compounds for Sodium Ion Battery Anodes: Phase Transformations and Performance. *Acc. Chem. Res.* **2015**, *48* (6), 1657–1665.

https://doi.org/10.1021/acs.accounts.5b00114.

(45) Mai, L.; Wei, Q.; Tian, X.; Zhao, Y.; An, Q. Electrochemical Nanowire Devices for Energy Storage. *Nanotechnology, IEEE Transactions on*. 2014, pp 10–15. https://doi.org/10.1109/TNANO.2013.2276524.

(46) Zhong, Y.; Li, X.; Zhang, Y.; Li, R.; Cai, M.; Sun, X. Nanostructued Core–Shell Sn Nanowires @ CNTs with Controllable Thickness of CNT Shells for Lithium Ion Battery. *Appl. Surf. Sci.* **2015**, *332*, 192–197. https://doi.org/10.1016/j.apsusc.2015.01.099.

(47) Kim, J.; Lim, J.; Kim, M.; Lee, H.; Jun, Y.; Kim, D. Fabrication of Carbon-Coated Silicon Nanowires and Their Application in Dye-Sensitized Solar Cells. **2014**.

(48) Nuli, Y.; Wang, B.; Yang, J.; Yuan, X.; Ma, Z. Cu5Si-Si/C Composites for Lithium-Ion Battery Anodes. *J. Power Sources* **2006**, *153*, 371–374. https://doi.org/10.1016/j.jpowsour.2005.05.023.

(49) Xu, K.; He, Y.; Ben, L.; Li, H.; Huang, X. Enhanced Electrochemical Performance of Si e Cu e Ti Thin Fi Lms by Surface Covered with Cu 3 Si Nanowires. **2015**, *c*, 455–460.

(50) Istratov, A. A.; Weber, E. R. Physics of Copper in Silicon. *J. Electrochem. Soc.* **2002**, *149* (1), G21. https://doi.org/10.1149/1.1421348.

(51) Harper, J. M. E.; Charai, A.; Stolt, L.; d'Heurle, F. M.; Fryer, P. M. Room-Temperature Oxidation of Silicon Catalyzed by Cu3Si. *Appl. Phys. Lett.* **1990**, *56* (25), 2519. https://doi.org/10.1063/1.103260.

(52) Liu, C. S.; Chen, L. J. Catalytic Oxidation of (001)Si in the Presence of Cu3Si at Room Temperature. *J. Appl. Phys.* **1993**, *74* (5), 3611–3613. https://doi.org/10.1063/1.354499.

(53) Cong, V. T.; Ganbold, E.-O.; Saha, J. K.; Jang, J.; Min, J.; Choo, J.; Kim, S.; Song, N. W.; Son, S. J.; Lee, S. B.; Joo, S.-W. Gold Nanoparticle Silica Nanopeapods. *J. Am. Chem.*

Soc. **2014**, *136* (10), 3833–3841. https://doi.org/10.1021/ja411034q.

(54) Hunyadi, S. E.; Murphy, C. J. Tunable One-Dimensional Silver−Silica Nanopeapod Architectures. *J. Phys. Chem. B* **2006**, *110* (14), 7226–7231. https://doi.org/10.1021/jp0603076.

(55) Kaushik, A.; Kumar, R.; Huey, E.; Bhansali, S.; Nair, N.; Nair, M. Silica Nanowires: Growth, Integration, and Sensing Applications. *Microchim. Acta* **2014**, *181* (15–16), 1759–1780. https://doi.org/10.1007/s00604-014-1255-0.

(56) Wang, S.-B.; Huang, Y.-F.; Chattopadhyay, S.; Jinn Chang, S.; Chen, R.-S.; Chong, C.-W.; Hu, M.-S.; Chen, L.-C.; Chen, K.-H. Surface Plasmon-Enhanced Gas Sensing in Single Gold-Peapodded Silica Nanowires. *NPG Asia Mater.* **2013**, *5* (5), e49. https://doi.org/10.1038/am.2013.17.

(57) Guo, X.; Ying, Y.; Tong, L. Photonic Nanowires: From Subwavelength Waveguides to Optical Sensors. *Acc. Chem. Res.* **2014**, *47* (2), 656–666. https://doi.org/10.1021/ar400232h.

(58) Shi, W.; Lu, W.; Jiang, L. The Fabrication of Photosensitive Self-Assembly Au Nanoparticles Embedded in Silica Nanofibers by Electrospinning. *J. Colloid Interface Sci.* **2009**, *340* (2), 291–297. https://doi.org/10.1016/j.jcis.2009.09.011.

(59) Wang, S.-B.; Chen, R.-S.; Chang, S. J.; Han, H.-C.; Hu, M.-S.; Chen, K.-H.; Chen, L.-C. Surface Plasmon Resonance-Induced Color-Selective Au-Peapodded Silica Nanowire Photodetectors with High Photoconductive Gain. *Nanoscale* **2014**, *6* (3), 1264–1270. https://doi.org/10.1039/C3NR04533A.

(60) Sığırcık, G.; Aydın, E. B. Electrochemical Synthesize and Characterization of ZnO/ZnS Nanostructures for Hydrogen Production. *Int. J. Energy Res.* **2020**, *44* (14), 11756–11771.

https://doi.org/10.1002/ER.5814.

(61) Ellis, B. L.; Knauth, P.; Djenizian, T. Three-Dimensional Self-Supported Metal Oxides for Advanced Energy Storage. *Adv. Mater.* **2014**, *26* (21), 3368–3397. https://doi.org/10.1002/ADMA.201306126.

(62) Md Jani, A. M.; Losic, D.; Voelcker, N. H. Nanoporous Anodic Aluminium Oxide: Advances in Surface Engineering and Emerging Applications. *Prog. Mater. Sci.* **2013**, *58* (5), 636–704. https://doi.org/10.1016/J.PMATSCI.2013.01.002.

(63) Basu, P. K.; Saha, N.; Maji, S.; Saha, H.; Basu, S. Nanoporous ZnO Thin Films Deposited by Electrochemical Anodization: Effect of UV Light. *J. Mater. Sci. Mater. Electron. 2008 196* **2008**, *19* (6), 493–499. https://doi.org/10.1007/S10854-008-9604-6.

(64) Bian, H.; Li, Z.; Xiao, X.; Schmuki, P.; Lu, J.; Li, Y. Y. Tunable Transformation Between SnS and SnOx Nanostructures via Facile Anodization and Their Photoelectrochemical and Photocatalytic Performance. *Sol. RRL* **2018**, *2* (11), 1800161. https://doi.org/10.1002/SOLR.201800161.

(65) Schimmel, M. I.; Bottechia, O. L.; Wendt, H. Anodic Formation of Binary and Ternary Compound Semiconductor Films for Photovoltaic Cells. *J. Appl. Electrochem. 1998 283* **1998**, *28* (3), 299–304. https://doi.org/10.1023/A:1003215716754.

(66) A novel superhydrophilic-underwater superoleophobic Cu2S coated copper mesh for efficient oil-water separation - ScienceDirect https://www-sciencedirect-com.ezproxy2.library.colostate.edu/science/article/pii/S0167577X16310424?via%3Dihub (accessed Aug 26, 2021).

(67) Kar, P.; Farsinezhad, S.; Zhang, X.; Shankar, K. Anodic Cu2S and CuS Nanorod and Nanowall Arrays: Preparation, Properties and Application in CO2 Photoreduction.

Nanoscale **2014**, *6* (23), 14305–14318. https://doi.org/10.1039/C4NR05371K.

(68) Vishwanath, R. S.; Kandaiah, S. Electrochemical Preparation of Crystalline γ-CuI Thin Films through Potential-Controlled Anodization of Copper and Its Photoelectrochemical Investigations. *J. Solid State Electrochem. 2016 207* **2016**, *20* (7), 2093–2102. https://doi.org/10.1007/S10008-016-3218-3.

(69) Huang, H. Y.; Chien, D. J.; Huang, G. G.; Chen, P. Y. Electrochemical Preparation of Photoelectrochemically Active CuI Thin Films from Room Temperature Ionic Liquid. *Electrochim. Acta* **2012**, *65*, 204–209. https://doi.org/10.1016/J.ELECTACTA.2012.01.044.

(70) Pasta, M.; Armstrong, D.; Brown, Z. L.; Bu, J.; Castell, M. R.; Chen, P.; Cocks, A.; Corr, S. A.; Cussen, E. J.; Darnbrough, E.; Deshpande, V.; Doerrer, C.; Dyer, M. S.; El-Shinawi, H.; Fleck, N.; Grant, P.; Gregory, G. L.; Grovenor, C.; Hardwick, L. J.; S Irvine, J. T.; Jeong Lee, H.; Li, G.; Liberti, E.; McClelland, I.; Monroe, C.; Nellist, P. D.; Shearing, P. R.; Shoko, E.; Song, W.; Spencer Jolly, D.; Thomas, C. I.; Turrell, S. J.; Vestli, M.; Williams, C. K.; Zhou, Y.; Bruce, P. G. 2020 Roadmap on Solid-State Batteries. *J. Phys. Energy* **2020**, *2*, 32008. https://doi.org/10.1088/2515-7655/ab95f4.

(71) Lu, Y.; Li, L.; Zhang, Q.; Niu, Z.; Chen, J. Electrolyte and Interface Engineering for Solid-State Sodium Batteries. *Joule*. Cell Press September 19, 2018, pp 1747–1770. https://doi.org/10.1016/j.joule.2018.07.028.

(72) Ding, Z.; Li, J.; Li, J.; An, C. Review-Interfaces: Key Issue to Be Solved for All Solid-State Lithium Battery Technologies. *J. Electrochem. Soc.* **2020**, *167*, 070541. https://doi.org/10.1149/1945-7111/ab7f84.

(73) Liu, B.; Gong, Y.; Fu, K.; Han, X.; Yao, Y.; Pastel, G.; Yang, C.; Xie, H.; Wachsman, E.

D.; Hu, L. Garnet Solid Electrolyte Protected Li-Metal Batteries. *Appl. Mater. Interfaces* **2017**, *9*, 18809–18815. https://doi.org/10.1021/acsami.7b03887.

(74) Bekaert, E.; Buannic, L.; Lassi, U.; Llordés, A.; Salminen, J. Electrolytes for Li- and Na-Ion Batteries: Concepts, Candidates, and the Role of Nanotechnology. In *Emerging Nanotechnologies in Rechargeable Energy Storage Systems*; Elsevier Inc., 2017; pp 1–43. https://doi.org/10.1016/B978-0-323-42977-1.00001-7.

(75) Zhou, C.; Bag, S.; Thangadurai, V. Engineering Materials for Progressive All-Solid-State Na Batteries. *ACS Energy Letters*. American Chemical Society September 14, 2018, pp 2181–2198. https://doi.org/10.1021/acsenergylett.8b00948.

(76) Sun, C.; Liu, J.; Gong, Y.; Wilkinson, D. P.; Zhang, J. Recent Advances in All-Solid-State Rechargeable Lithium Batteries. *Nano Energy*. Elsevier Ltd March 1, 2017, pp 363–386. https://doi.org/10.1016/j.nanoen.2017.01.028.

(77) Hayashi, A.; Sakuda, A.; Tatsumisago, M. Development of Sulfide Solid Electrolytes and Interface Formation Processes for Bulk-Type All-Solid-State Li and Na Batteries. *Front. Energy Res.* **2016**, *4*, 25. https://doi.org/10.3389/fenrg.2016.00025.

(78) Takada, K. Progress and Prospective of Solid-State Lithium Batteries. *Acta Mater.* **2013**, *61* (3), 759–770. https://doi.org/10.1016/j.actamat.2012.10.034.

(79) Goodenough, J. B.; Kim, Y. Challenges for Rechargeable Li Batteries. *Chem. Mater.* **2010**, *22*, 587–603. https://doi.org/10.1021/cm901452z.

(80) Manthiram, A.; Yu, X.; Wang, S. Lithium Battery Chemistries Enabled by Solid-State Electrolytes. *Nature Reviews Materials*. Nature Publishing Group February 14, 2017, pp 1–16. https://doi.org/10.1038/natrevmats.2016.103.

(81) Hueso, K. B.; Palomares, V.; Armand, M.; Rojo, T. Challenges and Perspectives on High

and Intermediate-Temperature Sodium Batteries. *Nano Research*. Tsinghua University Press December 1, 2017, pp 4082–4114. https://doi.org/10.1007/s12274-017-1602-7.

(82) Fu, L. J.; Liu, H.; Li, C.; Wu, Y. P.; Rahm, E.; Holze, R.; Wu, H. Q. Surface Modifications of Electrode Materials for Lithium Ion Batteries. *Solid State Sci.* **2006**, *8* (2), 113–128. https://doi.org/10.1016/j.solidstatesciences.2005.10.019.

(83) Ruffo, R.; Hong, S. S.; Chan, C. K.; Huggins, R. a.; Cui, Y. Impedance Analysis of Silicon Nanowire Lithium Ion Battery Anodes. *J. Phys. Chem. C* **2009**, *113*, 11390–11398. https://doi.org/10.1021/jp901594g.

(84) Chan, C. K.; Ruffo, R.; Hong, S. S.; Cui, Y. Surface Chemistry and Morphology of the Solid Electrolyte Interphase on Silicon Nanowire Lithium-Ion Battery Anodes. *J. Power Sources* **2009**, *189*, 1132–1140. https://doi.org/10.1016/j.jpowsour.2009.01.007.

(85) Soto, F. A.; Ma, Y.; Martinez de la Hoz, J. M.; Seminario, J. M.; Balbuena, P. B. Formation and Growth Mechanisms of Solid-Electrolyte Interphase Layers in Rechargeable Batteries. *Chem. Mater.* **2015**, acs.chemmater.5b03358. https://doi.org/10.1021/acs.chemmater.5b03358.

(86) Weiss, M.; Seidlhofer, B. K.; Geiß, M.; Geis, C.; Busche, M. R.; Becker, M.; Vargas-Barbosa, N. M.; Silvi, L.; Zeier, W. G.; Schröder, D.; Janek, J. Unraveling the Formation Mechanism of Solid-Liquid Electrolyte Interphases on LiPON Thin Films. *ACS Appl. Mater. Interfaces* **2019**, *11* (9), 9539–9547. https://doi.org/10.1021/acsami.8b19973.

(87) Biesinger, M. C. Advanced Analysis of Copper X-Ray Photoelectron Spectra. *Surf. Interface Anal.* **2017**, *49* (13), 1325–1334. https://doi.org/10.1002/sia.6239.

(88) Aurbach, D.; Weissman, I.; Schechter, A.; Cohen, H. X-Ray Photoelectron Spectroscopy Studies of Lithium Surfaces Prepared in Several Important Electrolyte Solutions. A

Comparison with Previous Studies by Fourier Transform Infrared Spectroscopy. *Langmuir* **1996**, *12* (16), 3991–4007. https://doi.org/10.1021/LA9600762.

(89) Malmgren, S.; Ciosek, K.; Lindblad, R.; Plogmaker, S.; Kühn, J.; Rensmo, H.; Edström, K.; Hahlin, M. Consequences of Air Exposure on the Lithiated Graphite SEI. *Electrochim. Acta* **2013**, *105*, 83–91. https://doi.org/10.1016/J.ELECTACTA.2013.04.118.

II. SINGLE STEP CHEMICAL VAPOR DEPOSITION SYNTHESIS OF HIGHLY BRANCHED SIO2 NANOWIRES FROM A MULTI-WIRE BACKBONE: INITIATING AND CONTROLLING BRANCHING VIA IN SITU CU-CATALYST LOADING.[ii]

2.1 Overview

Branched nanowires are a unique structure with the potential to impact the performance and practical use of nanowire devices. Previously however, in order to synthesize branched silicon-based nanowires, a multi-step CVD process has been used which involves first depositing a catalyst, then growing the primary backbone wire, followed by treatment of the product, secondary catalyst deposition, and a second growth step. Here we have demonstrated the ability to produce branched silica nanowires using a Cu catalyst in a single CVD reaction. The reaction can be initiated with pre-deposited Au nanoparticle catalyst, or Cu catalyst deposited in-line. Through continuous deposition of both SiO_x and Cu precursors, a multi-wire backbone is formed which allows for the co-deposition of copper silicide along the multi-wire interface. Continued SiO_x deposition promoted by the copper silicide catalyst results in a "nanopeapodded" wire structure, previously observed primarily in Au-SiO_2 systems. No previous report on nanopeapodding directly addresses the growth of the multi-wire backbone. Through studying and understanding the processes involved in the formation of these branched nano-wire structures, we provide evidence for the multi-

[ii] This chapter was formatted for the journal *Chemistry of Materials*.[1] The authors Shissler, Johnson, and Prieto contributed to the background and synthetic development for the work presented in the chapter, but nearly all writing, presented data, data analysis, and the entire multi-wire hypothesis is the work of the dissertation author. The one exception to this is the EELS analysis in this chapter, which was conducted by Prof. Beth Guiton, who also contributed to the data analysis and writing of that specific section.

wire hypothesis, as well as demonstrate how to manipulate the growth of the branched products through controlling synthetic variables. By understanding this system, we have been able to develop a CVD process which reliably and reproducibly synthesizes a high-density of branched nanowires.

2.2 Introduction

A significant portion of current academic materials research focuses on nanoscale materials, exploring the potential advantages over their bulk counterparts due to unique properties that emerge as a function of reduced size and high surface area. Nanowires are of particular interest due to their high aspect ratio and unique 1-dimensional transport properties, allowing new technologies to be developed for nanoscale applications including electronics, optics, energy storage and production, and sensors, such as those used for lab-on-a-chip devices.[1-7] One material currently under investigation for use in all of these fields is silica. Silica generally displays good chemical and physical stability and biocompatibility, and its properties can be altered through changes to morphology, doping, and surface modification or coating.[8-9] These synthetic controls allow nanoscale silica to be rationally designed for devices through manipulating the transport properties of electrons, photons, and plasmons.[5] Research on the controllable synthesis of nanowires has been ongoing for decades, with synthetic techniques including templated syntheses, solution based reactions, and chemical vapor deposition (CVD).[10-11] Chemical vapor deposition is particularly useful for the controllable synthesis of high-quality nanoscale materials when used in conjunction with catalyst-assisted growth mechanisms.

Research on nanowires of silicon and silica began with “whisker growth” studies, which likely synthesized nanowires primarily through axial screw dislocation-promoted growth or oxide-assisted growth.[10-11] While these processes allowed for the synthesis and study of nanowires, there

was little synthetic control until Wagner and Ellis reported the CVD synthesis of single crystal Si nanowires through a vapor-liquid-solid (VLS) growth mechanism using Au-nanoparticle catalysts.[12] Approximately three decades later, Morales and Lieber established the versatility of this synthetic technique by demonstrating that catalyst materials and wire growth conditions could be predicted from phase diagrams.[13] In addition to eutectic metal catalysts promoting growth through the VLS mechanism, later it was discovered that silicide-forming materials can also catalyze growth at sub-eutectic temperatures through a vapor-solid-solid (VSS) mechanism.[14] The use of catalysts and phase diagrams to predict the solubility of gaseous precursors in catalyst particles has allowed for rational synthetic design of more complex silicon-based nanowire products, including nanowire superlattices,[15] core-shell structures,[16-17] doped materials,[18] peapodded structures,[19-21] and 3-dimensional branched nanowires.[22-23] The variability and controllability of these products allows for numerous potential applications in nanoscale devices.

Branched silica nanowires are an interesting nanowire morphology as these structures may be uniquely suited for applications in fabricating nanoscale devices such as LED arrays or other optics, logic circuits, and for various biological and environmental sensors.[5-7, 24-25] The presence of branching can lead to higher surface area and an increased number of active sites per nanowire contact, which increases signal intensity and sensitivity for sensors, and may have additional impacts on other applications. Branched silicon nanowire structures have previously been synthesized though CVD using multi-step processing. Typically, the main or "trunk" wires are first grown via VLS growth and then the as-synthesized wires are removed from the reactor and treated in order to deposit a catalyst along the surface of the nanowires. Finally, a secondary growth process is initiated during which the branches are catalytically grown from the treated wires.[22]

The Elliman group previously reported the synthesis of branched silica nanowires in a single high-temperature annealing step.[26] To accomplish this, they used a thin film of Au deposited on a Si wafer substrate as the catalyst, and a second piece of Si was placed on the growth substrate to react with residual O_2 and form volatile SiO, resulting in the growth of substoichiometric SiO_x nanowire products.[26] This procedure resulted in the growth of Au nanopeapodded SiO_2 nanowires, with the Au nanoparticle deposits acting as the secondary catalysts. The branched nanowires synthesized through this method are a minority product, and the extent of branching is limited by both the initial Au catalyst deposition and diffusion of residual O_2.[26-27] The amount of Au deposited is unable to be significantly increased without preventing the initial nanowire growth necessary, and concentration and diffusion limitations on the residual O_2 further limit the ability to modify and control the growth of the highly branched nanowire species.

Herein, we present a method to synthesize branched SiO_2 nanowires with increased control over the number of branched structures and the extent of branching using an *in situ* Cu catalyst loading method. Figure 2.1 shows the schematic diagram of the home-built CVD system in which the

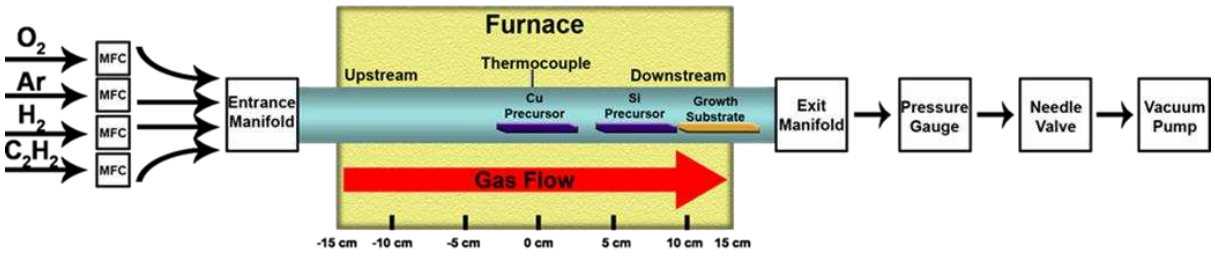

Figure 2.1. A depiction of the CVD reactor setup used to synthesize highly branched nanowires. Available carrier and reactive gasses (O_2, Ar, H_2, and C_2H_2) are depicted flowing from left to right through mass flow controllers (MFCs). Carbon coated quartz boats containing the solid Cu and Si precursors are located at the thermocouple located in center of the furnace and 8 cm downstream of the thermocouple respectively. The leading edge the of Si (100) growth substrates is placed 10-11 cm downstream of the thermocouple. The pressure of the system is regulated using a solenoid-controlled needle valve between the pressure sensor and vacuum pump.

branched SiO_2 nanowires are synthesized through the simultaneous thermal evaporation of Cu and SiO_x precursors in the horizontal reactor.

When both SiO_x and Cu are in the gas phase throughout the reaction, Cu can catalyze both the initial silica nanowire growth, as well as the growth of the branches as the reaction continues. As the Cu catalyst is deposited throughout the reaction, the extent of branching can be manipulated through controlling Cu and SiO_x partial pressures, and branching can be terminated through limiting Cu precursor present. The growth process uses a combination of the vapor-liquid-solid (VLS) and vapor-solid-solid (VSS) catalyst-assisted growth mechanisms simultaneously to synthesize branched nanowires whereby the size and morphology of the trunk as well as the branches can be manipulated. The simultaneous implementation of both growth mechanisms allows one to exercise a level of control over the final branched nanowire by controlling independent reaction parameters such as gas phase precursor concentrations, VLS catalyst loading, and VLS catalyst diameter. Additionally, the use of a peapodded structure as a foundation for synthesizing these branched structures not only allows for the unique, single step growth of highly branched structures, but the study of these branched wires also provides insights into the growth process of peapod structures not previously reported. Transmission electron microscopy (TEM), scanning electron microscopy (SEM), and elemental analysis are used to explain the branched nanowire growth.

2.3 Experimental

2.3.1 CVD apparatus

A schematic of the reactor setup used can be found in Figure 2.1. The synthesis of nanowires was carried out in a single zone, 30.5 cm horizontal tube furnace (Lindberg/Blue) in a 2.54 cm diameter (OD) quartz tube. The inner surface of the quartz tube was carbon coated through the thermal decomposition of methane at 1100 °C and 700 torr (15 sccm CH_4 and 100 sccm Ar).

Furnace temperature was measured via thermocouple and controlled through a LabView program interface. Pressure was monitored by thermocouple gauge (Kurt J. Lesker), and regulated by solenoid valve and driver (MKS Instruments) and mechanical rotary vacuum pump (Ulvac). UHP Argon and Hydrogen (Airgas) were used as carrier gases and were deoxygenated by passing the gas stream through columns containing BASF Puristar® Catalyst. Carrier gas flow rates were monitored and controlled by SmartTrak® mass flow controllers (Sierra Instruments).

2.3.2 Growth of branched silica nanowires

The reaction conditions described herein have been determined to give a high degree of branched product with relatively uniform structure and dispersion on the substrate surface. These are the conditions most often used for the data collected and presented. Many modifications to this procedure have been investigated which can affect the properties of the final products, and some of those modifications will be outlined at the end of the discussion and electronic supplementary information. The growth substrates were Si (100) n-type wafers (1-10 ohms-cm, Silicon Inc.) which were cut into strips (approximately 0.75 cm x 5 cm), cleaned by sonication (2 x 10 min. ethanol absolute, 2 x 10 min. Millipore water), and dried with N_2 blow. Two general synthetic procedures were followed, providing greater control over nanowire product morphologies observed and leading to a clearer understanding of the formation processes involved in the production of these complex structures.

Au-nanoparticle-initiated growth: Following Si substrate cleaning, poly-L-lysine (0.1% aqueous, Ted Pella) was applied for 2 min and then thoroughly removed with Millipore® water and dried with N_2 blow. A 30 nm Au colloid solution (Ted Pella) was then applied for 5 min and gently removed with Millipore® water and dried with a low flow of N_2 to ensure a high density of Au particles weakly bound to the poly-L-lysine treated Si surface.

Vapor-deposited Cu initiated growth: The native oxide layer of the substrate was removed using an HF bath (48%, 45 s), resulting in a hydrophobic Si-H surface layer. Following the HF bath, the substrate was quickly placed in a freshly prepared KOH bath for 15 seconds (4.5 M KOH in 4:1 H2O:IPA by weight) in order to remove the surface H, yielding a polar Si-OH surface. The substrate was thoroughly rinsed with Millipore® water upon removal from the KOH bath to prevent excessive etching, and dried with N_2 blow.

Reactor setup and conditions: To synthesize the nanowire products, a treated Si (100) substrate was placed on a C-coated quartz boat and inserted into the reaction tube with the leading edge 10 – 11 cm downstream from the thermocouple. Crushed Si precursor (10.0 mg) was placed in a boat 9 cm downstream of the thermocouple, and a mixture of CuO powder and powdered graphite (1:1 by weight, 3.0 mg) was placed in a boat at the thermocouple. The crushed Si was stored in ambient conditions, so the surface oxide could act as a SiO_x precursor. The CuO/C was used as similar metal oxide/carbon mixtures have been used in other high temperature CVD reactions for delivering metal atoms in the gas phase, as the metal oxide is reduced by the carbon releasing CO_2 and M(g). After three pump-purge cycles (<0.5 torr to 100 torr with 100 sccm Ar), the system was pressurized to 50 torr and the pressure was maintained by flowing UHP Ar (100 sccm). *Au-nanoparticle-initiated growth:* At the onset of the reaction, the carrier gas was switched to a Ar:H_2 mixture (70 sccm and 30 sccm respectively), and the furnace temperature was ramped to 1050 °C in 35 min. These conditions were held for 4 hrs.

Vapor-deposited Cu initiated growth: The growth conditions were analogous to the Au-catalyzed growth, but there was an initial Cu deposition step in which the carrier gas is only Ar (100 sccm) for both the 35 min ramp to 1050 °C and for 20 min at temperature to allow deposition of Cu catalyst. The carrier gas was then switched to the mixture of Ar and H_2, as H_2 promotes SiO_x

transport. These conditions were again held for 4 hrs. For both reactions, following the growth period, the furnace was turned off and the closed system was allowed to cool to room temperature under flowing Ar (400 sccm) and a system pressure of ~50 torr.

2.3.3 Characterization

Au-nanoparticle-catalyzed nanowire samples: Transmission electron microscopy (TEM) images were obtained using a JEOL JEM-2000 transmission electron microscope operating under an accelerating voltage of 160 kV. STEM images were obtained using a Hitachi HF-3300 FEG-TEM/STEM (ORNL SHaRE facility) operating at 300kV, and a VG Microscopes HB501 UX STEM with Nion aberration corrector, operating at 100kV. High spatial resolution energy-dispersive X-ray spectroscopy (EDS) data was collected on the Hitachi HF-3300 FEGTEM/STEM operated in bright field scanning mode, and electron energy loss spectroscopy (EELS) mapping was performed on the VG Microscopes HB501 UX STEM. The TEM samples were created by gently sonicating the nanowires from the growth substrate into 2-propanol (Sigma Aldrich, 99.5% anhydrous) and adding the solution, drop wise, to a copper or nickel TEM grid with a lacey carbon coating.

Vapor-deposited Cu nanowire samples: Low-resolution transmission electron microscope (TEM) analysis was carried out on a JEOL JEM 1400 instrument operated at an accelerating voltage of 100 kV. High-resolution TEM images were obtained with a JEOL JEM 2100F TEM operated at an accelerating voltage of 200 kV, and elemental mapping was collected with an Oxford Instruments energy dispersive spectroscopy (EDS) detector. For TEM imaging, wires were transferred from the growth substrate to carbon-coated Cu grids (Ted Pella, 200 mesh). Wires were transferred by freezing a droplet of $CHCl_3$ on the surface of the sample using a liquid N_2 bath and then removing the frozen solvent chip and allowing it to melt and evaporate on the TEM grid, leaving behind

wires initially trapped in the frozen $CHCl_3$. This method was chosen as it maintains the structure of the branched wires far better compared to traditional wire-transfer methods.

All samples: Scanning electron microscopy (SEM) images and EDS mapping and spectra were collected using a JEOL JSM-6500F field emission scanning electron microscope (FE-SEM) equipped with an EDAX Genesis EDS detector with an applied voltage of 15 kV.

2.4 Results and Discussion

2.4.1 General description of observed growth products along growth substrate

The growth of the silica nanowire trunk is initiated through the deposition of either gold nanoparticles or copper onto a silicon wafer, followed by a metal-catalyzed vapor-liquid-solid (VLS) nanowire growth mechanism. Following initial VLS growth, both Cu and Si are present in the gas-phase, resulting in a highly dynamic growth process. Nanowire products formed through this procedure display a wide variety of product morphologies as seen in Figure 2.2A, but through careful manipulation of the reaction conditions, predominantly branched nanowire products occur on the upstream edge of wire growth. Given the thermal gradient present in the reactor at the growth location, a gradient of products are deposited along the substrate surface. Figure 2.2B contains a photograph showing the gradient of nanowire species present on the substrate post Cu-vapor-initiated reaction, along with a graphic depiction more clearly highlighting the different regions present.

At the upstream region of the substrate (region i in Figure 2.2B) high temperature and the presence of Cu and/or Au cause etching of the surface and large Cu_3Si deposits to form. On the downstream end of this region, patchy growth of wires can occur from these large deposits, often through a combination of root and float growth as seen in Figure 2.S1. Regions ii and iii in Figure 2.2B are where primarily branched wire growth occurs, and a mixture of branched and unbranched

wire products are seen, respectively. Regions ii and iii are highlighted with a red box as all images and data presented when discussing the process of forming highly branched structures were collected from these regions. The SEM image in Figure 2.2A is an example showing the variety of products observed in region iii. Further downstream, region iv contains highly dense wire growth. Across this region, branched products are observed, but only as a minority species. Other nanowires in this region display a wide variety of morphologies consistent with previous reports of metal-catalyzed SiO_2 wire growth.[10, 28-29] Representative SEM images from the various regions, collected from the sample shown in Figure 2.2B, can be found in Figure 2.S2 A-G.

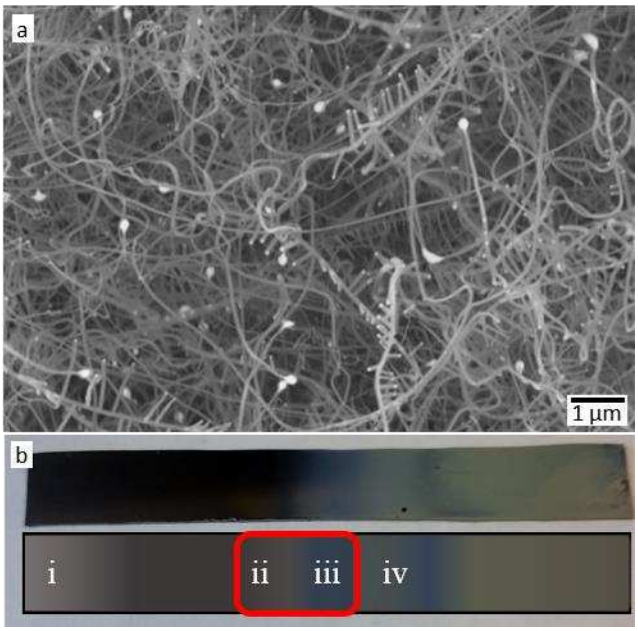

Figure 2.2. A) SEM image depicting a range of SiO_2 nanowire products grown through the thermal evaporation of Cu and SiOx precursors. B) Photograph of Si substrate partially coated with SiO_2 nanowire products along with a graphic highlighting regions along the substrate that display characteristic product morphologies. The branched nanowire morphologies of interest are primarily contained in regions ii and

2.4.2 Characterization of products synthesized using Au nanoparticle initiated growth

Figure 2.3a contains characteristic SEM images of the branched nanowire growth illustrating that the backbone can grow to lengths on the order of 100 µm. In addition to the length, the image contained in Figure 2.3a also shows the presence of a catalyst tip in white on the left of the image with a diameter larger than that of the nanowire; a characteristic feature of VLS growth.[10] Figures 2.3b and 2.3c are higher magnification images that demonstrate the relatively uniform branch nanowire diameter, which is controlled by the VSS catalyst, and spacing between the

branches. The images also clearly show the characteristic VSS catalyst tip at the end of the branches, as the catalyst diameter is consistent with that of the wire.[10, 30] To highlight the uniformity of the branching structure, an ADF STEM image illustrating a consistent VSS catalyst particle diameter of approximately 60 nm and a particle spacing of approximately 150 nm is contained in Supplemental Figure 2.S3. Through increasing reaction times and/or decreasing amount of solid Cu precursor, gas phase Cu can be depleted during a reaction, causing the deposition of Cu to cease. This prevents additional CuSi from being deposited along the backbone wire, but does not prevent continued growth of the wire, given sufficient SiO_x precursor. This is demonstrated by the TEM image in Figure 2.3d, which shows a gap of approximately 2 μm between the catalyst tip of the backbone nanowire and the closest VSS catalyst nanoparticle. Another feature to note from the images contained in Figure 2.3 is that the growth rate of the branches is much slower than that of the backbone nanowire; again indicating that the backbone growth is VLS catalyzed while the branch growth is VSS catalyzed in this case.

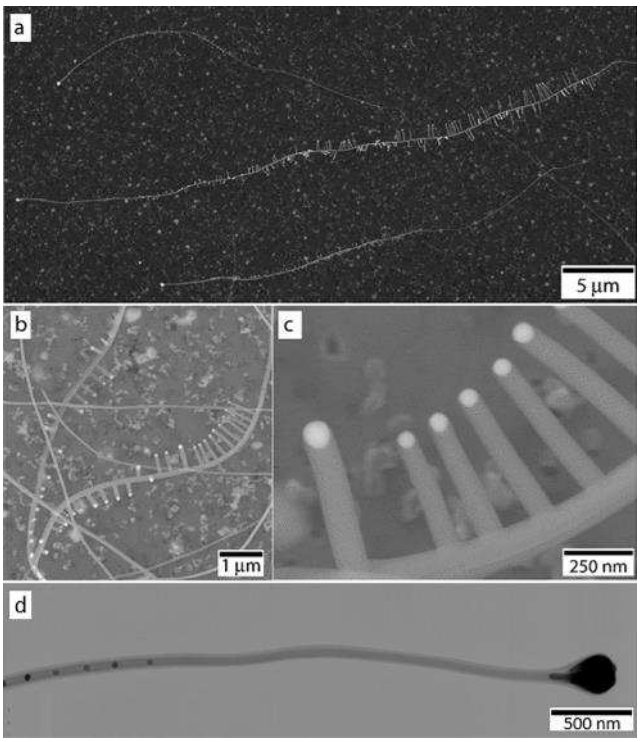

Figure 2.3. (a-c) Characteristic low and high magnification SEM images of the branched nanowires. (a) Demonstrates the high aspect ratio of the backbone nanowire and the low aspect ratio of the branched nanowires, suggesting different growth rates and thus different growth mechanisms. The characteristic catalyst tips for both the backbone and branches can be seen. (b) Illustrates the finger-like morphology of the branches, the consistent VSS catalyst diameter, and relatively consistent spacing between the branches. (c) The image shows that the branched wire diameters are consistent with the catalyst tip, which is indicative of VSS growth. (d) TEM image illustrating the ability to control secondary catalyst deposition through limiting gas phase Cu precursor.

A combination of EELS and EDS was used to determine the spatial location and relative atomic amounts of Au, Cu, and Si within the branched nanowire structure. Figure 2.4 contains EDS elemental mapping with the corresponding bright field STEM image of a branched nanowire grown using the Au-NP initiated reaction process. As illustrated in Figure 2.4 panels (a) through (e), the VLS catalyst tip at the end of the backbone contains a combination of Au and Cu with Si and O being confined to the perimeter. An EDS signal was not collected from the catalyst center due to beam attenuation. However, it is expected that Au is concentrated in the center of the catalyst with a smaller amount of Cu and an equilibrium concentration of Si. This is consistent with the additional EDS and EELS analyses contained in Figure 2.S4. Figure 2.S4 contains a characteristic SEM image of the catalyst tip, Cu/Si-rich EDS spatial phase map, and Au-rich EDS spatial phase map in panels a through c, respectively. This data demonstrates the presence of all three elements and a concentration of Au in the center of the VLS catalyst. In addition, EELS spatial elemental maps contained in Figure 2.S4, panels (d) through (g), provide high spatial resolution within the VLS tip for Cu, Si, and O. The enhanced spatial resolution illustrates the presence

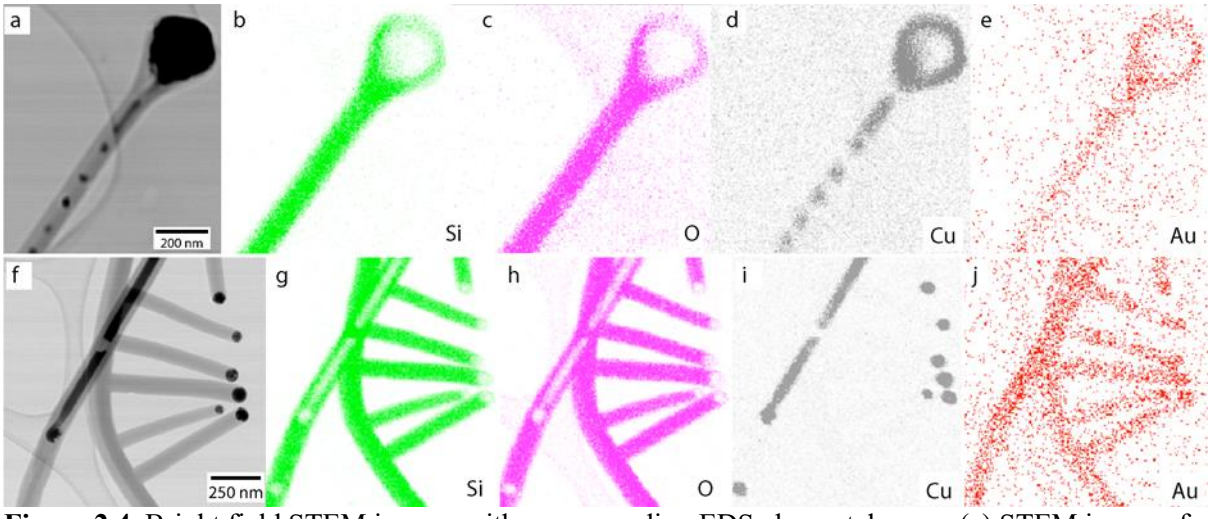

Figure 2.4. Bright field STEM images with corresponding EDS elemental maps. (a) STEM image of the backbone catalyst and wire with VSS catalyst particles as well as the corresponding spatial maps of (b) silicon, (c) oxygen, (d) copper, and (e) gold. (f) STEM image of the backbone with a VSS catalyst particle forming, as well as branches with VSS catalyst tips. Corresponding spatial elemental maps are shown for (g) silicon, (h) oxygen, (i) copper, and (j) gold.

of high concentrations of Cu and Si along the periphery of the VLS catalyst and in the portion that protrudes into the backbone.

To further characterize the nanowire products and better understand the growth process, EELS analysis was performed on the primary wire, branched wire, and secondary wire catalyst. Data collected from this analysis is presented in Figure 2.S5. With respect to the nanowire backbone, EELS analysis suggests that Si is in the 4+ oxidation state and that the relative atomic ratio of Si:O is 1:2. While the wires are expected to grow as a sub-stoichiometric SiO_x,[9, 24, 26, 29] the fully oxidized SiO_2 is observed due to the fact that Au, Cu, and Cu_3Si have all been shown to catalyze the room temperature oxidation of Si.[31-32] Additionally, this can be used to explain the complete oxidation of the branches to SiO_2. Like the backbone nanowire, the oxidation of the branches is based on data from the characteristic Si^{4+} EELS edge in these regions.

As shown in Figures 2.4e and j, there is an observable presence of Au throughout the branched structure and dopant level equilibrium concentrations of Cu and Cu_3Si. While the wires have undergone post-synthesis oxidation, the VSS catalyst particles are observed to be crystalline Cu_3Si. With respect to the VSS catalyst particles, Figure 2.4i shows that Cu is mostly confined to the internal VSS catalyst feed stream in the backbone and at the end of the branches in the secondary catalysts. To confirm that the Cu species detected by EDS is Cu_3Si EELS elemental maps were used to provide high spatial resolution of the VSS catalyst particle for Cu, Si, and O. Figure 2.S6a contains a STEM image of the VSS catalyst with corresponding spatial information for Cu, Si, and O contained in panels (b) through (d), respectively. It is clear that Cu is confined to the catalyst, O is not detected within the catalyst, and Si is observed throughout the branch. Additionally, unlike the Si^{4+} EELS edge observed in the backbone, the Si edge within the particle is characteristic of

SiO, suggesting that the VSS catalyst is Cu_3Si. The ratio of Cu:Si has also been determined by EELS to be approximately 3:1; further confirming the presence of Cu_3Si.

2.4.3 Characterization of vapor-deposited-Cu-initiated growth

The Cu vapor deposition method was developed to minimize the pre-synthetic processing, eliminate the cost of Au nanoparticles, and prevent Au doping in the wire structure. Additionally, using a Cu catalyst allows for a higher degree of branching due to higher concentration of Cu in the backbone catalyst. While the relative concentration of branched to unbranched species is observed to increase, the general structure of the nanowire products and growth process are consistent between the two methods. Using STEM along with EDS, the Cu-catalyzed structures were analyzed, again showing the backbone wires and branches to be SiO_2 with Cu as a dopant, as seen in Figure 2.5. Both the primary and secondary catalysts contain Cu and Si, and electron diffraction characterization further confirms the presence of crystalline Cu_3Si.

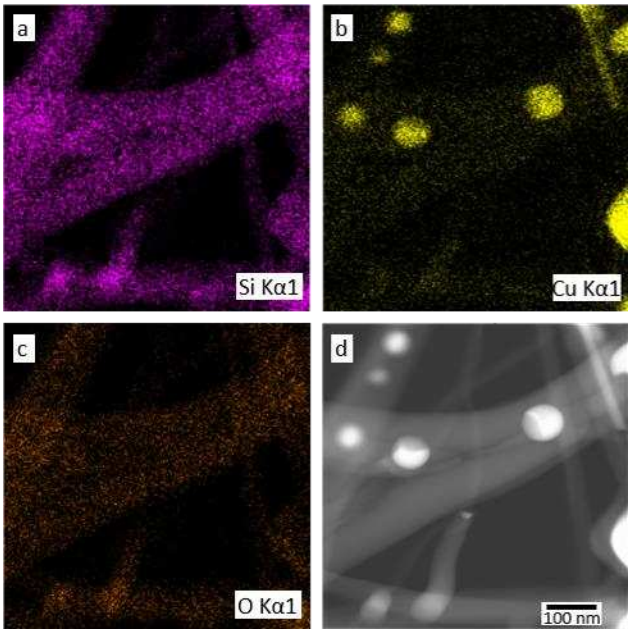

Figure 2.5. STEM EDS maps of (a) Si, (b) Cu, and (c) O. (d) ADF STEM image of nanowires and catalysts. The wire is SiO_2 with consistent Cu doping throughout. The catalyst droplets are composed of Cu and Si. A decrease in O concentration at catalyst sites indicates the lack of O present in the Cu_3Si products.

All branched nanowire products demonstrate consistent properties of amorphous SiO_2 backbone and branch wires, doped with Au and/or Cu. The presence of a Cu_3Si catalyst tip is observed for both the VLS and VSS grown wires, with the VLS backbone wire growing faster

than the VSS branched wires. While these general compositional and morphological components of the branched nanowire products are well characterized and consistent for every species analyzed, further investigation of the morphologies allows inferences to be made regarding various steps involved in the growth process of these unique structures.

2.4.4 Proposed steps involved in the process of forming highly branched silica nanowires

When considering the growth process of nanowire products that display branching, multiple structural differences are observed compared to the non-branching products. This suggests that while the synthetic procedure for these wires is straightforward, the growth mechanism that results in the branched nanowire structures is highly complex. While not comprehensively describing the mechanism, a series of discreet steps believed to be necessary to the growth mechanism of the branched species are outlined below in Figure 2.6.

Nanowire growth is initiated through a metal-catalyzed VLS growth mechanism as depicted in Figure 2.6A. A number of previous studies have investigated the VLS-catalyzed growth of silica nanowires using a variety of catalysts, and our observations are consistent with these studies.[7, 33-35] While some structures observed on the onset of wire growth demonstrate root growth (see Figure 2.S1), the vast majority of nanowire products appear to grow through the more common float growth. As wire growth continues, both the Cu and SiO_x species in the gas phase dissolve into the catalyst, as is evidenced by the diameter of the wire increasing toward the catalyst as depicted in Figure 2.6A(iii). This is unique due to our method of *in situ* catalyst loading, compared to other systems employing high temperature metal-catalyzed VLS growth, wire tapering is often seen due to catalyst evaporation and inclusion into the wire.[10, 36]

Continued growth leads to the formation of a "multi-wire" structure as illustrated in Figure 2.6B. The multi-wire structures as described here have not been extensively discussed or characterized elsewhere in literature to the best of our knowledge. While not previously described, similar structural architectures are likely present in other reported systems, in particular reports in which Au "nanopeapodding" in silica is observed.[6, 20-21, 36-38] The multi-wire structure consists of (typically) either two or three silica nanowires growing in parallel from a single catalyst, which allows CuSi to be co-deposited along the interface(s) between these wires. For this component of the discussion, CuSi is used because compositional information is not able to be collected *in situ* and is likely non-stoichiometric under the growth conditions present in this reaction. This process is exaggerated in Figure 2.6B for clarity of concept. The thin CuSi deposit catalyzes the deposition of SiO_x, leading to the fusing of the backbone wires and the formation of CuSi droplets along the wire interface surface. The resulting structures resemble nanopeapodded structures, as illustrated in Figure 2.6C. This is the first example of Cu-peapodded SiO_2 nanostructures formed through CVD processes to the best of our knowledge, as most all previous reports use Au. Of these previous reports, studies focusing on the formation of the peapodded structures either describe the wire as

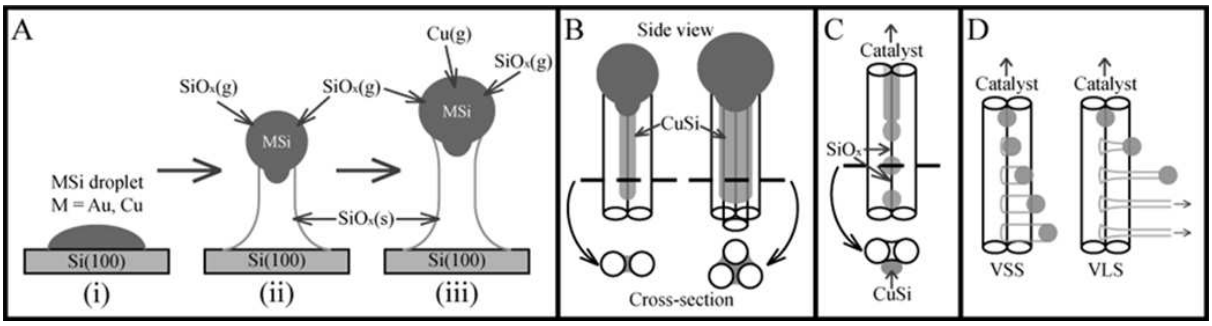

Figure 2.6. Depiction of proposed necessary steps for the branched nanowire growth hypothesis. A) (i) A metal (Au or Cu) silicide droplet forms on the substrate surface upon heating. (ii) As SiO_x is deposited from the gas phase, nanowire growth occurs through the float-growth VLS mechanism with the characteristic sloped base. (iii) Rather than reaching a steady diameter or tapering toward the catalyst, the wire diameter is seen to increase due to deposition of both Cu and SiO_x in the catalyst. B) Depiction of the multi-wire backbone structure consisting of either 2 or 3 wires growing in parallel, along with the co-deposited catalyst. C) Graphic showing the catalyzed deposition of SiO_x along the wire interface, and the formation of secondary catalysts along the wire interface. D) Representation of secondary wires growing from the trunk wire through either a VSS or VLS growth mechanism.

initially forming as a core-shell structure, followed by the separation of catalyst into droplets due to Rayleigh instability, or forming through a diffusion-limited process.[19, 36, 39-40] While this may be the correct process for some of these previous reports due to different experimental conditions, several reports display evidence consistent with the multi-wire hypothesis. In order to fully understand why the observed structures are forming, it is important to consider what is occurring chemically throughout the steps defined above based on our reaction design, which further helps to rationalize the oxidized product and support the synthetic hypothesis proposed.

2.4.5 Proposed chemical reactions relating to the nanowire growth process

The Cu precursor consisted of copper (I) oxide powder and graphitic carbon, but was kept in ambient environment resulting in a copper (II) oxide coating which could be observed by the change in color of the precursor and was confirmed through XPS. These copper oxide precursors can undergo carbothermal reduction in the presence of graphitic, which is a well-established procedure in literature at comparable and lower temperatures, as well as can be reduced by H_2. It is therefore important to identify what major reactions are believed to be contributing to the overall reaction. The first reactions are that of the carbothermal reduction of Cu_2O and CuO, some of which are shown in Reactions 2.1 – 2.4. These reactions are balanced with CO_2 as a product, but CO could also be a viable product formed, but those reactions are not included here due to redundancy. Reaction 2.3 shows the reduction of Cu^{2+} to Cu^{+}, with the other reactions showing metallic Cu being formed. While the $Cu_{(g)}$ precursors are being shown here are listed as individual atoms, it is likely they are forming some combination of vapor phase atoms and atomic clusters which would be consistent with other literature.

$$Cu_2O_{(s)} + C_{graphitic} \xrightarrow{\Delta} Cu_{(g)} + CO_{2(g)} \qquad \text{Reaction 2.1}$$

$$2Cu_2O_{(s)} + C_{graphitic} \xrightarrow{\Delta} 4Cu_{(g)} + CO_{2(g)} \qquad \text{Reaction 2.2}$$

$$4CuO_{(s)} + C_{graphitic} \xrightarrow{\Delta} 2Cu_2O_{(s)} + CO_{2(g)} \quad \text{Reaction 2.3}$$

$$2CuO_{(s)} + C_{graphitic} \xrightarrow{\Delta} 2Cu_{(g)} + CO_{2(g)} \quad \text{Reaction 2.4}$$

Reactions 2.1 – 2.4 show the gaseous oxide products being the inert CO and CO_2, there is also the possibility for Cu_xO to thermally decompose on its own as shown in Reactions 2.5 and 2.6, producing O_2 gas, which could contribute to the in-situ oxidation of the wire products.

$$2CuO_{(s)} \xrightarrow{\Delta} Cu_2O_{(s)} + \frac{1}{2}O_{2(g)} \quad \text{Reaction 2.5}$$

$$2Cu_2O_{(s)} + \xrightarrow{\Delta} 4Cu_{(g)} + O_{2(g)} \quad \text{Reaction 2.6}$$

When O_2 and CO are produced as a result of the above reactions, they can further react to form the stable CO_2 before being transported away as shown in Reactions 2.7 and 2.8, but these may be less likely to happen given the volatility of the initial products and the reaction conditions having a small physical location of the solid precursors under flowing gas.

$$C_{graphitic} + O_{2(g)} \xrightarrow{\Delta} CO_{2(g)} \quad \text{Reaction 2.7}$$

$$Cu_2O_{(s)} + CO_{(g)} \xrightarrow{\Delta} Cu_{(g)} + CO_{2(g)} \quad \text{Reaction 2.8}$$

Additionally the H_2 gas can react with the Cu_xO precursors in a variety of ways, only two of which are shown below in Reactions 2.9 and 2.10, but the notable product of such reactions is $H_2O_{(g)}$, which would likely go on to react with and oxidize potential Si products.

$$2CuO_{(s)} + H_{2(g)} \xrightarrow{\Delta} 2Cu_2O_{(g)} + H_2O_{(g)} \quad \text{Reaction 2.9}$$

$$Cu_2O_{(s)} + H_{2(g)} \xrightarrow{\Delta} Cu_{(g)} + H_2O_{(g)} \quad \text{Reaction 2.10}$$

The solid silicon precursor was kept close to the deposition substrate, and therefore only assumed to be evaporating and re-depositing over a short distance, simply through thermal decomposition or reaction with H_2 as shown in Reactions 2.11 and 2.12, but considering that the crushed

Si was kept in ambient condition, there is an appreciable oxide on the surface, which can lead to a variety of other gaseous products.

$$Si_{(s)} \xrightarrow{\Delta} Si_{(g)} \qquad \text{Reaction 2.11}$$

$$Si_{(s)} + 2H_{2(g)} \xrightarrow{\Delta} SiH_{4(g)} \qquad \text{Reaction 2.12}$$

Given that the intrinsic oxide layer on Si will consist of SiO_2 on the surface, Si in the core, and some gradient of suboxide SiO_x between the two, these species and the interactions between them must be considered. For balancing reactions SiO will be used for representing sub-oxide stoichiometries, but SiO_x would also be chemically relevant and will be used for certain sub-oxide species, such as clusters that can be released into the gas phase. For this oxide surface, first there is the potential reaction with H_2 as shown in Reactions 2.13 – 2.15, again notably making $H_2O_{(g)}$. In reaction 2.14 SiO is listed as either a solid or gas, because SiO does have a much higher vapor pressure than SiO_2 and could be an appreciable product given the reaction conditions. Therefore, the thermal evaporation of SiO shown in Reaction 2.16 is also an important consideration for the vapor phase products containing silicon, because it suggests that not only could the products be being oxidized *in situ* by the O_2 and H_2O being produced, but the products are likely also growing as some form of oxidized silica nanowire. While not perfect parallels to our reaction conditions, literate analysis of SiO evaporation suggests that the volatile species are some form of sub-oxide clusters, which is why reaction 2.16 is written as it is, but no specific compositions are proposed for this system, with the key feature being the production of a gas phase SiO_x species and additional O_2, which contribute to the growth of the silica nanowire products.

$$SiO_{2(s)} + 2H_{2(g)} \xrightarrow{\Delta} Si_{(g)} + 2H_2O_{(g)} \qquad \text{Reaction 2.13}$$

$$SiO_{2(s)} + H_{2(g)} \xrightarrow{\Delta} SiO_{(s\ or\ g)} + H_2O_{(g)} \qquad \text{Reaction 2.14}$$

$$SiO_{(s)} + H_{2(g)} \overset{\Delta}{\rightarrow} Si_{(g)} + H_2O_{(g)} \qquad \text{Reaction 2.15}$$

While not perfect parallels to our reaction conditions, literate analysis of SiO evaporation suggests that the volatile species are some form of sub-oxide clusters, which is why reaction 2.16 is written as it is, but no specific compositions are proposed for this system, with the key feature being the production of a gas phase SiO_x species and additional O_2, which contribute to the growth of the silica nanowire products.

$$ySiO_{(s)} \overset{\Delta}{\rightarrow} ySiO_{x(g)} + zO_{2(g)} \qquad \text{where z = ½ (y-x)} \qquad \text{Reaction 2.16}$$

Additionally, sub-oxide Si is known to undergo dissociation type reactions such as the one shown in Reaction 2.17, which the SiO_2 product can be reduced as shown in Reaction 2.14, producing the $SiO_{(s)}$ precursor once again and propagating the etching and evaporation of Si products.

$$2SiO_{(s)} \overset{\Delta}{\rightarrow} SiO_{2(s)} + Si_{(g)} \qquad \text{Reaction 2.17}$$

In order to initiate the growth of the nanowires through the VLS mechanism, both the Cu and Si vapor phase precursors can react with each other as they reach the lower temperature growth regime (approximately 850° C - 950° C) as shown in Reactions 2.18 and 2.19, as well as the Cu precursor can react with substrate during the temperature ramp and catalyst formation component of the reaction as shown in Reaction 2.20. No specific stoichiometry is given as explained in Chapter 1 do to the presence of a continuous liquid composition. These reactions correspond to the growth process step A(i) represented in Figure 2.6.

$$xCu_{(g)} + Si_{(g)} \overset{\Delta}{\rightarrow} Cu_xSi_{(l)} \qquad \text{Reaction 2.18}$$

$$xCu_{(g)} + SiH_{4(g)} \overset{\Delta}{\rightarrow} Cu_xSi_{(l)} + 2H_{2(g)} \qquad \text{Reaction 2.19}$$

$$xCu_{(g)} + Si_{(s)substrate} \overset{\Delta}{\rightarrow} Cu_xSi_{(l)} \qquad \text{Reaction 2.20}$$

As the $Cu_xSi_{(l)}$ droplet continues to catalyze the deposition of $Si_{(g)}$ out of the gas phase, the solubility limit of Si in the catalyst droplet is reached, resulting in the deposition of solid Si at the catalyst head/substrate or catalyst head/nanowire interface (Reaction 2.21), resulting in the upward growth of the product as represented in figure 2.6 A(ii).

$$Cu_xSi_{(l)} + ySi_{(g)} \xrightarrow{\Delta} Cu_xSi_{(l)} + ySi_{(s)solid\ nanowire} \qquad \text{Reaction 2.21}$$

The $Cu_{(g)}$ precursor, as well as the $Cu_xSi_{(l)}$ catalyst, can also react with the vapor phase SiO(g), resulting in different products based on the exact point in the growth procedure, with two general example reactions shown in Reaction 2.22 and 2.23. Generally the result is the continued growth of the silicon/silica product while maintaining the $Cu_xSi_{(l)}$ catalyst, consistent with Figure 2.6. resulting in the deposition of $SiO_{2(s)}$ and Si(s). Through these processes as Si continues to deposit out of the gas phase as it reacts with the liquid catalyst, the solubility limit of Si in the catalyst droplet is reached, resulting in the deposition of solid Si at the catalyst head/substrate or catalyst head/nanowire interface, resulting in the upward growth of the product (Reaction 1.7)

$$Cu_xSi_{(l)} + 2ySiO_{(g)} \xrightarrow{\Delta} Cu_xSi_{(l)} + ySi_{(s)core} + ySiO_{2(s)shell} \qquad \text{Reaction 2.22}$$

$$Cu_{(g)} + 2xSiO_{(g)} \xrightarrow{\Delta} Cu_xSi_{(l)} + xSiO_{2(s)fully\ oxidized\ product} \qquad \text{Reaction 2.23}$$

The catalyst is assumed to be Cu_xSi because the catalyst heads, which crystallize post-synthesis upon coolins, have been shown to be Cu_3Si using x-ray and e-beam diffraction and in the EELS analysis previous discussed. If the catalyst heads were oxidized, then the final cooled product should be an oxide product, as there are several stable copper silicates, and no precedence for a copper silicate to form Cu_3Si upon cooling or solidification. Additionally, the growth profile of the wires and temperature regime of reaction align well with well-established literature on the VLS growth of nanowire products. This is also why the SiO_x precursors are assumed to dissociate into an oxide shell with a crystalline core, or potentially react with the catalyst head, diffusing along

the surface, in order to be precipitated out at the interface, as the oxidized species have very limited solubility in the silicide catalyst.

Growth then continues through reactions 2.21 – 2.23, and the catalyst head swells as Cu is also being added from the gas phase as shown generally in Reaction 2.24, which is consistent with Figure 2.6 A(iii).

$$Cu_xSi_{(l)} + \ x\ Cu_{(g)} + Si_{(g)} \xrightarrow{\Delta} 2Cu_xSi_{(l)} - product\ swelling \qquad \text{Reaction 2.24}$$

This swelling combined with reaction 2.21 – 2.23 are one facet of what can lead to the nucleation of additional wires, and the formation of the multi-wire interface as shown in Figure 2.6 B. Once the multi-wire interface is formed, a combination of Reactions 2.21 – 2.24 lead to the deposition of both the multi-wire backbone and the secondary catalyst, which precipitates out along the inter-stitial space between the multi-wires minimizing surface energy interactions between the catalyst and growing wires.

As the wires continue to grow, depending on the dominant precursor and growth reaction, the nanowire species can either be formed as a combination of oxidized an unoxidized silicon, or as oxidized silicon if the surface level precipitation and diffusion mechanism is dominant. If the products are grown as a combination of silicon and silica, the oxygen can difuse rapidly given the size of the structure, the temperature, and the presence of Cu, which is known to catalyze oxidation. Furthermore, even if crystalline Si is being precipitated out at the catalyst interface, O_2 and H_2O, which are in our system as established by Reactions 2.5, 2.6, 2.9, 2.10 and 2.13 – 2.16 can rapidly oxidize any remaining unoxidized Si as shown in the generalized Reaction 2.25.

$$Si_{(s)} \underset{or}{\overset{and}{}} SiO_{(s)} \ + H_2O_{(g)} + O_{2(g)} \xrightarrow{\Delta} SiO_{2(s)} + H_{2(g)} \qquad \text{Reaction 2.25}$$

There are several observations which support a multi-wire process rather than a core-shell process for the branched nanowire products studied in this system. The first observation is the presence of branching in general. If this was a core-shell structure, there would be little driving force for the bulky nanoparticle of CuSi to diffuse through the SiO_2 shell to the surface in order to catalyze the growth of branches. Second is the ordering of the branches along the surface, such as the three-fold branching which is consistently observed, as seen in Figure 2.7A,B. If the CuSi was diffusing through an amorphous SiO_x shell, then the regular observation of highly ordered branching would be unlikely. Additional images such as those seen in Figure 2.7B show the dip seen along the surface, sometimes previously explained through the wire collapsing due to the vacancy remaining after the Au droplets form, but is better explained through the multi-wire hypothesis.

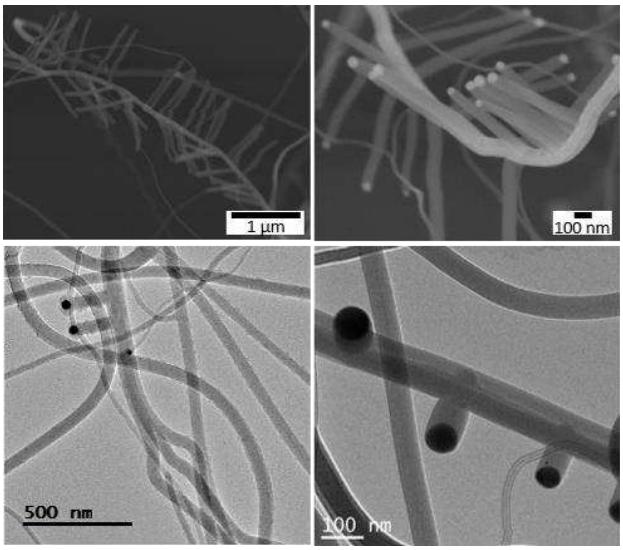

Figure 2.7. Evidence supporting the multi-wire hypothesis. A) SEM image showing the three-fold branching often observed. B) SEM image also showing three-fold branching, as well as "dip" observed on surface between branches and most clearly on the right side of the image. C) TEM image showing 3 independent wires aligning, with branching occurring in the multi-wire region. D) TEM image showing the contrast differences observed due to overlapping wires.

The most compelling evidence comes from TEM in which multiple contrast differences are observed, as seen in Figure 2.7C,D. Elemental analysis and diffraction done in the TEM show the structure to be completely amorphous SiO_2, so the contrast differences are not a result of a core-shell structure or different crystallographic orientations, but instead is simply a result of multiple overlapping wires. Lastly, as seen in Figure 2.7D, it is observed that often prior to regions

that display the features of CuSi co-deposition, peapodding, or branching, a “split” is observed. Figure 2.7C shows where three wires growing from a single catalyst have come together, aligned, and shortly thereafter, branching is present.

Additional discussion and support for the multi-wire hypothesis can be found in the supplemental data, along with a discussion of two potential processes for initially forming the multi-wire structure in the section *Formation of Si multi-wires through two separate processes* and accompanying figures 2.S7 – 2.S10.

Following the formation of the CuSi droplets on the surface of the trunk multi-wire, they can then act as secondary catalysts resulting in the branched wire structures as illustrated in Figure 2.6D and seen in Figure 2.7. Typically the branches appear to grow through a VSS-catalyzed growth mechanism, showing consistent growth diameter from catalyst to base, and relatively slow growth compared to the faster VLS process responsible for the trunk wire. Branches can grow through the VLS mechanism as well, displaying much narrower diameters, a tapered base, and rapid growth compared to branches growing through the VSS mechanism, but VLS branches are the minority species.

2.4.5 Manipulating growth conditions and synthetic control over products

Identifying individual processes that occur throughout the growth mechanism has allowed reaction conditions to be systematically modified in order to exert a degree of control over the resulting growth. For example, the initial wire growth step, illustrated in Figure 2.6A, can be manipulated by using the different catalyst deposition procedures of either Au nanoparticles or Cu from the gas phase, as discussed above in the experimental section. This allows for control over the density and dispersion of nanowire products on the substrate surface. In addition to altering the catalyst deposition procedure, a number of reaction conditions were modified, and the effects were

monitored through comparing the resulting product morphologies using electron microscopy. These tests were done multiple times to ensure that any observed synthetic control was reproducible and consistent with the growth hypothesis previously described. The experimentally tested variables with reproducible results are listed in Table S1 of the electronic supplementary information. The results described are qualitative observation made by researchers when comparing products of analogous reactions with only the variable in question being altered.

The control available using the system of *in situ* Cu loading is valuable as it further supports the wire growth hypothesis outlined previously, as well as benefits the ability to rationally design products for future incorporation of such materials into nanowire devices. The various observations relating to the presence of Cu and SiO_x species in the gas phase illustrate the balance required between wire growth rate and catalyst deposition rate for the formation of these structures. This is consistent with the growth hypothesis described as these rates impact the formation of the multiwire backbone and subsequent co-deposition of secondary catalyst.

As such, the reaction conditions outlined in the experimental section have been determined to consistently and reproducibly result in the formation of a high degree of branched nanowire species, which display high aspect ratios and significant branching. A control reaction was conducted using Au nanoparticle catalysts and no Cu precursor which demonstrated that our system can grow nanowire products consistent with literature reports of high temperature annealing growth of silica nanowires that do not include the branched nanowire products observed when the Cu precursor is present. One control experiment not included in Table S1 incorporates low concentrations of C_2H_2 throughout the reaction. When C_2H_2 is present in the gas phase no silica nanowire growth is observed due to C_2H_2 acting as an oxygen getter. The SiO_x precursors and volatile species are quickly reduced to Si in the presence of C_2H_2 and high temperatures, and CO_2 flows

out of the system without further reacting. This confirms that the wires are growing as a SiO_x, as opposed to pure Si being the volatile precursor species with the nanowires being oxidized post-synthesis.

2.5 Conclusions

Highly branched silica nanowires have been controllably synthesized in a single step CVD reaction through employing a method of *in situ* Cu catalyst loading. Characterization of these products using a combination of electron imaging and elemental analysis shows these products are made up of amorphous SiO_2, doped with Au and/or Cu, for both the primary (backbone) and secondary (branch) wires. The growth of the multi-wire backbone occurs through a metal-catalyzed VLS growth mechanism, while secondary growth typically occurs through a Cu_3Si-catalyzed VSS mechanism. Post-synthetic elemental analysis and diffraction data confirm the secondary catalyst to be crystalline Cu_3Si following the reaction (under ambient conditions). The structural observations made in this system relating to these growth processes are consistent with literature describing similar metal-catalyzed growth of nanowires.

Through manipulation of reaction conditions and extensive, careful characterization of branched nanowire products, several steps necessary for the growth mechanism can be inferred. These steps include: (1) initiation of primary wire growth through a metal-catalyzed VLS mechanism, (2) formation of a multi-wire backbone and deposition of the secondary catalyst (Cu_3Si) along the multi-wire interface, (3) catalyzed deposition of SiO_x along the multi-wire interface and formation of "nanopeapodded" type architecture, with Cu_3Si beaded regularly along the wire surface, and (4) Cu_3Si-catalyzed growth of SiO_x branches. Following synthesis, the sub-stoichiometric SiO_x nanowire products are catalytically oxidized to SiO_2. Understanding this growth process and being able to experimentally manipulate product properties can hopefully influence work

on synthesizing related materials in the future. Notably, the intermediate steps (2) and (3) may have a significant impact on not only research relating to branched nanowire products, but also when investigating nanopeapodded materials for sensing and optoelectronic applications.

2.6 Supporting Information

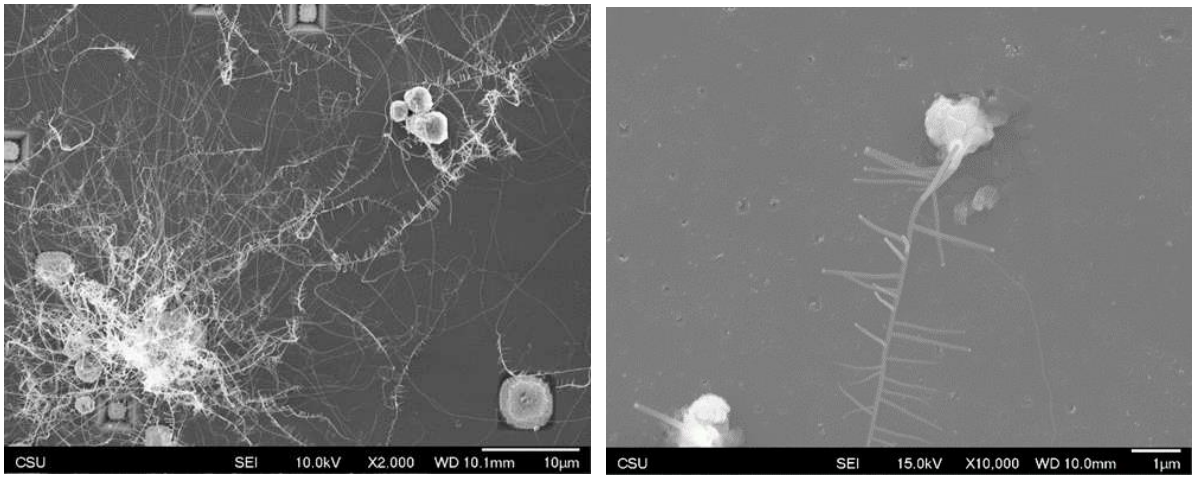

Figure 2.S1. (Left) SEM image showing an overview of many highly branched nanowires growing up from large deposits of Cu_3Si on the downstream end of region i, near region ii (shown in dark grey in Figure 2.2B). (Right) Higher magnification SEM image showing the branched nanowire growing through a root growth process.

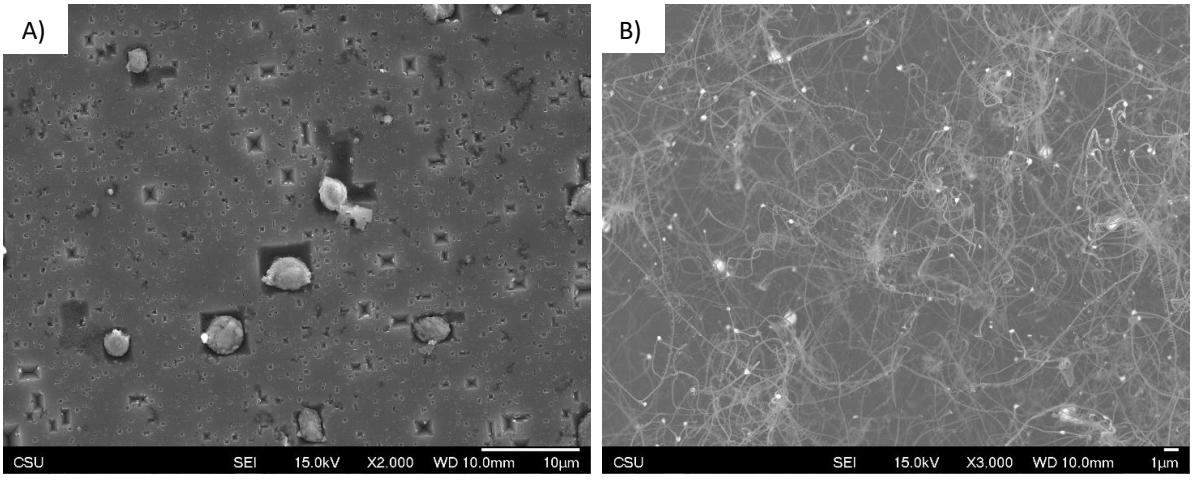

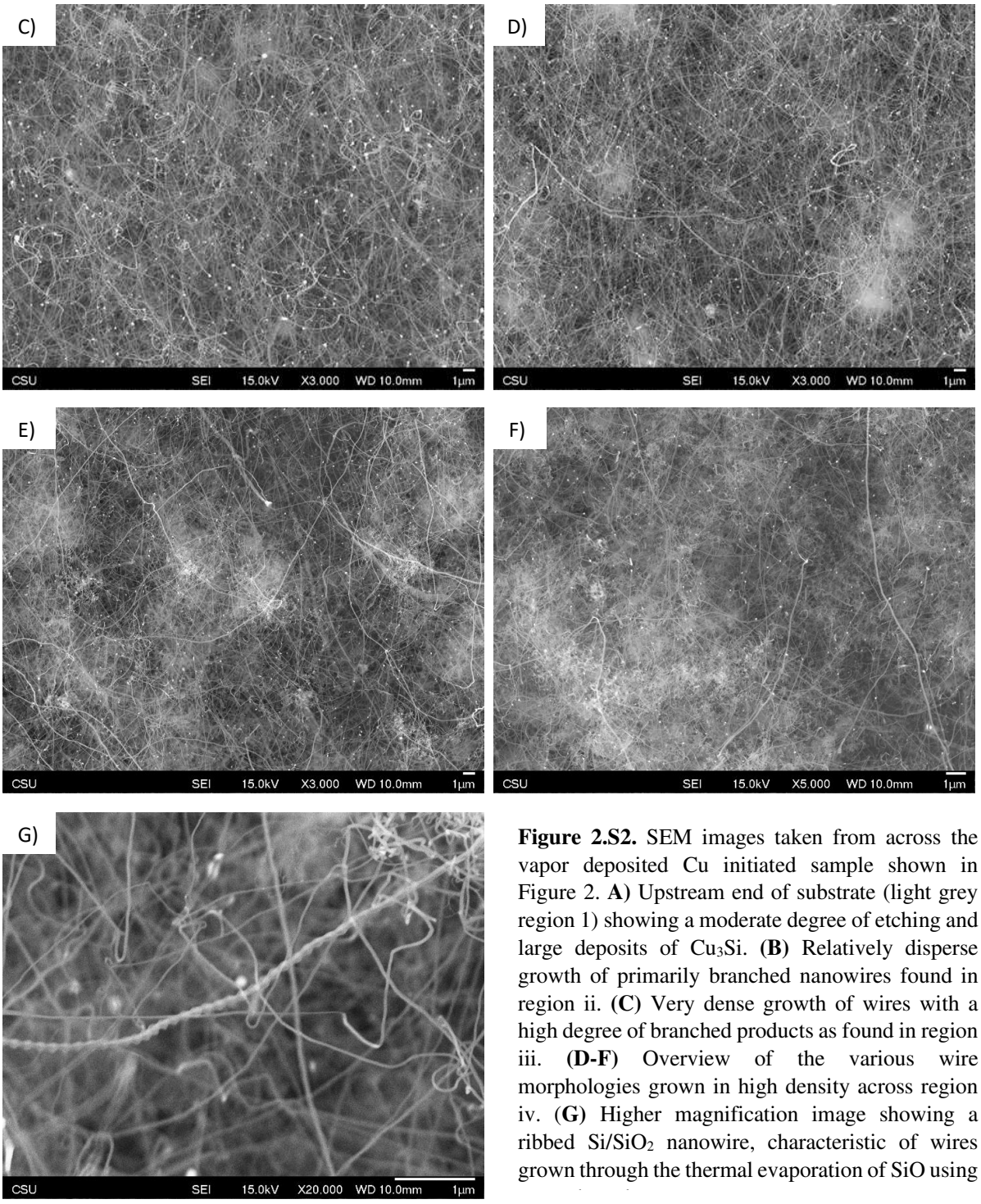

Figure 2.S2. SEM images taken from across the vapor deposited Cu initiated sample shown in Figure 2. **A)** Upstream end of substrate (light grey region 1) showing a moderate degree of etching and large deposits of Cu_3Si. **(B)** Relatively disperse growth of primarily branched nanowires found in region ii. **(C)** Very dense growth of wires with a high degree of branched products as found in region iii. **(D-F)** Overview of the various wire morphologies grown in high density across region iv. (**G)** Higher magnification image showing a ribbed Si/SiO_2 nanowire, characteristic of wires grown through the thermal evaporation of SiO using

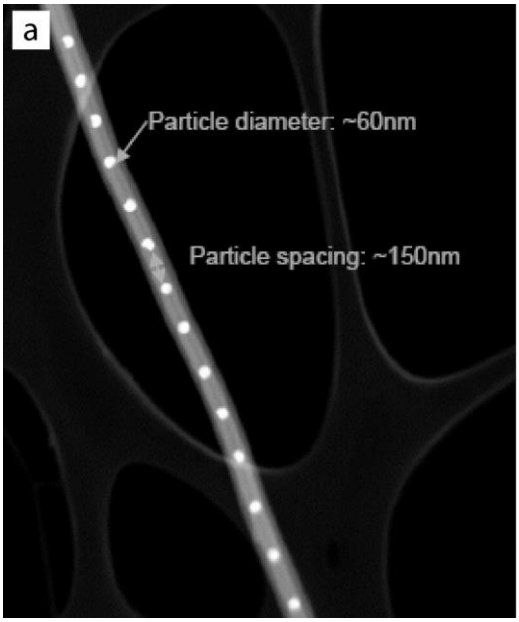

Figure 2.S3. ADF STEM image of a nanopeapodded wire showing uniform secondary catalyst diameter and separation. Also seen in this image is the multiple contrast lines characteristic of the multi-wire backbone structure.

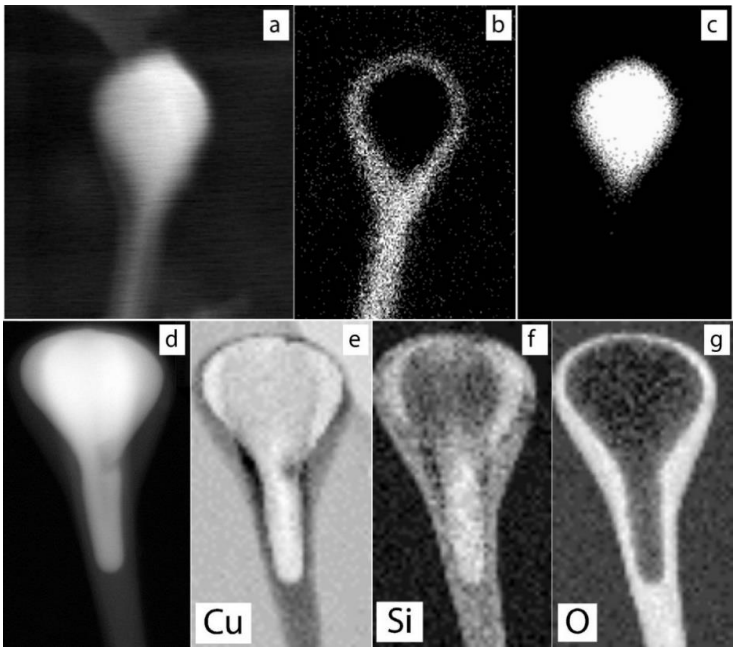

Figure 2.S4. SEM-EDS mapping images for (a) the time averaged electron micrograph representing the duration of the EDS collection time, (b) the copper-silicon rich phase, and (c) the gold rich phase. (d) Characteristic ADF STEM image of the backbone nanowire catalyst with corresponding EELS elemental edge maps for (e) copper, (f) silicon, and (g) oxygen.

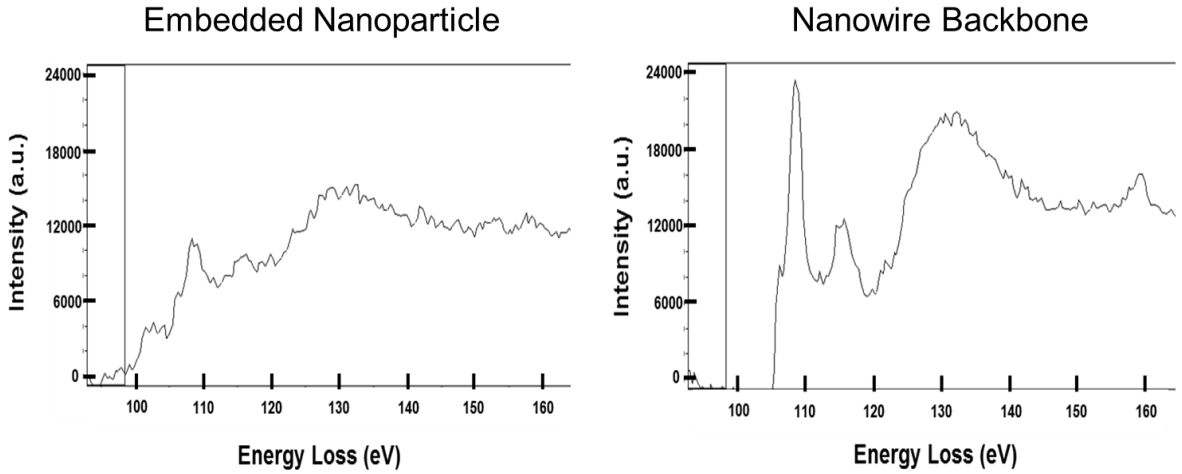

Figure 2.S5. Characteristic EELS spectra from the embedded VSS nanoparticle and nanowire backbone demonstrating Si in the zeroth oxidation state and Si in the +4 oxidation, respectively, as demonstrated by the Si L2,3 edges. These spectra are characteristic of the heterostructure nanowires discussed in this manuscript. The heterostructure nanowire sample spectra were extracted from data collected in the 50-550 eV region.

2.6.1 Formation of Si multi-wire through two separate processes

Two potential processes for forming multi-wire structures are the convergence of multiple wires, as shown in Figure 2.S7A, or the nucleation of multiple wires from a single catalyst head as shown in Figure 2.S7B1 and 2.2.

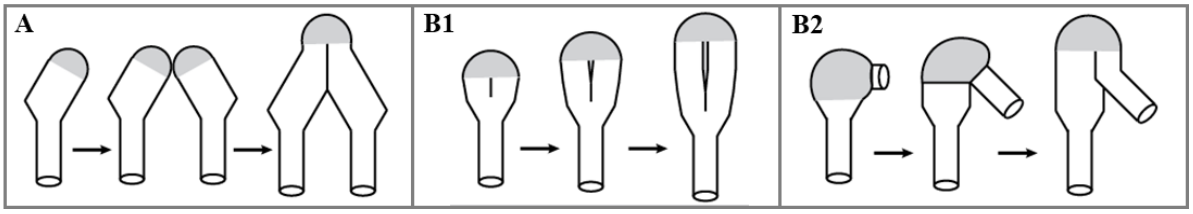

Figure 2.S7. Illustration of potential processes through which multi-wire formation can occur. **A)** The wires' diameter and growth direction change throughout the synthetic process which leads to catalyst heads coming into contact. Following catalyst head merging, wires can align to form the multi-wire backbone structure. **B)** Secondary nucleation from a swelling catalyst head. This secondary wire can nucleate either at the existing wire/catalyst interface **(B1)** directly forming an aligned multi-wire backbone, or it may occur away from the primary wire **(B2)** where it may or may not eventually align.

Given the disorder and density of wires as seen in Figure 2.S2, it is expected that catalyst heads will frequently come into contact. The disorder in the system is a direct result of the dynamic nature of growth in the reported system. Due to the initial $Cu_xSi_{(l)}$ catalysts forming as a result of deposition from the gas phase, the resulting wires will have different sizes, and therefore different growth rates and growth directions. When catalysts connect with a large angle between the individual wires, these wires will not align initially. Growth continues for both wires, but the physical growth direction (translation of the catalyst through space) cannot continue linearly for each wire after combination. This results in the spiraling of the two wires prior to alignment. This spiraling and subsequent alignment and formation of the multi-wire structure is seen in Figure 2.S8.

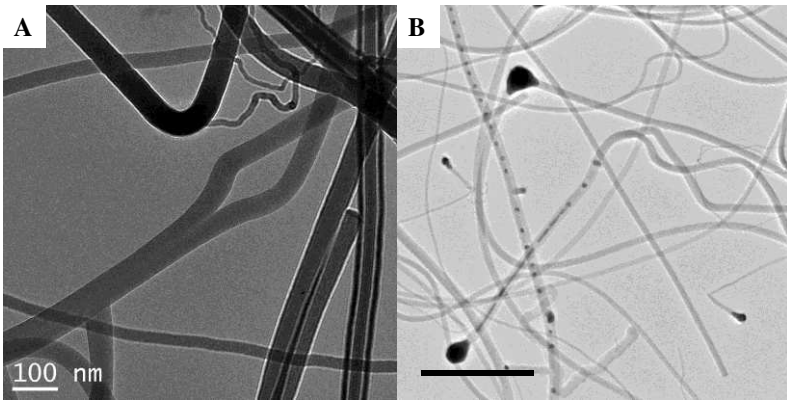

Figure 2.S8. TEM images of two wires spiraling, converging, and forming a multi-wire structure. **A)** Branched growth is observed shortly after the formation of the multi-wire with the branch pointing down. **B)** Deposition of Cu_xSi_y along the multi-wire interface is observed shortly after wire merging along with a peapodded structure with limited branching.

While individual catalysts may merge during growth to form a multi-wire structure, it is more likely that a single catalyst undergoes multiple wire nucleations. As the catalyst swells throughout the growth period, new nucleation sites can form either at the interface between the wire and catalyst, directly forming a multi-wire structure as depicted in Figure 2.S7B1, or it can occur away from previous wire growth, and these wires can later align, as shown in Figure 2.S7B2. This latter process is analogous to the procedure described for the aligning of wires following the merging of multiple catalysts. The reason the hypothesis of multiple nucleation is sometimes

preferred compared to the catalyst merging hypothesis is supported by the high number of wires often observed growing from a single catalyst as seen in Figure 2.S9.

While catalyst merging is likely in our system, and may be the case seen in figure 2.S8B and in higher density wire situations, the probability that catalyst collision is the cause for an observed multi-wire structure decreases with the number of wires involved and in low-density growth regions. In cases where there is a large number of wires growing from a single catalyst head, like those shown in Figure 2.S9, a secondary nucleation hypothesis makes more sense. Also seen in Figure 2.S9 are other pieces of evidence strongly supporting the multi-wire hypothesis for the peapodded structures compared to a core-shell structure. In both images contrast differences are seen in the backbone structures due to overlapping wires. We know these backbones are amorphous silica (not including the higher contrast due to the Cu_3Si co-deposition), so the contrast cannot be attributed to differences in phase, composition, or crystallographic orientation. Also seen in Figure 2.S9B is an apparent dip in the wire surface when looking along the edge. This is due to there being two wires fused together as shown in Figure 2.6.

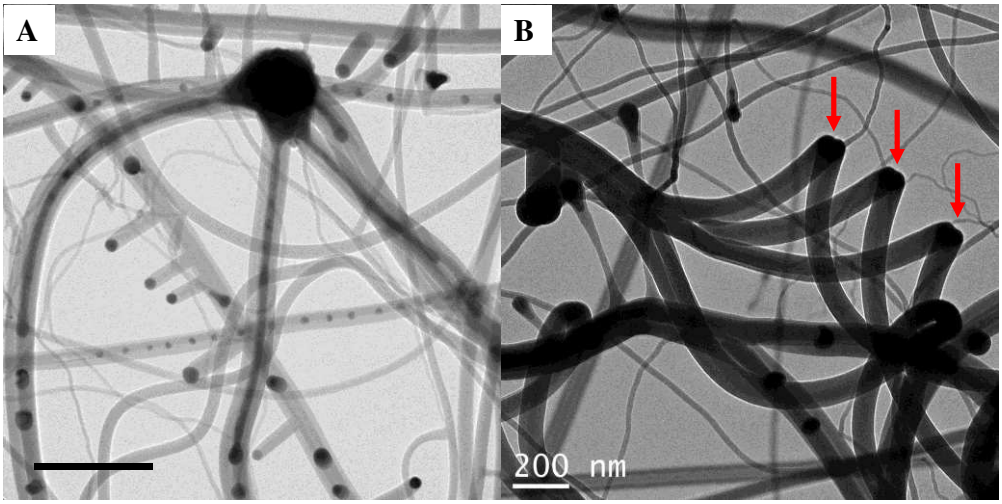

Figure 2.S9. A) TEM image showing the growth of 4 multi-wire structures, each with Cu_xSi_y deposition, all from a single large catalyst. **B)** TEM image showing the convergence of 4 bi-wires. The red arrows point to the dip observed when looking along the length of the wire due to the interface between the two wires of the bi-wire. A second multi-wire is seen below this structure, with two multi-wire backbones exhibiting secondary catalyst deposition merging.

Further evidence for the multi-wire growth hypothesis is presented in Figure 2.S10. In early growth regions where wire density is low but the relative percentage of branched product is high, we observe a series of structural features that commonly correspond to the formation of aligned multi-wire backbones which can lead to branched species. One feature is two individual wires that seem to be spiralling around one another which eventually converge, leading to a bi-wire. This is seen circled in Figure 2.S10A. Following the formation of the bi-wire, there is often another "kink" in the wire, indicated by arrows in Figure 2.S10A and shown at higher magnification using TEM in Figure 2.S10B. The presence of this kink comes from a third wire nucleating at the bi-wire interface. Following the formation of the tri-wire backbone, co-deposition of CuSi along the inter-face typically begins and branching follows.

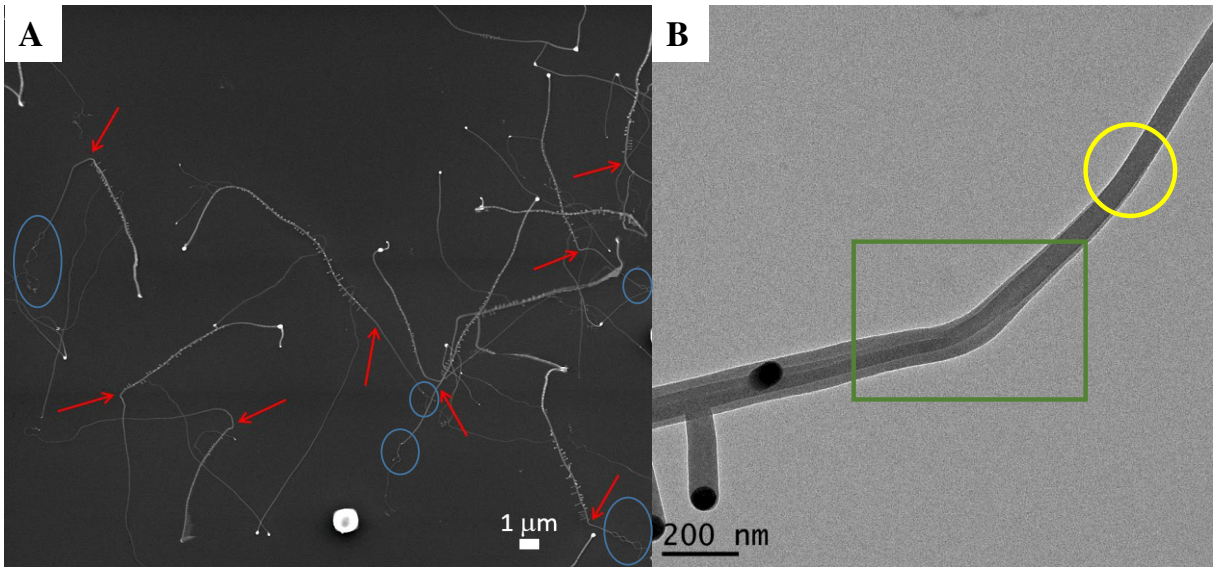

Figure 2.S10. A) SEM image of branched nanowires, which show an increasing diameter and a kink (indicated by the red arrow) prior to branching. The blue circle shows the presence of two wires converging early in growth which later splits into a multi-wire. **B)** TEM image showing that the observed increase in diameter and kinking in the wire is a result of the formation of the multi-wire. The yellow circle highlights when the wire first splits into two wires, as is evidenced by the formation of the contrast lines due to wire overlap, and the kink is due to the slight difference in growth rates of the bi-wire. The green box highlights the region where a third wire forms, resulting in the growth of three aligned wires. The tri-wire structure allows for the co-deposition of Cu_xSi_y at the interface between these three wires, which can then act as the catalyst for branched wire growth. Images adapted from reference (1).

Table 2.S1. Modifications to the experimental conditions tested and qualitative observations relating to how these modifications impact the growth of branched nanowire products observed.

Variable	Experimentally tested	Result
Initial catalyst composition	Au	Consistent dispersion of nanowire products, consistent initial wire diameter, low concentration of branched products
	Cu	Increased presence of branching, increase of variability in wire diameters
Catalyst deposition procedure	Poly-L-Lysine + AuNP	High degree of surface etching
	HF, KOH, vapor phase Cu	Large deposits of Cu_3Si upstream, mixture of root growth and float growth upstream
AuNP deposition time	2-10 minutes	Short times: decrease in the number of nanowire products and high degree of dispersion of products on surface. Long times: dense nanowire growth across surface

Substrate	N-type Si (100)	Moderate dispersion of wires, generally product can be manipulated through substrate preparation and reaction times
	Fused quartz slide (SiO_2)	Excessive wire growth across surface at short reaction times with limited branching due to excess concentration of SiO_x
Cu precursor	Cu powder (native CuO_x layer)	Moderate wire growth showing low concentrations of branched wire species. Due to volatile CuO only on surface, branching can cease at long growth times (see Figure 5d)
	CuO/C	Increases the presence of branched products
	None (Au NP initiated growth)	Mixed Si and SiO_x wire growth, variable morphologies with no branched nanowire products
Si precursor (non-substrate)	None	Limited growth and high degree of substrate surface etching
	Crushed Si wafer	Varying amount of precursor can control presence of SiO_x in the gas phase, corresponding to increasing the rate and extent of growth. Amount of solid precursor directly relates to concentration of SiO_x in gas phase
	SiO powder	SiO powder displays increased volatility compared to the native oxide of the crushed Si wafer (nominally SiO_2 on Si) resulting in higher concentrations of grown products, and an increase in product variability.
Time	1-10 hours	Longer growth times lead to an increase in wire length and an increase in the presence of branched species. Almost no branching was observed at $T \leq 3hr$ for Au initiated reactions, and $T \leq 1hr$ for Cu initiated reactions

REFERENCES

1. Agarwal, R.; Lieber, C. M., Semiconductor nanowires: optics and optoelectronics. *Applied Physics A* **2006,** *85* (3), 209.
2. Rao, C. N. R.; Deepak, F. L.; Gundiah, G.; Govindaraj, A., Inorganic nanowires. *Progress in Solid State Chemistry* **2003,** *31* (1), 5-147.
3. Chan, C. K.; Peng, H.; Liu, G.; McIlwrath, K.; Zhang, X. F.; Huggins, R. A.; Cui, Y., High-performance lithium battery anodes using silicon nanowires. *Nat Nano* **2008,** *3* (1), 31-35.
4. Bierman, M. J.; Lau, Y. K. A.; Jin, S., Hyperbranched PbS and PbSe Nanowires and the Effect of Hydrogen Gas on Their Synthesis. *Nano Letters* **2007,** *7* (9), 2907-2912.
5. Kaushik, A.; Kumar, R.; Huey, E.; Bhansali, S.; Nair, N.; Nair, M., Silica nanowires: Growth, integration, and sensing applications. *Microchimica Acta* **2014,** *181* (15), 1759-1780.
6. Wang, S.-B.; Huang, Y.-F.; Chattopadhyay, S.; Jinn Chang, S.; Chen, R.-S.; Chong, C.-W.; Hu, M.-S.; Chen, L.-C.; Chen, K.-H., Surface plasmon-enhanced gas sensing in single gold-peapodded silica nanowires. *NPG Asia Mater* **2013,** *5*, e49.
7. Murphy-Perez, E.; Arya, S. K.; Bhansali, S., Vapor-liquid-solid grown silica nanowire based electrochemical glucose biosensor. *Analyst* **2011,** *136* (8), 1686-1689.
8. Wang, Z. L.; Gao, R. P.; Gole, J. L.; Stout, J. D., Silica Nanotubes and Nanofiber Arrays. *Advanced Materials* **2000,** *12* (24), 1938-1940.
9. Wang, J. C.; Zhan, C. Z.; Li, F. G., The synthesis of silica nanowire arrays. *Solid State Communications* **2003,** *125* (11), 629-631.
10. Wang, N.; Cai, Y.; Zhang, R. Q., Growth of nanowires. *Materials Science and Engineering: R: Reports* **2008,** *60* (1), 1-51.

11. Schmidt, V.; Wittemann, J. V.; Senz, S.; Gösele, U., Silicon Nanowires: A Review on Aspects of their Growth and their Electrical Properties. *Advanced Materials* **2009,** *21* (25-26), 2681-2702.

12. Wagner, R. S.; Ellis, W. C., VAPOR-LIQUID-SOLID MECHANISM OF SINGLE CRYSTAL GROWTH. *Applied Physics Letters* **1964,** *4* (5), 89-90.

13. Morales, A. M.; Lieber, C. M., A Laser Ablation Method for the Synthesis of Crystalline Semiconductor Nanowires. *Science* **1998,** *279* (5348), 208-211.

14. Wang, Y.; Schmidt, V.; Senz, S.; Gosele, U., Epitaxial growth of silicon nanowires using an aluminium catalyst. *Nat Nano* **2006,** *1* (3), 186-189.

15. Gudiksen, M. S.; Lauhon, L. J.; Wang, J.; Smith, D. C.; Lieber, C. M., Growth of nanowire superlattice structures for nanoscale photonics and electronics. *Nature* **2002,** *415* (6872), 617-620.

16. Cui, L.-F.; Ruffo, R.; Chan, C. K.; Peng, H.; Cui, Y., Crystalline-Amorphous Core−Shell Silicon Nanowires for High Capacity and High Current Battery Electrodes. *Nano Letters* **2009,** *9* (1), 491-495.

17. Lauhon, L. J.; Gudiksen, M. S.; Wang, D.; Lieber, C. M., Epitaxial core-shell and core-multishell nanowire heterostructures. *Nature* **2002,** *420* (6911), 57-61.

18. Johnson, D. C.; Mosby, J. M.; Riha, S. C.; Prieto, A. L., Synthesis of copper silicide nanocrystallites embedded in silicon nanowires for enhanced transport properties. *Journal of Materials Chemistry* **2010,** *20* (10), 1993-1998.

19. Gentile, A.; Ruffino, F.; Boninelli, S.; Grimaldi, M. G., Silica nanowire–Au nanoparticle pea-podded composites: Synthesis and structural analyses. *Thin Solid Films* **2015,** *589* (Supplement C), 755-763.

20. Wang, S.-B.; Chen, R.-S.; Chang, S. J.; Han, H.-C.; Hu, M.-S.; Chen, K.-H.; Chen, L.-C., Surface plasmon resonance-induced color-selective Au-peapodded silica nanowire photodetectors with high photoconductive gain. *Nanoscale* **2014,** *6* (3), 1264-1270.

21. Cong, V. T.; Ganbold, E.-O.; Saha, J. K.; Jang, J.; Min, J.; Choo, J.; Kim, S.; Song, N. W.; Son, S. J.; Lee, S. B.; Joo, S.-W., Gold Nanoparticle Silica Nanopeapods. *Journal of the American Chemical Society* **2014,** *136* (10), 3833-3841.

22. Jiang, X.; Tian, B.; Xiang, J.; Qian, F.; Zheng, G.; Wang, H.; Mai, L.; Lieber, C. M., Rational growth of branched nanowire heterostructures with synthetically encoded properties and function. *Proceedings of the National Academy of Sciences* **2011,** *108* (30), 12212-12216.

23. Zhu, J.; Peng, H.; Chan, C. K.; Jarausch, K.; Zhang, X. F.; Cui, Y., Hyperbranched Lead Selenide Nanowire Networks. *Nano Letters* **2007,** *7* (4), 1095-1099.

24. Yu, D. P.; Hang, Q. L.; Ding, Y.; Zhang, H. Z.; Bai, Z. G.; Wang, J. J.; Zou, Y. H.; Qian, W.; Xiong, G. C.; Feng, S. Q., Amorphous silica nanowires: Intensive blue light emitters. *Applied Physics Letters* **1998,** *73* (21), 3076-3078.

25. Kulkarni, S.; Patrikar, S., Detection of propane gas adsorbed in a nanometer layer on silica nanowire. *Optik - International Journal for Light and Electron Optics* **2016,** *127* (1), 465-470.

26. Shalav, A. E., R. G., Hierarchal silica nanowire growth via single step annealing. *International Conference on Nanoscience and Nanotechnology* **2010,** *(ICONN 2010)*, 203-206.

27. Shalav, A.; Kim, T.; Elliman, R. G., SiOx Nanowires Grown via the Active Oxidation of Silicon. *IEEE Journal of Selected Topics in Quantum Electronics* **2011,** *17* (4), 785-793.

28. Yoon, J.-H., Alternative vapor–liquid–solid process in Au-assisted growth of silica nanowires. *Materials Letters* **2014,** *123* (Supplement C), 131-134.

29. Kim, H. W.; Hyun Shim, S.; Woo Lee, J., Characteristics of SiOx nanowires synthesized via the thermal heating of Cu-coated Si substrates. *Physica E: Low-dimensional Systems and Nanostructures* **2007,** *37* (1), 163-167.

30. Wen, C. Y.; Reuter, M. C.; Tersoff, J.; Stach, E. A.; Ross, F. M., Structure, Growth Kinetics, and Ledge Flow during Vapor−Solid−Solid Growth of Copper-Catalyzed Silicon Nanowires. *Nano Letters* **2010,** *10* (2), 514-519.

31. Harper, J. M. E.; Charai, A.; Stolt, L.; d'Heurle, F. M.; Fryer, P. M., Room-temperature oxidation of silicon catalyzed by Cu3Si. *Applied Physics Letters* **1990,** *56* (25), 2519-2521.

32. Stolt, L.; Charai, A.; D'Heurle, F. M.; Fryer, P. M.; Harper, J. M. E., Formation of Cu3Si and its catalytic effect on silicon oxidation at room temperature. *Journal of Vacuum Science & Technology A* **1991,** *9* (3), 1501-1505.

33. Zheng, B.; Wu, Y. Y.; Yang, P. D.; Liu, J., Synthesis of ultra-long and highly oriented silicon oxide nanowires from liquid alloys. *Adv Mater* **2002,** *14*.

34. Xiao, Z.; Zhang, L.; Meng, G.; Tian, X.; Zeng, H.; Fang, M., High-Density, Aligned SiO2 Nanowire Arrays: Microscopic Imaging of the Unique Growth Style and Their Ultraviolet Light Emission Properties. *The Journal of Physical Chemistry B* **2006,** *110* (32), 15724-15728.

35. Sun, S. H.; Meng, G. W.; Zhang, M. G.; Tian, Y. T.; Xie, T.; Zhang, L. D., Preparation and characterization of oriented silica nanowires. *Solid State Communications* **2003,** *128* (8), 287-290.

36. Fletcher, N. H.; Elliman, R. G.; Kim, T. H., Gold bead-strings in silica nanowires: a simple diffusion model. *Nanotechnology* **2009,** *20* (8), 085613.

37. Wang, S.-B.; Hu, M.-S.; Chang, S. J.; Chong, C.-W.; Han, H.-C.; Huang, B.-R.; Chen, L.-C.; Chen, K.-H., Gold nanoparticle-modulated conductivity in gold peapodded silica nanowires. *Nanoscale* **2012,** *4* (12), 3660-3664.

38. Shi, W.; Lu, W.; Jiang, L., The fabrication of photosensitive self-assembly Au nanoparticles embedded in silica nanofibers by electrospinning. *Journal of Colloid and Interface Science* **2009,** *340* (2), 291-297.

39. Molares, M. E. T.; Balogh, A. G.; Cornelius, T. W.; Neumann, R.; Trautmann, C., Fragmentation of nanowires driven by Rayleigh instability. *Applied Physics Letters* **2004,** *85* (22), 5337-5339.

40. Chen, P.-H.; Hsieh, C.-H.; Chen, S.-Y.; Wu, C.-H.; Wu, Y.-J.; Chou, L.-J.; Chen, L.-J., Direct Observation of Au/Ga2O3 Peapodded Nanowires and Their Plasmonic Behaviors. *Nano Letters* **2010,** *10* (9), 3267-3271.

III. EXPLORING ELECTROCHEMICAL ANODIZATION AS A SYNTHETIC APPROACH TO PRODUCE IONICALLY CONDUCTING MATERIALS[iii]

3.1 Overview

The objective of this project was to explore the feasibility of using electrochemical anodization as a synthetic method to conduct targeted synthesis of ionically conducting materials. The hypothesis is that if a system is properly designed, using this technique will require ionic conductivity – the specific property of interest – in order for any significant synthesis to occur. This approach will naturally select for systems that exhibit desired properties and accelerate the discovery of chemically-dynamic, ionically conducting materials. As this is an exploratory research direction, an initial system of AgI was proposed as a "proof of concept" target and one to inform research directions moving forward. Using electrochemical anodization allowed for successful synthesis of AgI with a variety of morphologies and other unexpected properties. Insights into the fundamental processes of electrochemical anodization were gained through analyzing this system and alternative hypotheses surrounding product formation are proposed. Stemming from this initial system CuI and Cu_xS were synthesized through comparable methods and compared to literature reports. With the successful syntheses of these Cu and Ag binary systems, moving toward more complex materials and systems with greater relevance to the study of ionic conductivity was pursued. Alternate systems that will be touched upon in this chapter include exploratory results on the synthesis of Na_3PS_3, the cationic exchange of Li^+ and Cu^+ in

[iii] Th initial concept for this chapter of using electrochemical corrosion for synthesis in such a unique way, and the background for the fundamental science and research targets, came from Dr. Amy Prieto and Dr. Jamie Neilson. Unless otherwise noted, all work, results, figures, writing, and proposed research directions presented in this chapter are solely that of the author, Jacob Boissiere. This has been written and formatted for the dissertation and has not been formatted or submitted to any journal at this time.

Cu_6PS_5Cl, and future research directions involving pursuing additional chalcogenide anion reactions targeting $Cu_{2-x}Se$ and Ag_3SI. Overall, the pursuit of synthesizing ionically conductive materials through the use of electrochemical anodization methods has yielded many challenges and failed attempts, even more than are included herein. Despite that, there are valuable conclusions and insights to be drawn from this work, both the successes and failures, and numerous opportunities for expansion upon present work and pursuing new and informed research directions.

3.2 Motivation, Introduction, and research objectives

3.2.1 Motivation for the investigation of inorganic solid state electrolytes

Ionic conductivity is a fundamentally important mechanic for many technological devices and industrial applications.[1–5] Historically and practically, liquid electrolytes are the most well understood and widely utilized electrolyte systems with their modern roots dating back to the beginning of the 19th century with Volta's voltaic pile and Galvani's frog leg experiments, The discovery of electrolytic properties in the solid state is nearly as old with Faraday observing the conductivity of PbF_2 and Ag_2S, which are commonly accepted to be the first reported solid electrolyte and intercalation electrode, respectively.[6,7] While continuous study and countless advances have been made to both liquid and solid systems, the vast majority of commercial electrochemical processes and manufactured devices, such as batteries, use liquid electrolytes. While liquid electrolytes provide many practical benefits and proven performance, several applications would benefit favorably through the incorporation of solid electrolytes, namely secondary battery technologies. A secondary battery refers to a device which stores energy utilizing differences in chemical potential, and importantly this process for storing and releasing this energy is reversible.[8]

Lead acid batteries were invented in the mid-19th century and are not only the first rechargeable battery produced and remains in widespread use in vehicles and a variety of other applications. The world of battery technologies was forever changed in 1991 when the first lithium-ion battery (LIB) was commercially produced, quickly becoming the dominant source of energy for portable electronics. As technological improvements continued to advance the widespread use of portable electronics in everyday life, LIB technology has continued to progress, providing higher energy density, longer cell lifetime, smaller device size, improved rate capabilities, and peripheral advances such as adaptive and wireless charging. As a result, LIBs have been incorporated into a wider variety of devices and applications, most notably for use in transportation such as aviation and the production of hybrid and fully electric vehicles.

While LIBs dominate the fields of consumer electronics and electric vehicles in terms of utility and volume of production, redox-flow batteries, molten salt batteries, and sodium-ion batteries (NIBs) are all commercially produced technologies of interest for a variety of other applications, in particular grid-level energy storage.[1,4,9–12] Of these examples mentioned, only molten salt batteries typically use solid electrolytes at this time, while liquid electrolytes are most prevalent for the other applications, specifically carbonate-based organic liquid electrolytes for LIBs and NIBs, and aqueous electrolytes for redox flow devices.[11,13–16] Moving from liquid electrolytes to solid state electrolytes (SSEs) for secondary battery systems has several potential advantages but needs to overcome a variety of limitations of current technologies. The primary advantages for integration of SSEs into batteries used for mobile energy storage is the theoretical increase in energy density, lifetime, and safety as discussed in Chapter 1, Section 1.4.2. Moving to such an architecture also is proposed to have a more significant impact on the design and implementation of non-Li technologies, as Na lacks the well-developed or commercially produced

anodes that Li uses, and multivalent systems such as Ca and Mg-ion batteries currently lack both anode and electrolyte technologies that demonstrate device level performance for any systems that may be commercially relevant.[1,17–22]

3.2.2 Classification of ionic materials and research objectives

In addition to performance metrics, solid ionic conductors are classified by the mobile ion and the structural and chemical characteristics of the solid lattice or immobile component. An initial distinction separates ionically conducting materials into the classes of anionic and cationic conductors. The majority of solid anionic conducting materials are either oxide or fluoride conductors, with some additional examples of hydride and other halide conductors.[7,23] For the current research objectives, no anionic conducting materials where targeted, nor general design principles commonly related to structures associated with anionic materials. When considering cationic conduction, there exists a much greater variety of materials that fit this classification, with the most common examples being Li^+, Na^+, Ag^+, and Cu^+ conducting materials.[4,22,24,25] These are all mobile ion systems of interest and are viable targets for the proposed electrochemical anodization synthetic method. While the goal of the project is to ultimately focus on the development of exploratory methodologies, rather than targeting specific product morphologies or compositions, it is beneficial to identify, and target established systems that be used as a test bed of synthetic targets. By first focusing on known systems, results can be used to test the basic synthetic hypothesis, identify key parameters and considerations regarding design of experiment, teach the research the fundamental synthetic and characterization methods relevant to the field, and establish the currently theoretical procedure as relevant to practical applications. Following work targeting known systems, the intention is for the method to be applied to a wide range of

systems and explore the inclusion of new and varied components with the ultimate goal of new materials discovery.

While the common mono-valent cation systems mentioned above encompass a wide variety of well-known solid ionically conducting materials, being able to apply learned techniques to target advanced technologies such as multivalent Ca^{2+} or Mg^{2+} ion conductors are of particular interest. These systems are limited in their current capabilities and new materials could have an even greater impact on developing the next generation of energy storage than the current focus on incorporation of SSEs into LIB technologies.[18] Due to the limited number of viable materials and lack of well-defined parameters for determining the conductivity of such multivalent systems, following more traditional routes of systematic modification of existing materials or computational prediction of potential compounds is challenging for this class of ion conductors.[26,27] Therefore, corroding these metals to potentially identify new multivalent ionically conducting materials is a perfect future goal and the ultimate actualization of the proposed work.

Beyond classifying ionic conductors by the mobile ion, the structure and composition are equally, if not more important. Compositionally, solid electrolytes can be split into polymer and inorganic solid electrolytes. Polymer solid electrolytes have captured much of the attention of the battery community recently, with several companies promising new advances in commercial battery technology using polymer electrolytes, and polymeric components already being incorporated in a variety of applications. While employing electrochemical methods to initiate polymerization and regulate polymer deposition onto an electrode is known and demonstrated to be an exciting and beneficial technique, polymer electrodes will not be discussed in the context of this project. The anodization method proposed here specifically deals with oxidizing a metal anode in the presence of dissolved inorganic anionic species, resulting in the formation of solid, inorganic

product formation. Given the proper knowledge of polymer synthesis and precursor chemistry, an analogous technique could be used to potentially deposit polymer through anodically initiated polymerization, and such films could regulate cation flow in a similar manner, but that is outside the scope of the project at this time. For inorganic solid electrolyte systems, these are largely divided into crystalline and non-crystalline electrolytes.

Classes of solid crystalline ionic materials are typically defined ether by the crystal structure or by a combination of their mobile ion and primary anionic lattice constituent. Certain families of materials are sometimes referred to by special terms coined in the field (i.e. NaSICon and subsequently LiSICon), or generalized according to a foundational compound that has since

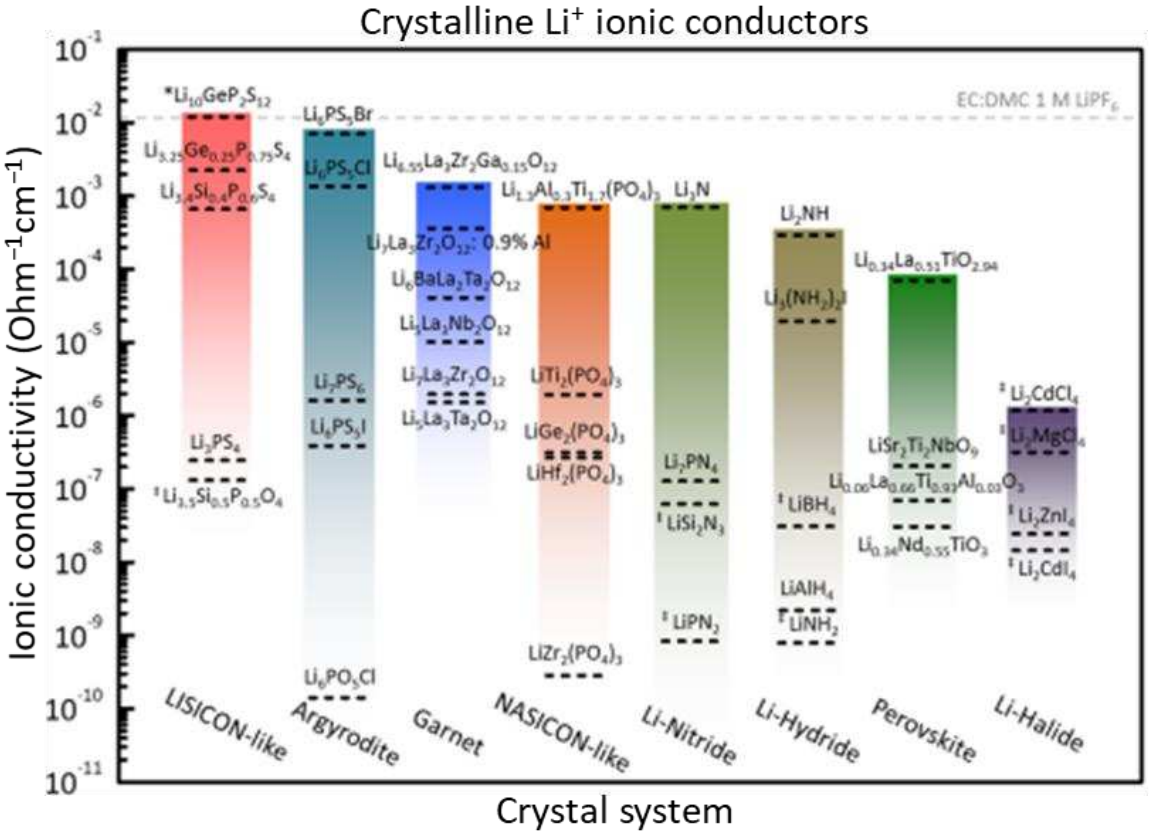

Figure 3.1. Chart showing 8 different classes of crystalline solid Li-ion conducting materials. Notable examples of materials that fit into these classes are listed and positioned with respect to their ionic conductivities (values correspond to the y-axis, a log scale of $\Omega^{-1}cm^{-1}$). The dotted line above 10^{-2} $\Omega^{-1}cm^{-1}$ corresponds to the ionic conductivity of a common carbonate-based liquid electrolyte for LIB applications. Figure reproduced from Shao-Horn, Y.; et al. *Chem. Rev*. **2016**, 116, 140-162.[22]

been modified, for example when garnet materials are described by their relation to lithium lanthanum zirconium oxide (LLZO).[1,4,9,22,28,29] An overview of several of these classifications or families of structure for Li, along with their ionic conductivity ranges and various specific compounds which have been produced and characterized, is shown in Figure 3.1. This overview also compares the conductivities to a carbonate liquid electrolyte, relevant to current Li-ion battery technologies.

A similarly diverse subset of materials can be found for the non-crystalline solid ionic conductors including notable example of $(Li_2S)_x \cdot (P_2S_5)_y$ or "LPS" glassy electrolyte and lithium phosphorous oxynitride or LiPON and related compounds.[1,26,29–32] Amorphous or glassy electrolytes are of particular interest due to exhibiting excellent ionic conductivities due to their structural and thermodynamic properties. A variety of glass formers can be used to influence local structure and result in increases in ionic conductivity or manipulation of other properties. Alkali oxides and halides can be doped or substituted into these structures to manipulate the conductivities of the products, resulting in some of the best reported ionic conductors to date, displaying conductivities on the order of 10^{-1} $\Omega^{-1}cm^{-1}$. These amorphous materials may also display certain advantageous properties relative to their crystalline counterparts, as they are more likely to have isotropic properties with good conductivity in 3 dimensions, can be modified through the incorporation of a number of different dopants and substitutions without destroying structure, have reduced presence of grain boundaries or instances of significant interfacial impedance within the structure, more likely to exhibit favorable materials properties relating to cost of synthesis or device incorporation, and can be relatively stable or inert. Because of these benefits and the increased difficulty in modeling and challenges relating to the ability to predict new materials of

such highly disordered structures, it was of particular interest to be able to synthesize such materials when defining our proposed synthetic technique.

Despite this wide range of available materials, none of these examples have adequately satisfied all of the requirements for widespread practical use in solid state batteries. This relates to the various limitations and considerations outlined in Chapter 1. Because of these limitations, it is important to continue pursuing the discovery of new materials, outside of these existing classes, but there are no widely accepted design principles for coming up with novel ionic conductors, especially not for materials with very high ionic conductivities (superionic conductors). This challenge is not unique to ionic conductors; most classes of materials with unusual and potentially interesting properties also lack unifying, robust design principles.

Because of these challenges, we wanted to take a step back and think about how rationally designing a different approach to fundamentally synthesizing and discovering ionically conducting materials could be achieved. Therefore, we sought to undertake establishing a synthetic paradigm where materials that have the properties desired for a particular application are the only materials that would form under the reaction conditions. Our focus on materials that permit ion mobility meant that we must therefore employ conditions where the only materials that could theoretically be synthesized, are the materials that allow for ion mobility. The intent was for this limitation to be achieved by requiring one reactant (the metal cation produced at the anode) to be able to move through the solid inorganic material being formed at the surface under the given reaction conditions. The ultimate goal will be the discovery of solid electrolytes for next-generation batteries.

3.2.3 Motivation for targeting new synthetic paradigm for ionically conducting materials

Our goal was to use the concept of 'natural selection' to accelerate the discovery of chemically-dynamic, ionically conducting materials for applications in electrolytes. The proposed method is a modification of electrodeposition, in that the mobile ion comes from the electrochemical corrosion of a working electrode. This electrode is submersed in a complex solution with multiple reagents that may be chemically or electrochemically reactive. Employing various electrochemical techniques of constant current or applied potentials will drive an electrochemical reaction, which provides the overall driving force to form products on the electrode surface. However, in order for current to flow, any deposited material must also allow for ionic mobility through the solid in order to the reaction to continue at the electrolyte interface. This will be enabled through design of the external circuit, electrodeposition potential waveform, and precursor selection, to ensure that the new materials that grow are naturally selected. The approach outlined here theoretically selects for the ideal combination of structure and imperfections that enable the transformative properties of chemically-dynamic materials. Further discussion of the fundamental concept behind this approach can be found in the following section.

The distinctive challenge is designing the experimental framework that applies a selective pressure for the self-selective synthesis of materials with desired properties. We focus on chemical dynamics because the structural or compositional descriptions of these materials are less defined and those structures that are highly defected are often advantageous. Predictive theories for these types of materials simply do not yet exist to guide the discovery. With our proposed approach the specific structure is almost irrelevant; just by formation under the reaction conditions, the compound should inherently display the desired ionic properties

The goals when pursuing this project involve the systematic, tiered approach to materials discovery, targeting ionically conducting properties. Ultimately, if new superionic conductors

could be found using these techniques, this would enable technologies that reach beyond the energy storage applications previously discussed. The potential to discovery advanced ionically conductive materials with complex structures or multivalent conduction have the potential to be high impact, because accurate and predictive theories simply do not yet exist to help guide exploratory synthesis for these cases, so existing approaches currently yield only incremental advances. In this new synthetic paradigm, no specific structure needs to necessarily be known or expected, as the structure that is consistent with the selected property will be the only material that forms. Following synthesis, any resulting product can then be thoroughly characterized, and the knowledge gained from understanding the structure property relationships of potentially newly discovered materials can be used to help improve current theoretical methods.

3.2.4 Fundamental hypothesis for utilization of electrochemical anodization

A diagram outlining the fundamental synthetic paradigm being proposed regarding the electrochemical anodization synthesis and discovery of ionically conducting materials and be found in Figure 3.2. This diagram shows how the synthesis begins with a solid metal anode of the desired mobile cation, which is placed in a solution containing counter ions in their preferred oxidation state. The lattice constituents could also be electrochemically activated instead of existing in their anionic form in solution. This could occur via the anion being formed at the counter electrode and then diffusing across to the anode, or the solution could contain compounds that oxidatively decompose at the anode resulting in the release of cation components and the subsequent anionic decomposition product being the reactive constituent.

Once the reaction is prepped an oxidizing potential is applied to the anode resulting in the oxidation of metals at the surface which then react with solution components and form a film on the anode (Figure 3.2 (1)). The reaction must be designed and prepared such that the

electrochemically initiated reaction can uniformly and completely react with the exposed anode surface. This coating can either be ionically insulating or conducting. If a deposited product does not allow for ion conduction, then the surface becomes passivated, not allowing the reaction to continue (Figure 3.2 (2a)). This is easily observed electrochemically; if a constant potential is being applied, the current will plummet, and if constant current techniques are being used, the voltage will spike, indicating a passivated surface. This is one way the synthetic methodology provides rapid feedback. In the event that a non-conducting product is formed, initial solution

conditions and electrochemical methods employed must be revisited (Figure 3.2 (3a)). This feedback loop results in iterative feedback and reaction design.

Once a surface is formed that allows ions to move through it, the charge transfer reaction will then occur through the net motions of ions through the surface as shown in Figure 3.2 step

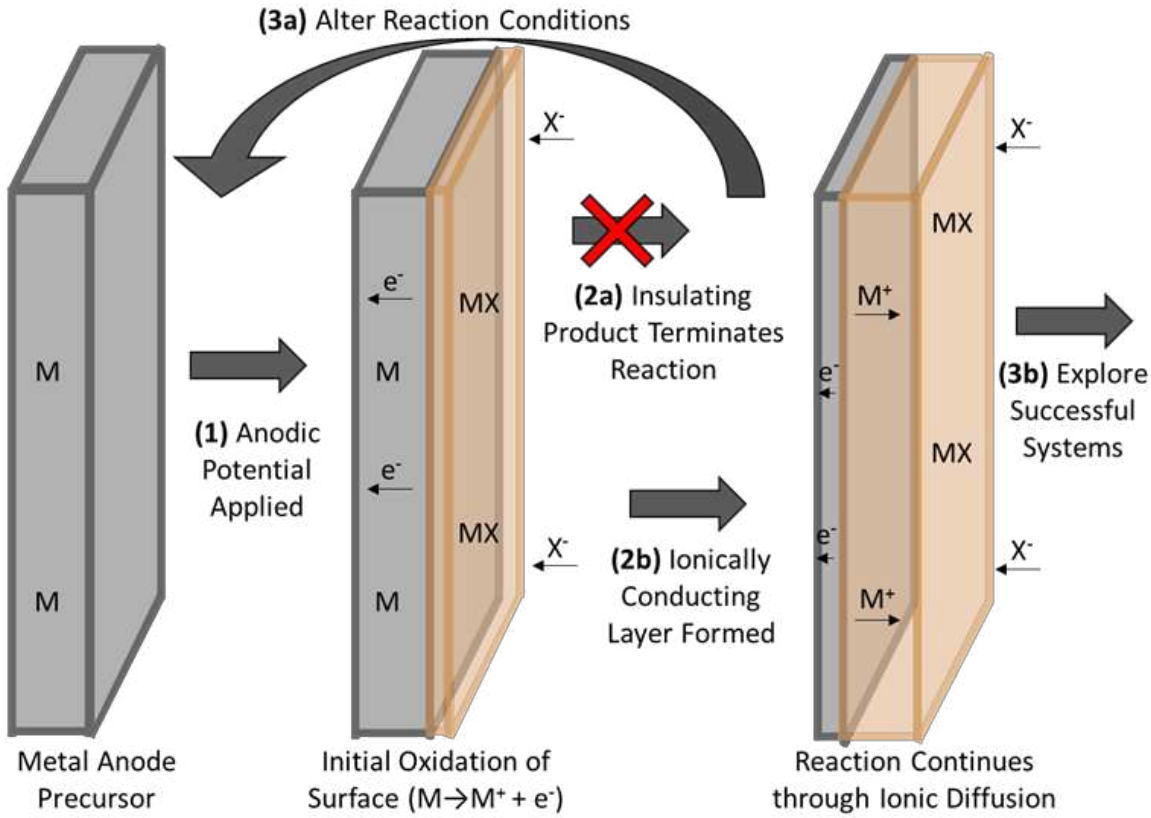

Figure 3.2 (1) Begin with a metal anode of the desired mobile ion (M and M+) and apply an oxidizing (anodic) potential in a solution containing reduced precursor ions (X-).

(2a) If the reaction between the oxidized metal and solution results in an ionically insulating product, then **(3a)** the reaction will cease and conditions must be altered and additional reactions performed.

(2b) If the reaction yields an ionically conducting material, the reaction can proceed as the mobile ion (M+) moves through the produced surface (MX) to continue reacting. **(3b)** Successful systems will be characterized exploring the composition, morphology, atomic structure, and ionic and electronic properties. These reactions can then either be further optimized or adapted to explore new systems

(2b). This means that whatever material is being formed necessarily has the properties of ion conduction and relatively low ion-transfer resistance. The thickness of the deposited film can be monitored and regulated by net current passed and the rate of reaction determined by applied

potential/ current density. This ionically conducting product can then be characterized and reaction conditions can be manipulated and optimized accordingly by adding dopants or changing electrochemical technique used (Figure 3.2 (3b)). By applying consistent over-potentials, ion-conductivity can be approximated by current density. Additionally, larger changes to established reactions can be made, such as switching the anode between lithium and sodium, or moving toward the study of multivalent mobile anodes. Through this iterative and explorative synthetic paradigm, new material systems can be targeted, and the resulting product properties can be explored.

3.3 The corrosion synthesis of AgI and related compounds

3.3.1 Motivation for studying AgI as an initial target and synthetic design

The motivations for using silver iodide (AgI) as the initial test system for anodization synthesis is that 1) it is a well-studied, known superionic conductor (SIC) at elevated temperature, 2) the product is a binary system with a single stable composition, 3) the electrochemistry is relatively straightforward with a focus on the Ag/Ag^+ redox couple and readily produced I^- solutions, 4) the electrode and electrolyte are stable, relatively cost effective, and able to worked with on in air at ambient conditions, and 5) there are a number of known related compounds and modifications to the simple AgI system that allow for continued work moving forward. Under ambient conditions AgI can exist as a mixture of the β phase, which is a hexagonal wurtzite ($P\bar{6}3mc$) and is the most thermodynamically stable phase, and γ phase, which is a metastable cubic zincblende ($F\bar{4}3m$).[7,33–35] These phases exhibit modest ionic mobility, on the order of 10^{-5} ($\Omega^{-1}cm^{-1}$) at room temperature, suggesting that the proposed driven ionic synthetic method can be pursued at or above room temperature, but AgI undergoes a phase change around 420 K, to the FCC α-AgI phase. This high temperature α phase is a SIC, with ionic conductivity greater than 1 ($\Omega^{-1}cm^{-1}$).

This drastic change in ionic conductivity corresponding to the phase change can be seen in Figure 3.3.A. The arrows in this figure indicate the melting point of the compounds shown, demonstrating that AgI has liquid-like ionic conductivity in the α phase while remaining solid. This is due to the α-AgI phase being described by a rigid body-centered cubic (bcc) sublattice of I^- (space group Im^-3m), while the Ag^+ ions can occupy any of the tetrahedral (red), octahedral (black), or trigonal (gold) sites as depicted in Figure 3.3.B.[7]

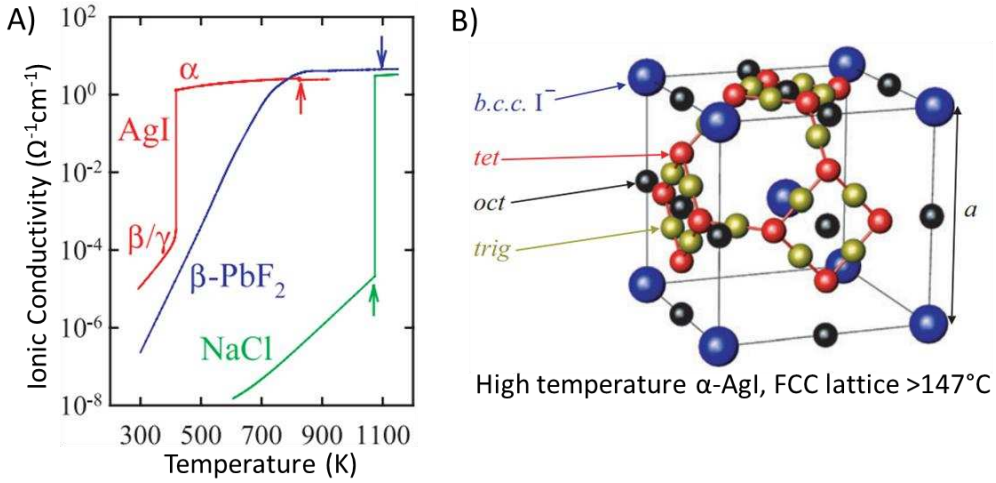

Figure 3.3. A) The variation of the ionic conductivities of NaCl, β-PbF2 and AgI with temperature. The vertical arrows denote the melting points of each compound B) The crystal structure of the high temperature α-AgI phase, showing the bcc anion sublattice and the locations of the octahedral (oct), tetrahedral (tet) and trigonal (trig) interstices. Figure modified from ref. 7.

This arrangement of Ag^+ ions in a highly disordered sublattice is what allows for the ionically conductive properties of the material, and as such is referred to as a "liquid-like" or "molten" sublattice of the Ag^+. While similar terms have been used to describe the behavior of other SICs, this is not a common crystallographic property of the majority of ionically conducting materials and therefore cannot be used as an indicator or predictor of material targets. Figure 3.3.A also contrasts the unique property of an abrupt change in properties for AgI to superionic conductivity as the result of a phase change, compared to another canonical "standard" ionic conductor, β-PbF_2, which shows the more typical trend of a linear increase in ionic mobility, with

high ionic mobility being achieved in the solid-state at elevated temperatures. These two ionic conductors are compared to NaCl, which is considered a non-conducting ionic compound, where the drastic change to high ionic mobility corresponds to the melting of the material, indicated by the green arrow in Figure 3.3.A.

While the phase space is still a point of study for the AgI system, with work being conducted to balance and isolate these phases more purely and exact the mechanisms for ionic conductivity and exact site preference of the high-temperature phase using neutron studies, those aspects of the material do not directly hinder the present motivation to study the synthesis of this material through anodization. To the best of this research group's knowledge, this synthesis of AgI using electrochemical corrosion has never been reported. There has been a report of CuI,[36,37] which will also be discussed and compared to later, but CuI does not exhibit such interesting properties related to ionic conductivities, and Ag has the added benefit of only one cationic oxidation state, which minimizes one aspect of the electrochemistry as opposed to having to balance the $Cu/Cu^{+}/Cu^{2+}$ oxidation states. Additionally, there are a wide range of related Ag systems, such as cation modified $RbAg_4I_5$ (a low temperature SIC) or anion modified Ag_3SI, which are much better understood and investigated compared to Cu analogs when considering ionically conducting materials.[7,38] These related compounds also demonstrate the rich compositional phase space that can be explored related to this base system. Initially however, AgI was targeted for learning purposes, proof of concept, and to begin to learn how to manipulate and control anodization synthesis of solid inorganic films.

3.3.2 Anodization reaction design, modifications, results, and conclusions for AgI and related systems

3.3.2.1 Generalized anodization synthesis from aqueous solutions and systematic modifications

The electrochemical anodization synthesis of AgI involves using a potentiostat (Gamry Reference 3000) to apply an oxidizing potential to a silver film in aqueous I^+ containing solutions. The aqueous iodide solutions were prepared by dissolving an iodide salt (either potassium iodide, KI, sodium iodide, NaI, or tetrabutylammonium iodide, TBAI) in Millipore water that was degassed through sparging with Ar. The majority of reactions used KI as the I^- source, and no appreciable difference was observed compared to NaI. Use of TBAI resulted in spotty and inconsistent films, and SEM and EDS analysis indicated there were amorphous organic deposits on films. Concentrations of I^- in solution were varied, and fresh solutions were produced for each series of reactions.

The silver anode is prepared by evaporating thin layers of chromium (15 nm), gold (100 nm), and silver (variable thickness) sequentially onto substrates via thermal evaporation. The substrates consisted of glass slides that were cut into pieces of ~1 cm x 5 cm and attached to the deposition stage using 2-sided copper tape. This process yields uniform films with controllable thickness. Initial studies were conducted using a thinner Cr wetting layer and without the use of the gold layer, but excessive corrosion led to film failure and uneven current densities across the film surface. Increasing the Cr wetting layer and adding the Au conduction layer resulted in more robust films and more uniform products. The use of thin metal foil substrates were also investigated, but the process of insulating the back of the metal films, mounting, and removing the Ag coated samples from the stage resulted in bending, yielding foils with variable surfaces and compromised Ag films. Additionally, the Au has the added benefit of not being susceptible to oxidation at the conditions investigated, so no decomposition of the substrate should occur upon excessive oxidation of the Ag. Following evaporation, the Ag films are highly pure and pristine with a mirror finish. Minimum variation to the surface is observable using optical and electron

microscopy. These films are observed to form a patchy white coating over time. Analysis of these films using scanning electron microscopy (SEM), energy dispersive spectroscopy (EDS), and X-ray diffraction (XRD) suggests the presence of a thin oxide forming. It was observed that this oxide film formed more rapidly when left on the benchtop, due to either exposure to the ambient conditions in the lab, and/or light exposure. Because of this, evaporated film samples were typically used within a week of preparation.

To set up a reaction the silver anode is placed vertically in an aqueous I^- electrolyte solution with a saturated calomel reference electrode (SCE) placed offset between the working electrode and a platinum mesh counter electrode, as is depicted in Figure 3.4. Later studies switched to using larger stainless steel mesh counter electrodes to increase surface area and minimize certain edge effects, with no appreciable changes observed to the electrochemical processes. The 3 electrodes are contacted using foil wrapped clips and the electrochemical reaction is controlled and monitored using a Gamry Reference 3000. The reaction and subsequent products can be controlled through manipulating a variety of parameters including concentration of iodide ions in solution, the electrochemical technique employed, reaction time, temperature, stirring, and the addition of other

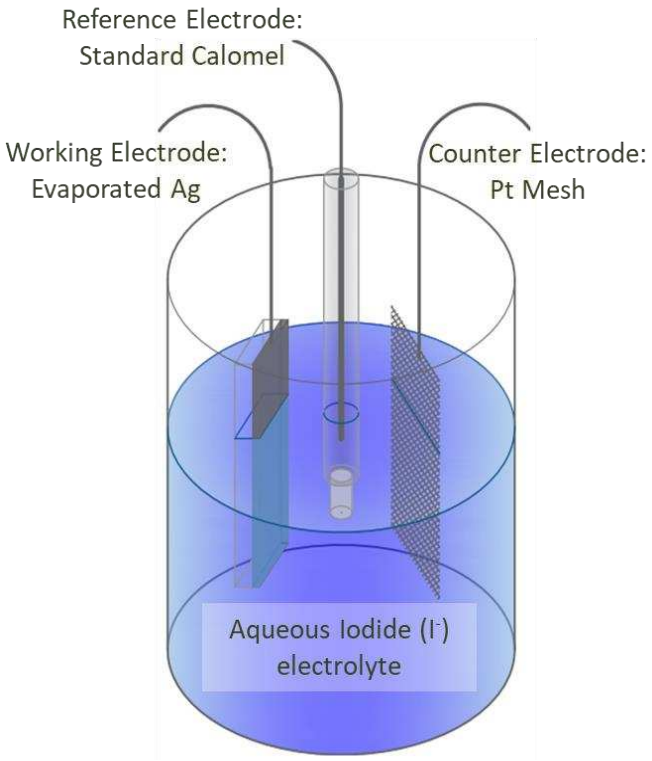

Figure 3.4. Graphic depicting the standard 3 electrode cell used to conduct the anodization synthesis of AgI.

constituents to the electrolyte solution. Using this reaction design, AgI has been able to be formed repeatedly and reproducibly through a series of anodization reactions.

Limited comparable studies were done using a Cu-foil anode forming CuI. These Cu films were prepared by covering the back of the Cu foil with Kapton tape so only the counter-electrode facing surface would react. These foils were then cut to ~1 cm x 3 cm strips, flattened, and the surface oxide was removed using an acid bath. Aside from the preparation and composition of the working electrode, reaction parameters and setup was analogous to the AgI reactions described above. This investigation came about as a way to compare to literature, as well as investigate systems with multiple potential oxidation states and move toward even more cost effective and device relevant ionically conducting materials.

3.3.2.2 Electrochemical anodization of Ag in aqueous iodide solutions: Results and discussion

Cyclic voltammetry: Cyclic voltammetry was done on aqueous I^- solutions (0.1 M) using a Pt working electrode, a Pt counter electrode, and a saturated calomel reference electrode (SCE). A representative CV is shown in Figure 3.5.A in which the potential was swept starting from open circuit potential to -1.0 V and +1.0 V vs SCE. The key features of this experiment are the onset of I^- oxidation above ~0.35 V and the relatively broad lower range of stability until water

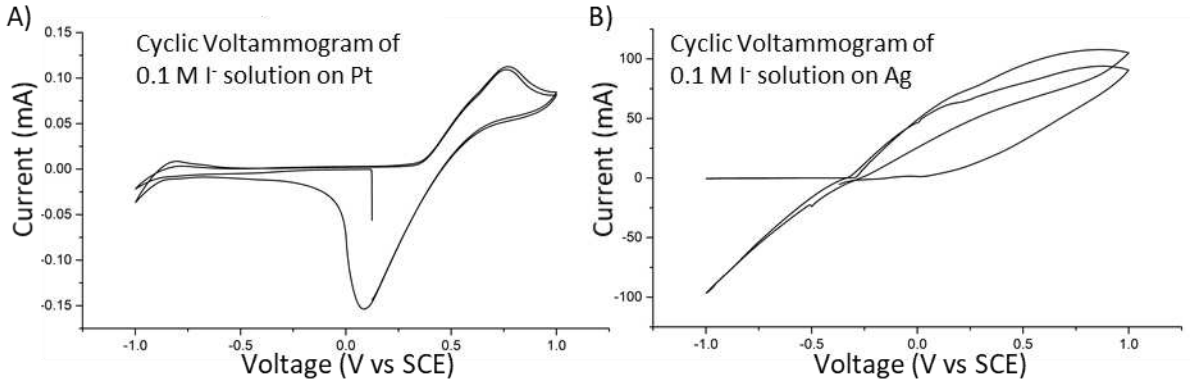

Figure 3.5. Cyclic voltamagrams (CVs) of 0.1 M I^- solution on A) Pt and B) Ag working electrodes from -1.0 V to +1.0 V vs a saturated calomel reference electrode (SCE).

electrolysis. Cyclic voltammetry was also done in the same setup using a Ag working electrode instead of a Pt working electrode, and a representative CV is shown in Figure 3.5.B. This voltammogram shows the onset of oxidation of Ag in the presence of I^- at ~ -0.3 V with some additional variation observed around 0.2 V. Therefore, the optimal operating voltage for anodization experiments was determined to be between approximately ±0.3 V vs SCE. Reactions were carried out above the upper end of the solution stability and AgI products were reproducibly formed under these conditions while also oxidizing the iodide in solution.

Electrochemical corrosion techniques: Multiple electrochemical techniques were employed to oxidize the Ag electrode including chronoamperometry (CA), chronopotentiometry (CP), chronocoulometry (CC), cyclic voltammetry (CV), and pulsed potential techniques. Chronoamperometry was the primary technique used initially, as a set potential is applied, and the resulting current is measured over time. An example of the data obtained using this technique is show in Figure 3.6.A along with a scanning electron microscope (SEM) image of the AgI film produced below. Multiple series of reactions were carried out comparing differences in potential over time, but as the analysis of the AgI products shifted away from imaging and electrochemistry toward diffraction, which will be discussed later, CC was used. Chronocoulometry applies a constant potential comparable to that of CA, but rather than applying for a given amount of time, the potential is held until a set amount of total current (coulombs) is passed. The motivation for this shift was to focus on making films of comparable thickness as opposed to focusing on the duration of the reaction, so the Ag substrate and relative intensities seen in powder X-ray diffraction patterns (PXRD) were more readily comparable. A representative potential vs time graph is shown in Figure 3.6.B for a CP reaction carried out with a constant current of 2.5 mA using a 0.1 M KI solution. A SEM image of the AgI film grown using these conditions is shown

below in the same figure. For the corrosion of the CuI system, constant potential techniques were used as comparable to that found in the Vishwanath study.[37]

The rough, highly facetted crystalline films shown in the SEM images of Figure 3.6. were determined to be AgI based on EDS and XRD characterization. Looking at both reactions and the subsequent films produced, it is demonstrated that AgI can be synthesized through electrochemical

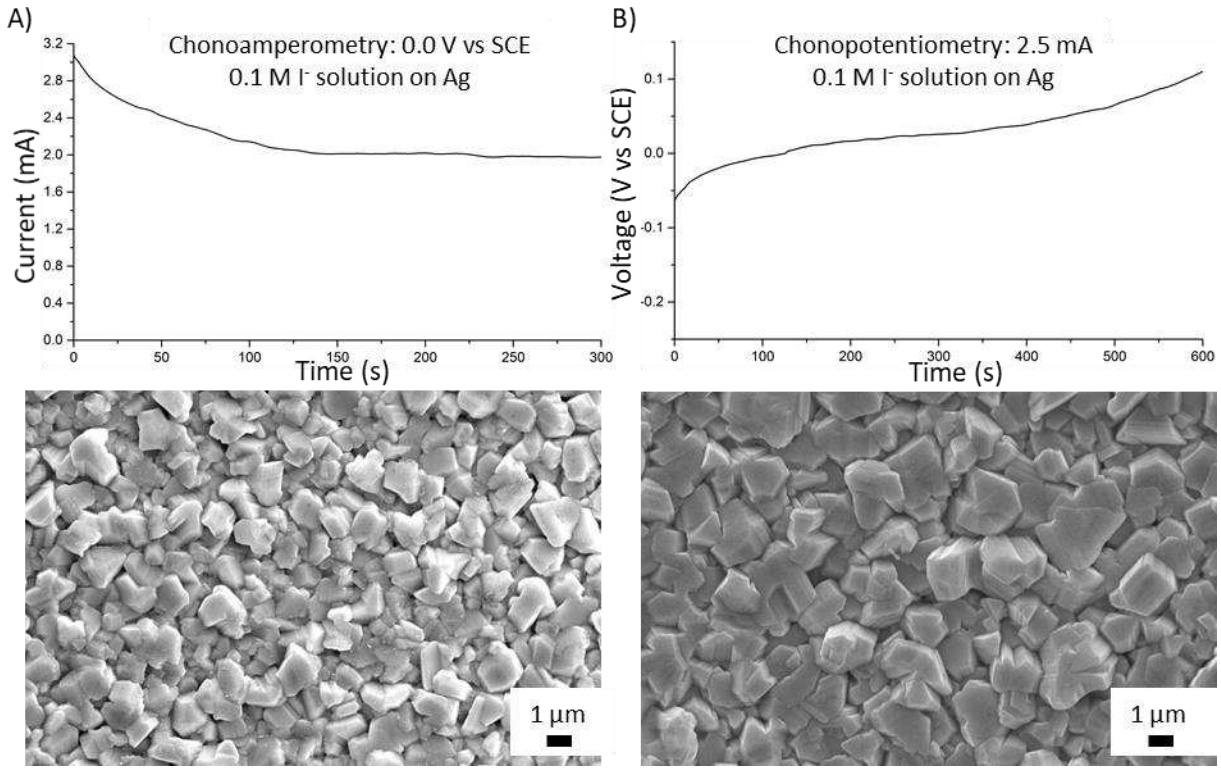

Figure 3.6. A) Graph of current vs time resulting from the chronoamperometric anodization of a Ag film in 0.1 M KI aqeuous electrolyte. **B)** Graph of voltage vs time resulting from the chrono-potentiometric anodization of a thin Ag film in 0.1 M KI aqeuous electrolyte. The SEM images below each graph depict the crystalline AgI product formed from the respective reactions.

anodization methods, and these results are reproducible given similar conditions, even when minor changes occur due to variations in current and potential. Additional reactions conducted using variable potentials applied such as CV and pulsed potential were conducted. These corrosion methods produced AgI, but no noteworthy observations were made beyond what was observed for the constant potential and current techniques and will not be presented for this material.

Scanning Electron Microscopy: Imaging of the anodized AgI and CuI films yielded a range of interesting results and insights into processes that may be occurring during synthesis as well as features of the products that may have impacts for their use in other applications. Figure 3.7 A-C show SEM images of the highly faceted CuI product that formed after a chronoamperometric reaction applying 800 mV vs SCE for 300 s to a Cu-foil in a 0.5 M KI solution. The resulting images show a difference in features across different regions of the product. Figure 3.7.A corresponds to the upper end of the corroded product as represented in graphic D, where the surface of the solution interacted with the submerged film. This region produced smaller, protruding CuI features along with incomplete or reduced extent of oxidation, as some metallic Cu was still observable as well as the film was more conductive overall (less charging effects in SEM). Comparing this upper product to the edge of the sample shown in Figure 3.7.B, a dense film of large CuI crystals (note the difference in scale bar) was formed. The middle portion of the sample C) has a consistent, yet highly facetted film of micron size crystalline

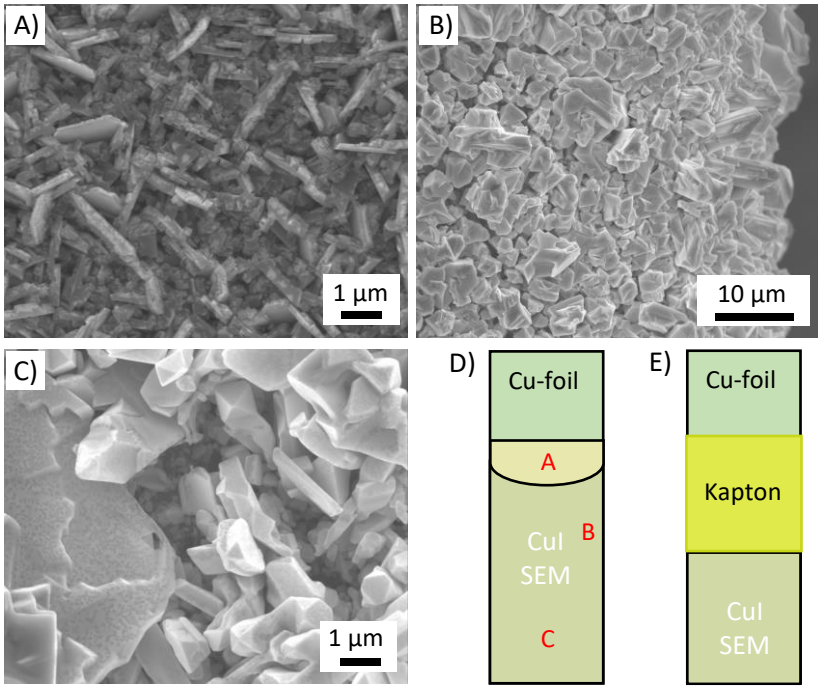

Figure 3.7. A CuI product was formed through applying 800 mV vs SCE for 300 s to a Cu-foil in a 0.5 M KI solution. SEM images A), B), and C) were collected from the regions of the sample as indicated in graphic D). These images show a variety of structures and feature dimensions despite being formed simultaneously. To prevent surface effects, Kapton tape was placed on the surface of the sample as shown in graphic E) and the electrode was submerged so the electrolyte solution went ~3/4 of the way up the tape prior to reaction.

CuI. Slight variation in surface brightness or apparent surface level features are the result of CuI decomposition under the electron beam resulting in small domains of metallic Cu.

These observations led to several systematic changes being implemented for both the Cu and Ag systems. The first change is indicated in Figure 3.7.E which involved placing a 1" stip of Kapton tape ~1 cm from the bottom of the sample. This provided two benefits, first, it minimized the edge effects seen at the surface of the electrolyte, and secondly, it resulted in a more consistent area of the reactive substrate being exposed. Previous studies had inconsistent depth of films, so when applying constant current or potential over time, different current densities were being passed, adding complexity to comparing across samples and trials. Additionally, the counter electrode was switched to stainless steel, allowing for a larger counter electrode cross section and an increase in overall surface area. This helps to create more uniform potential lines and therefore more uniform reactivity, helping to partially reduce the edge effects observed. Additional systematic variables were more carefully regulated such as ensuring parallel surfaces between electrodes and maintaining consistent distance between counter and working electrode (~1").

While the CuI reaction most clearly demonstrated the varieties across surfaces and directly led to the process improvements outlined, the majority of work was done on the AgI system. Solution concentrations were varied from 1.0 M to 0.01 mM I^-, but reactions were exceedingly slow below ~1 mM, and the majority of experiments used solutions between 1 – 100 mM. Initial studies focused on constant current (CP) reactions due to the interest in the kinetics of the reaction, and current passed can be related to rate. This resulted in 3 common morphologies of AgI products being observed. Representative images for these morphologies are shown in Figure 3.8 with A) showing dense films of large AgI crystallites, B) showing porous faceted product, and C) having pseudo 1-dimensional rods. The reaction conditions used for the synthesis of the exact products

being imaged in Figure 3.8 are given in the figure caption, but repeated experiments demonstrate that these images are representative of products formed under a variety of conditions.

Generally, dense films are made at low potentials or current passed, meaning these are formed at low rates of reaction. Similar products can be made at higher rates given sufficiently

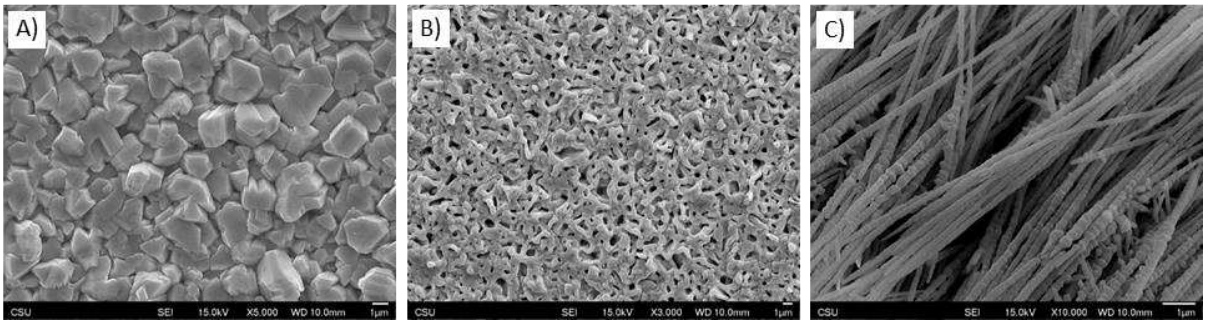

Figure 3.8. SEM images showing the three representative morphologies of anodically produced AgI products. A) Dense highly crystalline film synthesized using a 0.010 M KI solution and a constant applied current of 2.5 mA. B) Porous film from a 0.10 M KI solution and a constant current of 50 mA. C) Pseudo one-dimensional structure from a 0.01 M TBAI solution and a constant current of 5 mA.

high I^- concentration. When reaction rate is significantly increased (for example current densities greater than 20 mA/cm$^{2)}$ but I^- concentration is maintained between 10 – 100 mM, porous films are produced. The rod like structures shown in Figure 3.8 C) were formed through balancing reaction rate and diffusion of I^- in solution, and were formed when reacting 10 mM I^- with the Ag film at a current density of ~0.5 mA/cm^2 to ~5.0 mA/cm^2 (current densities are approximate due to how the glass sides were broken to form substrates and masking, resulting in a significant decree of surface area variability. Concentrations other than 10 mM were not tested to determine specific limits, but wires were not observed for I^- concentrations of ≥100 mM or <1mM.

While investigating different electrochemical techniques and reaction conditions, a patterning was observed on the surface of the silver iodide films which was determined to be metallic silver. An example of this can be seen in Figure 3.9, where the darker “spots” on the surface are silver, and the brighter material is AgI. This effect is also seen when the samples are

exposed to light for extended periods of time due to the relative instability of the material, which also corresponds to a visible change in the appearance of the film. Due to using electrochemical synthesis, the surface of these materials can be systematically manipulated using variable potential techniques. This is an interesting property that has potential impact on the properties and performance of this and similar materials for applications such as a reactive surface for photoelectrocatalytic reduction.

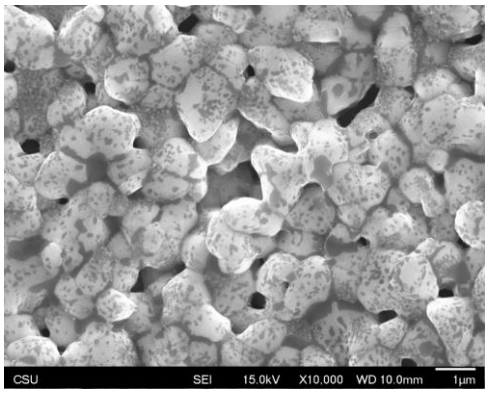

Figure 3.9. SEM image showing the patterning of reduced silver on the surface. This was synthesized using cyclic voltammetry, cycling between -1.0 V and 1.0 V vs SCE. Similar results can be obtained through pulsed potential techniques.

Powder X-ray diffraction: X-ray diffraction (XRD) was conducted on the majority of films synthesized, further supporting that AgI had been successfully produced. Several representative XRD patterns for a variety of conditions are shown in Figure 3.10 along with a pattern of the AgI substrate and a simulated pattern of AgI based on the β-AgI hexagonal wurtzite ($P\bar{6}3mc$) phase. The reactions represented in Figure 3.10 were all carried out using a 100 mM I^- precursor solution and a variety of electrochemical techniques and times of reaction. While all products have peaks that clearly align with the simulated AgI pattern, the relative peak intensities vary greatly. Most notably, there is a significant difference to the two peaks on the left corresponding to the (100) plane at ~22.3 degrees 2θ and the (002) plane at ~23.7 degrees 2θ. This observation motivated additional study into what causes these inconsistencies.

Series of reactions were done where variables of solution concentration, reaction time, applied potential, and current density were systematically altered. This produced a significant number of samples and corresponding data, but no definite conclusions were drawn when comparing diffraction data, SEM images, and reaction conditions. When looked at individually, certain series of diffraction data seemed to show trends, such as a consistent increase in the relative peak intensities of the (100) plane compared to the (002) plane for samples produced by increasing the current from 1mA to 20 mA for a system containing 10 mM KI. However, when comparing the morphologies observed for this series, which included both the rod-like structures, and more porous structures, to diffraction trends of similar morphologies and other reaction conditions, no clear trend was able to be determined that adequately addressed all observations. Likely there are a number of competing factors, and the similar structures may be a result of "local minima" in a varied 3-dimensional reaction landscape.

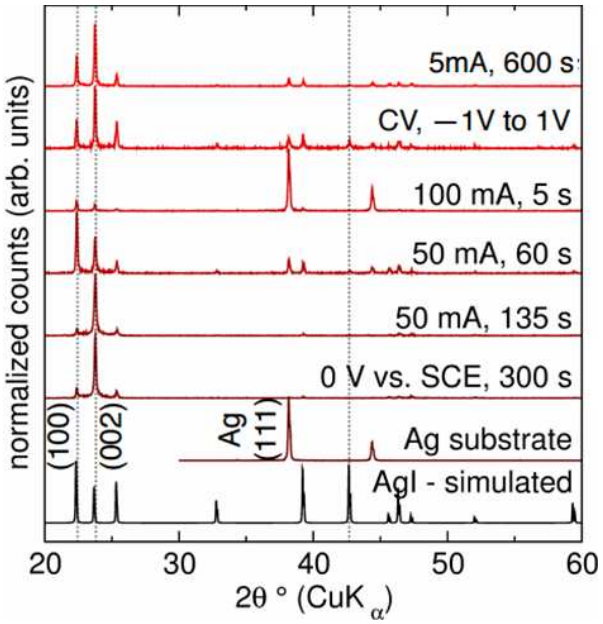

Figure 3.10. Powder XRD patterns of AgI produced through a variety of anodization reactions. All reactions represented here used 100 mM KI solutions. The peaks corresponding to the (100) and (002) indices are noted due to their variable intensities and the (103) is highlighted due to the apparent lack of signal apart from the CV pattern.

While conducting this more cross-sectional study, samples continued to be studied and hypotheses generated surrounding explanations for varieties of peak intensities and deviation from expected patterns from literature or modeled patterns. In order to fit the collected diffraction patterns, two possible rationales were proposed. The first hypothesis, strongly motivated by the

presence of the pseudo-one-dimensional AgI products, was to use preferred orientation. Examples of fitting the data of a film produced through the chronopotentiometry reaction of a film where 1 mA current was passed for 120 s in a 10 mM KI solution is shown in Figure 3.11 A) and B). This is one film that was part of the series mentioned in the previous paragraph and is notable due to the greatly reduced intensity of the the (100) plane compared to the (002) compared to predicted peak intensity as seen in Figure 3.10. While a fit can be calculated that appears to more accurately represent the data, the uncertainty estimate ($\sigma[y_{O,I}]$) used was unrealistic and the weighted profile R-factor still showed significant deviation from expected values. Similarly, the potential presence of the metastable γ phase (zincblende) could influence peak intensities due to the primary

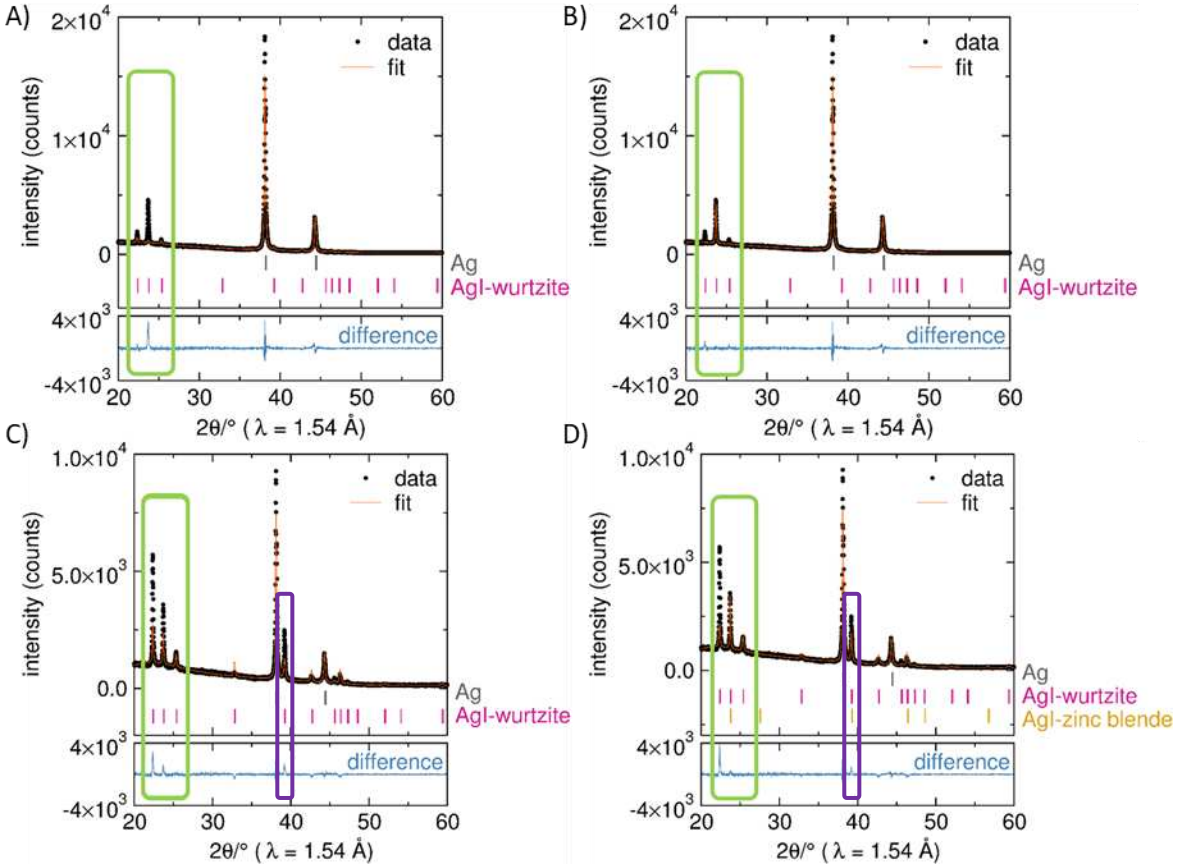

Figure 3.11. Diffraction patterns of 2 samples of AgI fitted using manipulated Rietveld refinements, with difference in observed vs calculated intensity shown in blue. The patterns A) and B) are the same pattern, but B) is fit with a preferred orientation parameter for the (002) plane. The patterns C) and D) are the same pattern, but D) is fit with a both wurtzite and zincblende AgI phases.

reflections of this phase overlapping with the wurtzite (002) and (110) planes around 23.6 degrees 2θ and 39.2 degrees 2θ respectively. This approach was utilized for a sample synthesized through the chronopotentiometry reaction of a film where 20 mA current was passed for 60 s in a 10 mM KI solution, and those results are shown in Figure 3.11 C) and D). When utilizing multi-phase fitting including both the β and γ phases of AgI, no drastic improvement of overall fitting was achieved. For the mixed phase fitting shown in Figure 3.11 D) corrections for preferred orientation were not used.

Additional work was conducted pursuing *in-situ* diffraction analysis using an electrochemical cell which is designed to be integrated into the Bruker D8 Advance DaVinci stage and operated with an external potentiostat. The cell measures the diffraction of a thin material through a Be window, which is also used as the electrical contact for the electrode of interest. This cell is ideally used for Li-ion or Na-ion systems, typically for anode studies in which the mobile ion is being intercalated or alloying with an anode material under a cathodic (negative) potential. This type of reaction is preferred as the Be window has a relatively low reduction potential, meaning there is the possibility to oxidize that component under oxidizing potentials, resulting in a corroded surface which limits or ruins the cell's capabilities depending on the extent of the reaction. Despite this the *in situ* XRD cell was tested using Cu metal foil and Ag evaporated onto a thin Al foil, which were then oxidized in the presence of an aqueous solution of KI (0.10 M). The thin Cu and Al foils were able to protect the Be window and anodization of the material occurred, but the metal iodide products formed were not observed through diffraction due to the X-rays not penetrating the film to the deposited surface. In order to measure the reactive surface directly, attempts were made switching to a Cu-foam electrode, which permitted the solution to penetrate the electrode to the Be window, allowing electrochemically active surfaces on the upper

portion of the foam to be measured through diffraction. When an oxidizing current was applied (10 mA) no change was observed in the diffraction pattern after repeated reactions: multiple chronopotentiometric scans applying 10 mA for periods of time from 2-10 minutes, taking diffraction after applying current. Following these tests, corrosion had visibly occurred on the surface of the Be window as well as the Cu, and subsequent tests were not conducted. Because of this, *ex-situ* electrochemistry and diffraction was used to collect all data presented.

The data presented in this chapter is a small subset of the overall data analyzed, with key, representative pieces of information and data being presented, which were used to inform research decisions and contribute to developing hypotheses.

3.3.2.3 Electrochemical anodization of Ag and Cu in aqueous iodide solutions: Conclusions

These results demonstrate the successful and reproducible synthesis of silver iodide (AgI) through electrochemical anodization techniques, as well as reproduce previously reported synthesis of CuI. While the formation of AgI using anodization was expected to be successful, the variety of product morphologies was surprising and the crystallographic data presented additional considerations relating to the complexity of synthetic processes, even for a system that was intended to be straightforward. Through investigating these products, morphology and reaction conditions do not adequately describe inconsistencies observed in relative peak intensities of the AgI films produced. While attempts to fit the data using preferred orientation or mixed phases was unsatisfactory, this does not rule out either aspect from contributing to these results. In the case of the rod-like structures particularly, it is highly likely that there is a preferred orientation to the products being produced.

One aspect to data collection and analysis that was not significantly discussed is the instability of the products. The AgI films decompose over time, forming deposits of metallic silver.

This process is accelerated with exposure to light, so all samples were kept in drawers in petri-dishes covered in foil if analysis could not be done quickly following synthesis. This decomposition occurs at a significantly faster rate upon heating or in an electron microscope. Due to the decomposition of the product in the electron microscope, no meaning transmission electron microscopy (TEM) or electron diffraction was able to be conducted, even following evaporating a thin film of gold onto the surface. This prevented the direct characterization of lattice planes of individual crystallites or rods formed, which would be a straightforward method to determine the orientation of growth.

While the synthesis was described along with the products' microscopic morphologies and diffraction patterns, the films also varied in color from white to a gradient of yellowish greens to dark browns. The rod-like structures were consistently white in color, as would be expected of pure AgI. The films varied in color depending on duration of reaction and applied potential. This likely indicates the integration of either nano-domains of Ag metal, or likely the presence of triiodide or iodine species being incorporated into the films. If the AgI films contain domains of metallic Ag, triiodide substituted for I^-, or trapped I_2, this not only explains the colors observed, but would also create significant strain and distortion throughout the as-synthesized films. Therefore, it is likely that the presence of these species contributes significantly to the observed differences to the diffraction patterns. While the measurement of nano-Ag may be difficult due to the convolution of any data as a result of the previously described ambient decomposition of AgI, an investigation into the presence and abundance of I^-/ I_3^-/ I_2 in the film could prove insightful. These species could be measure through the use of Raman spectroscopy, or potentially X-ray photoelectron spectroscopy (XPS). Confirming the incorporation of oxidized iodide species could contribute to better understanding reaction conditions needed to optimize film properties

depending on the desired application, but that does not directly contribute to the present study of investigating electrochemical anodization as a synthetic method for ionically conducting materials.

The various morphologies observed were originally hypothesized to demonstrate the effect of balancing the solid-state diffusion conditions of the Ag^+ through the deposited product and the diffusion of the anionic I^- precursor in solution. However, this is not consistent with all observations made regarding product morphologies, most notably the rod-like structures. As a result, a new hypothesis is proposed for the production of the observed crystalline AgI structures formed via the electrochemical anodization method, which we had previously not considered and greatly impacts how the technique can be used to selectively target ionically conducting materials. This insight relates to the fundamental mechanism of film formation through oxidative syntheses as represented in Figure 12. It was previously predicted film formation would initially occur through an anodic electrodeposition (Figure 3.12(A)) where metal cations produced electrochemically would react at the metal surface with counter-anions from solution forming a relatively uniform thin film. Following this film formation, in order for the reaction to proceed, metal cations would diffuse through the thin film, thereby continuing to react with counter-anions at the precipitated film surface, depositing subsequent layers of the product. An alternative synthetic mechanism is now being considered in which products are formed through a process of "anodic electrocrystallization" (Figure 3.12(b)). In this process the electrochemically generated cations are locally solubilized due to the applied potential, initially reacting with counter-anions and nucleating crystalline deposits on the substrate surface due to the low solubility of the salt product. Following this nucleation, cations continue to be solubilized into the electrolyte solution, where they then react with the counter-anions present and form precipitates due to the low solubility of the salt species. The morphology of precipitates is then determined by a balance in

concentration and diffusion of the dissolved anion precursor and the local solubility, diffusion, and oxidation of the metal cation.

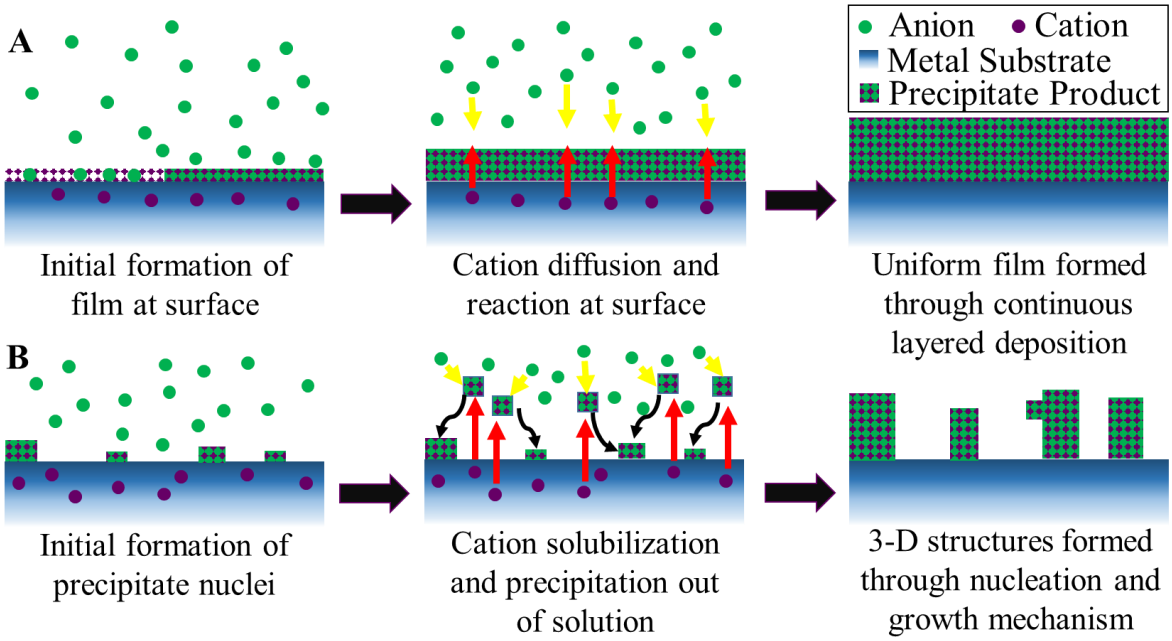

Figure 3.12. Schematic of two potential mechanisms of product formation through electrochemical oxidative synthesis. **A)** Anodic deposition through the uniform diffusion of ionic species through a thin film. **B)** Electrocrystallization mechanism occurring through the local dissolution of cationic species into solution and subsequent precipitation of an insoluble salt. This follows a nucleation and growth process which can yield a variety of 3-dimensional structures being formed depending on reaction conditions.

Given the variety of morphologies we have observed for the AgI and CuI products, we now believe that these products are forming through this described electrocrystallization mechanism. This conclusion is vitally important as it means products formation is not being regulated or driven through the solid-state diffusion of metal cations, as was the original proposal of the project. Therefore, modifications to reaction design are necessary in order to force conditions that result in the ion-diffusion limited synthetic process. Initial tests involved conditioning the precursor metal substrate to produce a uniform thin film of the salt on the surface. Completely passivating the metal film would prevent exposed metal sites that could allow for the direct dissolution of cations into solution, which is required for the electrocrystallization mechanism to proceed.

Through passing low oxidation currents for an extended period of time in relatively high concentration anion solutions, initial passivating surfaces can be formed. After initial passivation, reaction solutions can be manipulated, and higher currents or other electrochemical techniques can be employed to attempt to kinetically drive reactions forward. Limited attempts were made using such techniques on the AgI system, which appeared to result in the formation of a dense film of crystalline products with large grain sizes upon initial treatment. Following this however, when attempting to force cations through this surface by applying greater anodizing potentials, either no current was passed at modest potentials due to the insulating nature of the products, or at higher potentials, films became unstable and degraded, resulting in precipitates flaking off into solution. This stripping of the passivating surface is analogous to anodic electropolishing techniques employed to remove surface oxides from metals. Achieving a balance between cation solubility, anion reactivity with the electrode and general solubility of interesting precursors and developing passivating surfaces that are both robust and allow for ionic mobility has proven to be a significant challenge.

3.4 Targeting alternate ionically conducting systems

3.4.1 Na_3PS_4

The sodium fast-ionic conductor Na_3PS_4 was identified early on as a synthetic target for the anodization project. While investigation into the AgI system continued on the benchtop, targeting a system which involved electrochemically reacting a battery-relevant alkali metal with the intention of demonstrating the production of a solid electrolyte on the metal anode surface was pursued. Investigation of the Na-P-S system was met with great challenges, with most problems pertaining to finding acceptable solvents and soluble precursors which could together form an adequate electrolyte containing some form of anionic P-S compound. The initial objective for the

anodization synthesis of Na_3PS_4 began with a goal of finding a way to have the correct charge of precursors in the solution for the oxidized sodium to react with (i.e. P must be 5+ and S must be 2-). In order to have the correct charge solvation of P_2S_5 was initially targeted. While CS_2 was identified to be able to dissolve thiophosphate compounds, it was also discovered that CS_2 is not a viable solvent for use in electrochemical systems (Figure 3.13). The cyclic voltammogram in Figure 3.13 demonstrates that the solution reacted over all measured applied potentials, and the solution readily darkened during the analysis with significant formation of precipitate. To make this system viable for testing as a precursor to electrochemical anodization, a combination of a new solvents and supporting electrolytes that could be mixed homogeneously into CS_2 was investigated. Initially a solution of $TBAPF_6$ dissolved in acetonitrile was tested due to the well-established literature using such a system for electrochemical applications. Upon mixing the acetonitrile solution with CS_2/ P_2S_5 system, the two solvents proved to be immiscible and readily separated.

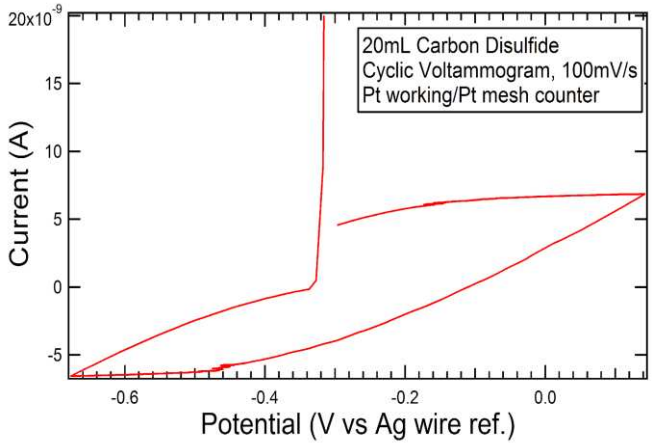

Figure 3.13. Cyclic voltammogram of 20mL carbon disulfide between -0.7 V and 0.1 V vs Ag wire reference. Platinum working and platinum counter electrodes were used at a scan rate of 100mVs^{-1}.

Many additional mixed solvent experiments yielded similar results, testing combination of MeCN, THF, and various carbonate systems otherwise used for Na-ion battery electrolytes. One potential combination was identified of a 1:3 ratio of CS_2 : DMF being initially promising. Cyclic voltammetry was performed on these combined solvents using $TBAPF_6$ supporting electrolyte without dissolved P_2S_5 to identify the electrochemical stability window of the solution, which was

found to be approximately 1.5 V. Outside of this window visual degradation of the solvent was observed resulting in discoloration. Moving forward, the $TBAPF_6$ was substituted with $NaPF_6$, to prevent any unwanted side reaction with the TBA, and P_2S_5 was reintroduced into the solution and initial electrochemical testing using a small platinum working electrode in a two-electrode setup with a platinum counter suggested the solution was stable at open circuit potential with an operating voltage of around 1 V. However, when moving from a platinum electrode to a sodium working electrode, spontaneous reaction of the solution and the Na electrode surface occurred. The solution rapidly changed color with the Na surface fouling and pitting. Leaving the sodium in the solution overnight resulted in the consumption of the sodium metal in the solution, with limited precipitate forming. No data was collected for the precipitate, and any analogous Na products were assumed to be unstable in that solvent system.

Additional work on the system involved collaborating with the Dr. Martinolich of the Nielson group who synthesized Na_3PS_4 through solid state techniques. This allowed characterization and analysis of the target material, as well as testing for solubility and solution stability. The goal was to find a solvent system which the Na_3PS_4 was insoluble in and stable with (did not appear to decompose the solid powder or discolor the solution or powder) and then purse reverse engineering a method or chemical system that could decompose the product resulting in the solublization of the P-S constituent. The logic was to pursue essentially a metathesis reaction in which the non Na-P-S precursor is initially soluble in a solution which the Na-P-S would be insoluble. The reaction would then proceed yielding a soluble theoretical P-S product, and an insoluble NaX product. This precursor could then be used to attempt the electrochemically driven reverse reaction, and removal of Na-P-S product in order to investigate any results of producing the material electrochemically instead of through traditional solid-state methods. No such system

was discovered, but the theoretical concept is still valid for pursuing electrochemical anodization in the future. An additional recommendation for future directions would be to investigate ionic-liquid or molten-salt type electrolyte solutions, or potentially some type of micellular or water-in-salt system which could solubilize relevant precursors but not react with a metal sodium electrode until the external oxidative potential is applied.

While investigating the CS_2 : DMF solvent system containing P_2S_5 and $NaPF_6$, due to the failure upon addition of the Na metal electrode, the use of a Cu electrode was speculated. While of less relevance to device integration than their Na and Li counterparts, Cu-based ionic conductors are established in literature, including Cu_3PS_4 and related compounds. Despite the spontaneous reaction observed with Na, the previously prepared P_2S_5 solution did not appear to appreciably react with a Cu electrode with an oxidative potential applied within the electrolyte's solubility window. Due to the complications that arose with the Na system, focus shifted toward Cu-ion conductors. This continued to build on the work established by the AgI and CuI systems but moved toward systems with more complex electrochemistry and compositions.

3.4.2 Advanced Cu-ion conductors and proposed Cu^+/ Li^+ ion-exchange system

3.4.2.1 Pursing chalcogenide anions: initial reactions using sulfide solutions

One of the few literature examples of non-oxide corrosion synthesis is on the formation of Cu_2S and CuS.[39] Limited preliminary initial investigations were conducted on this system to compare experimentally synthesized products to literature reports. As such, no attempts were made to limit cation solubility or unchecked growth of structures into solution as described at the end of section 3.3. Electrochemical anodization reactions were conducted based on the Kar report, and analogous CuS structures were able to be produced including rectangular crystallites, and wavy 2D sheets as shown in the SEM images of Figure 3.14 A) and B) respectively. Also synthesized

through variations to the synthetic parameters were more dendritic plate-like structures not included here, but represented by Figure 3.14 image C, which is from the Kar Paper.[39] Figure 3.14, image C and D are from the Kar paper which was investigating anodically synthesized Cu_xS for its use as a photoreduction electrode material. While the synthetic mechanism does not directly affect the utility or performance of the material for the purpose of their report, the authors describe the growth process and explain the observed morphologies as a result of Cu-ion diffusion through the platelets to the edge allowing for continued growth as shown in Figure 3.13.D. If this is true, then it means these platelets have particularly good Cu-ion conductivity along the crystalline axis related to that growth direction, and we should study that system. However, I suspect the products may be growing through an anodic electrocrystallization mechanism.

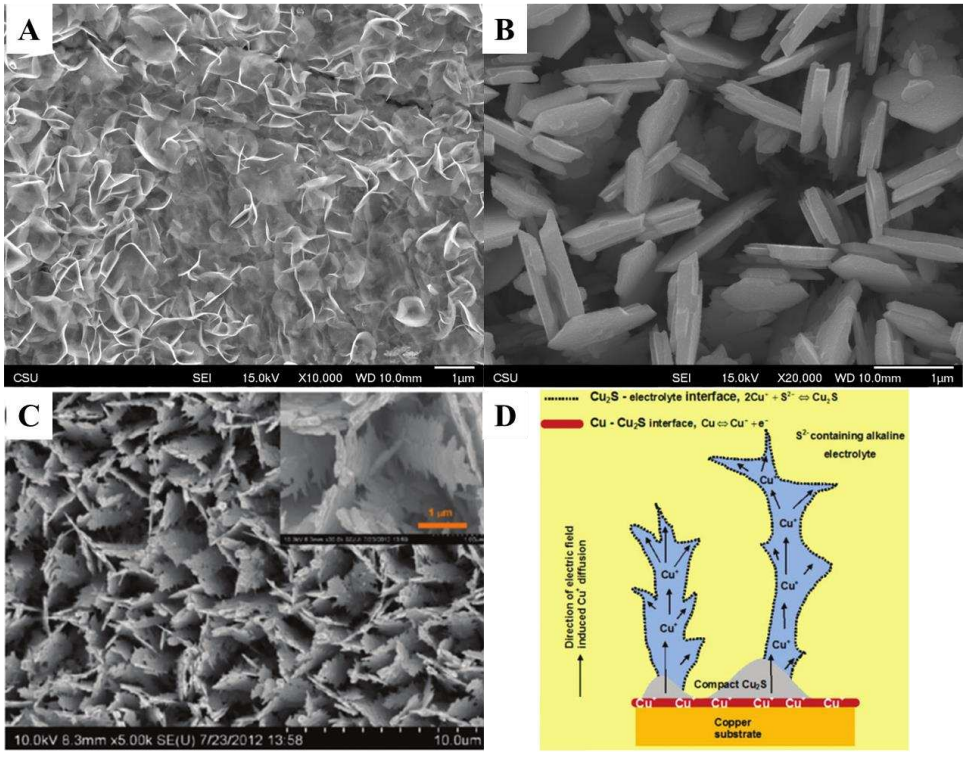

Figure 3.13. A) SEM images of wavy 2D sheets of Cu_xS and **B)** formed via electrochemical oxidation. **C)** SEM image of platelets of Cu_2S reported by Kar and **D)** a schematic explanation of the growth mechanism through Cu^+ ion solid state diffusion through the product.[39]

While the structures are related to those of the AgI and CuI systems, much less work was conducted, and the proposal of the electrocrystallization mechanism as the primary synthetic route for these products is based primarily on qualitative observation and chemical intuition. This system may be ideal to be able to provide insight into which growth mechanism is occurring through measuring the electrochemical properties of the larger platelet structures. Through reproducibly synthesizing these structures over a series of time scales, reasonable length estimates could be measured in the SEM, and longitudinal growth rates could be estimated. Through knowing the duration of the electrochemical synthesis and approximate maximum length from base to dendrite tip, a minimum net ionic conductivity for the Cu^+ ion can be estimated, assuming it is growing through the solid-state-diffusion method. These platelets could then be removed from the growth substrate and deposited onto an insulating slide, and electrical contacts could be made to single sheets using E-beam and optical lithography. Electrochemical analysis can be conducted on a single platelet, along the axis of growth, to determine ionic conductivity. The electrochemically measured ionic conductivity could then be compared to the minimum ionic conductivity calculated based on the estimated growth rate of the solid products. In the event that the calculated growth rate for the crystals is greater than the measured solid ionic conductivity, then some type of solution based electrocrystallization is likely the mechanism. If the measured rate of solid ionic conductivity is greater than or equal to the calculated rate of growth, than either process is possible and additional investigations are required to disprove either method.

A test reaction was done using leftover Ag substrates in the sulfide solution following the Cu reactions. The Ag was able to be electrochemically corroded resulting in a dark grey film indicating the formation of Ag_2S. No additional work was done on this system as it did not directly correlate to the objective of targeting ionic conductors. Generally, the work on the sulfide anion

system was limited, as it was mostly done in tandem to the work being conducted on the Na_3PS_4. Neither returning to this system, nor switching research efforts to pursuing this and related systems sooner was an oversight, and a shortcoming of the presented work.

3.4.2.2 Pursing chalcogenide anions: future directions

While neither CuS, Cu_2S, nor Ag_2S are significantly relevant to the study of ionically conducting materials, $Cu_{2-x}Se$ does display appreciable ionic conductivity. Pursuing the anodization synthesis of the Cu-Se phase space is an exciting next step that is proposed to be a practical and attainable target. The production of the various compositions and structures related to Cu-Se system are established for solid state reactions, as well as solution reactions and even nanoparticle synthesis. Therefore, investigating the ability to control and manipulate the oxidation state of Cu-Se products through electrochemical methods would allow for the as synthesized products to be directly compared to the purity, morphologies, and material properties of comparable products formed through a variety of methods. Additionally, the complexity of the phase space and balance of Cu oxidation state may require the synthetic control to be more finely tuned and potentially showcase the value of electrochemical synthesis if it is successful. Looking forward to pursuing such a synthesis, several synthetic considerations will be briefly introduced.:

While Na_2S was able to be purchased and used for the Cu-S and Ag_2S reactions, Na_2Se is both less stable in aqueous media and significantly more expensive. Using Na_2Se as a precursor source for preparing aqueous Se^{2-} electrolyte solutions is still a valid starting point, and there are literature preparation methods that can be used to synthesize Na_2Se with sufficient purity and low cost to make these studies practical. An additional reagent of potential interest was initially identified as a source of anionic sulfide during the study of Na_3PS_4 which is Lawesson's reagent, as seen in Figure 3.14, but the Se analogue (Woollins' reagent also shown in Figure 3.14) is also

commercially available. This molecular precursor has the potential to be dissolved in a variety of electrochemically relevant organic solvents, and could then be a stable, yet moderately costly precursor for the $Cu_{2-x}Se$ studies.

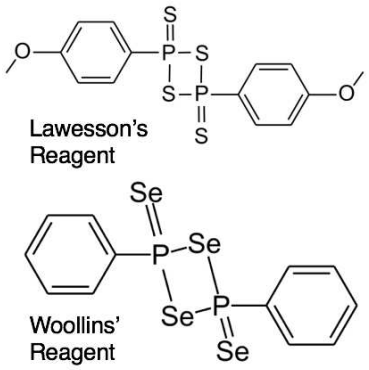

Figure 3.14. Chemical structure of Lawesson's reagent and Woollins' reagent.

The other direction pertaining to the future direction of chalcogenide ion studies should be to investigate the electrochemical anodization synthesis of Ag_3SI. Having been able to demonstrate the anodization synthesis of both AgI and Ag_2S from aqueous electrolyte solutions containing the anion precursor that was prepared through dissolving a sodium salt, it is the logical next step to combine these syntheses and determine if a product can be consistently produced which contains a mixed anion lattice.

3.4.2.3 Proposed Cu^+/ Li^+ ion-exchange system

One system conceived during the investigation of these various ion-conducting electrochemical systems was the concept of a "mixed ion conductor." It was proposed that through synthesizing a Cu-ion conducting solid electrolytes, that there would be the potential to incorporate this product into a system where cation exchange can be electrochemically driven in the solid state. In this case the objective would be to synthesize a Cu-ion conducting solid and exchange the Cu^+ for Li^+. This would be accomplished through reducing the Cu^+ from the electrolyte onto a Cu electrode with the counter electrode being Li which is in turn oxidized to Li^+ and diffuses into the electrolyte as shown in Figure 3.15. Lithium and copper were selected for this concept due to both being used in a variety of fast ion conducting architectures as well as having comparable ionic radii.

Investigation into mixed-ion conducting materials and device design may be of interest due to electrochemically driven all-solid-state cation exchange a relatively unexplored scheme. It is reasonable to expect that for certain systems crystalline structure can be maintain throughout the Cu^+/ Li^+ ion-exchange process due to the comparable ionic radii. If structure is maintained, the resulting electronic and ionic conducting properties of the mixed-ion electrolyte will contribute new information for the field of ionic conductors. Additionally, if this ion exchange is reversible, then this has the capability of potentially functioning as an all-solid-state battery architecture, or at least for use in ion-exchange membranes or other applications. For a system using a Li/Cu metal electrode structure, the difference in their standard reduction potential is ~3.5 V. As standard reduction potentials are determined by aqueous solutions, the actual cell voltage would need to be measured for individual systems of solid ionic conductors. In between the anode and cathode, the volume of the Li^+/Cu^+ conducting solid electrolyte and the ability to selectively and reversible plate the two metals would determine the maximum potential capacity of the cell. As this such a device would function through the plating and stripping of the metals on both sides as shown above in Figure 3.15, the amount of electrons that could practically be stored or released would be determined by the amount of the Li^+/Cu^+ ions the electrolyte can exchange. If such a system could be produced, it would be different from the lithium solid state systems otherwise being investigated, as capacity will no longer be reliant on the cell's cathode or anode. Similarly, such a system would have an

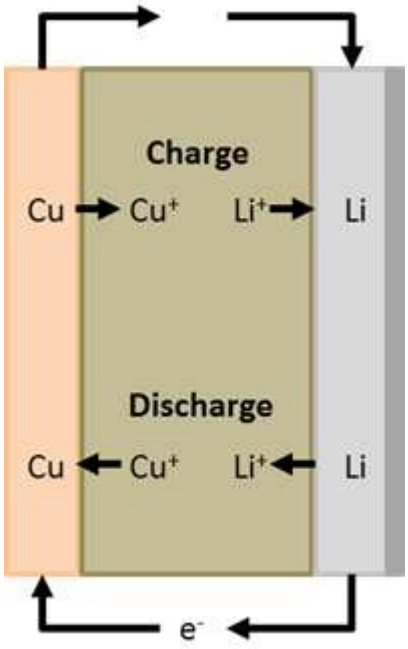

Figure 3.15. Depiction of a mixed Cu^+/Li^+ exchange system.

even greater energy density than lithium solid state systems, as copper is denser than any typical Li cathode materials.

While this was an interesting hypothetical system, upon further investigation it is unlikely to operate in any manner close to the described method. The potential required to plate Li^+ onto the Li surface is obviously well below the plating potential of Cu, so any Cu that can make it across the electrolyte would plate out onto the Li surface. Upon discharging, it is impractical that all Cu^+ would be plated onto the Cu metal cathode and replaced by Li, therefore, some would remain throughout the electrolyte, which could then subsequently migrate to the Li electrode during charging and plate out, consuming irreversible energy and degrading the cell potential. As a result, the battery would likely fail quickly in the as-described setup, resulting in a minimization of cell potential, and a mixed Li^+/Cu^+ conducting electrolyte with some energetically minimized composition of Li^+ and Cu^+ distributed throughout the structure. This last point however is of interest, as using pulsed potential or cyclic electrochemical methods to drive the reversible exchange of ions into and out of a structure, could act to result in the formation of ionically conducting side products, or some material that exhibits a higher overall ionic conductivity due to the disorder of mixed mobile ions.

A series of potentially relevant starting materials for such an investigation was identified including Cu_6PS_5Cl, Cu_3PS_4, Cu_7PS_6, $Cu_{2-x}Se$, and $LiS_2(P_2S_5)$. These were considered due to literature precedence for exhibiting sufficient ionic conductivity and relation to other experimental work being conducted at the time. A series of objectives for this project was outlined, beginning with a Cu-ion conducting material due to the cost benefit and ability to work with it under ambient conditions. Once synthesized this material could be characterized and it's electrochemical properties measured. Once a baseline of properties was established, it would be placed into a cell

comparable to that shown in Figure 3.15, the reduction of Cu^+ and Li^+ incorporation into the structure would be electrically driven.

The argyrodite structured material Cu_6PS_5Cl was chosen as the target candidate due to the ionic conductivities and structures being reported in literature for the Cu and Li analogues. The Cu_6PS_5Cl material was successfully synthesized through solid-state methods and characterized by Dr. Andy Martinolich of the Nielson group. Attempting the all-solid-state ion exchange consisted of setting up a cell similar to that depicted in Figure 3.15, but with a stainless-steel current collector in place of the Cu contact, as this would allow for us to detect any potentially plated Cu. The cell was prepared in a Swagelok device in which the solid Cu_6PS_5Cl electrolyte was formed into a compressed pellet and the two current collectors and Li metal electrode were compressed on either side using a non-conductive clamp. In this setup no charge was passed within the voltage capabilities of our available potentiostats (10V difference applied). This is likely due to large interfacial impedances at the electrode-electrolyte interfaces. Therefore, the Cu_6PS_5Cl pellet and electrodes were saturated with a carbonate-based Li^+ ion containing electrolyte for the subsequent test, and current was passed using a large applied overpotential of 5 V. The presence of metallic Cu was confirmed by XRD, and no new crystalline products were observed for the solid electrolyte, but this does not account for potentially amorphous products that could form as a result of Cu extraction, or other decomposition products that may have been lost as a result of the post-synthetic processing conditions. Limited elemental analysis of the post-reaction solid electrolyte suggests the presence of Li by XPS, but the signal was low enough to be accounted for by residual salt deposited upon solvent evaporation or electrolyte decomposition during the course of the reaction. As the practical issues of cell design, interfacial impedance limitations, deconvolution of data, and overall effort vs results gained were realized, further pursuit of the specific Cu^+/ Li^+ ion-

exchange system were suspended

Despite the limited results and insights gained, I believe there is still value to this concept which is why the process of the project conception, approach, and results are presented here. While the specific system explored here did not produce meaningful outcomes, it highlights an alternative approach to the other systems described in this Chapter. Through targeting a solid-state ion-exchange process, there is the potential to essentially trap precursors such as P and S in their desired oxidation state and local geometries, with Cu^+ as a charge balance in this case. Therefore, when Cu^+ is reduced and the Li counter electrode is oxidized, the resulting Li^+ can react with these P and S "precursors", thus eliminating many of the issues we have encountered with the solution stability of comparable systems that were highlighted during the investigation of Na_3PS_4. Similarly, this concept can be applied for alternate mobile ion systems such as Na and Mg, in order to pursue the investigation of the products which would result from exchanging ions with significantly different ionic radii. The initial hypothesis and motivation for exchanging Li^+ and Cu^+ was that the comparable ionic radii would allow for the system to maintain its structure and ionic conductivity would occur through analogous pathways, but that is fundamentally not the primary objective of this research. The objective is to use electrochemistry in new ways to see if new results are gained.

Therefore, there remains merit to the ion-exchange hypothesis, that I believe is bolstered when thinking about preparing "sacrificial" electrolytes to react with alternate mobile cations of interest. In this case, rather than focusing on the mobility of the ions across some deposited surface, the reaction would need to be designed such that the rate of removal and reduction of the sacrificial mobile ion species is sufficiently fast, therefore the rate of the reaction would be predicated on the subsequent mobility of the new mobile cation either into the structure, or through decomposing

the existing structure and forming new compounds.

3.5 Conclusion on the preliminary anodization reactions of AgI/CuI related systems: emphasis on potential studies and future directions involving non-iodide products

There are a variety of challenges when discussing this proposed mechanism of "anodic electrocrystallization" in current literature. First, that specific term itself is rarely found and can also be referred to simply as anodization, electrocrystallization, electrodeposition (this now tends to refer to reductive depositions), oxidation, or corrosion, and sometimes a combination or variation of those terms (oxidative electrochemical deposition). This is why the usage of the terms anodization, corrosion, and oxidation were defined at the onset of this report. Such ambiguity of language convolutes the process of finding information relating to the proposed mechanism and limits the clarity of discourse in the field overall. Therefore, it would be beneficial to attempt to provide some definition for "anodic electrocrystalliztion" as a means to oxidize and locally solubilize some cationic species, which then reacts with electrolyte constituents resulting in the crystallization of some ionic solid at the electrode interface. This is complicated by the use of molecular species and cluster chemistries to form electrodeposited products through analogous methods. With this and other considerations in mind, this definition buried in a dissertation is not intended to be the foundation for establishing the language of field, but instead act as a commentary for how to consider the communication of concepts uniformly. Building on this, anodic electrocrystallization has primarily been studied for oxide systems, yielding numerous metal-oxide products of advanced and hierarchical geometries, optimizing products for a range of applications. Despite this, there seems to be a general lack of awareness of this subset of electrochemical synthesis in the broader electrochemistry and inorganic communities. I believe this is in part due to the unclear and widely varied language used to describe the technique, with the notable Kar

report simply describing the product as “anodic CuS” which in no way indicates the use of electrochemistry and could simply refer to a chemical bath deposition technique. Additionally, because there are so few examples of non-oxide products formed using these methods, when researchers dive into literature investigations for systems that could utilize this synthetic technique and exploit the controls over surface modification, these reports are unlikely to stand out in the sea of “high impact” reports or systems that are more optimized and therefore yield higher efficiencies or better properties. Additionally, the lack of unique, established, and compelling language describing this process may contribute to the fact that such reports are unlikely to be recognized or found without specific intent, as even regular consumers of scientific literature are unlikely to come across multiple of these reports, and even less likely to draw connections between them without explicitly reading and processing the information contained within.

Because of this I believe it is important for this project moving forward to use what has already been observed and hypothesized to this point and continue to build upon these results focusing on the use of halide and chalcogenide counter anion species to synthesize materials through anodic electrocrystallization. Initially, work should continue to utilize Ag and Cu systems to continue to establish the theory and language surrounding this subset of non-oxide systems that undergo anodic electrocrystallization using halides and chalcogenides as our counter-anion species. If multi-anion species can be produced, such as the Ag_3SI proposed, this would be a significant step toward highlighting the as-yet unexplored potential of the technique. Additionally, through collaboration with analytical groups that can conduct tests on the photo and electrocatalytic properties of these materials, and work to optimize performance through manipulation of product morphology, surface modification, dopant inclusion, or other variables,

this would expose the potential benefits of the synthetic method to a broader audience and demonstrate value from a practical perspective.

REFERENCES

(1) Zhou, C.; Bag, S.; Thangadurai, V. Engineering Materials for Progressive All-Solid-State Na Batteries. *ACS Energy Letters*. American Chemical Society September 14, 2018, pp 2181–2198. https://doi.org/10.1021/acsenergylett.8b00948.

(2) Park, M.; Zhang, X.; Chung, M.; Less, G. B.; Sastry, A. M. A Review of Conduction Phenomena in Li-Ion Batteries. *J. Power Sources* **2010**, *195* (24), 7904–7929. https://doi.org/10.1016/j.jpowsour.2010.06.060.

(3) Chen, H. M.; Maohua, C.; Adams, S. Stability and Ionic Mobility in Argyrodite-Related Lithium-Ion Solid Electrolytes. *Phys. Chem. Chem. Phys.* **2015**, *17* (25), 16494–16506. https://doi.org/10.1039/C5CP01841B.

(4) Wang, Y.; Song, S.; Xu, C.; Hu, N.; Molenda, J.; Lu, L. Development of Solid-State Electrolytes for Sodium-Ion Battery-A Short Review. *Nano Mater. Sci.* **2019**, *1* (2), 91–100. https://doi.org/10.1016/j.nanoms.2019.02.007.

(5) Ding, Z.; Li, J.; Li, J.; An, C. Review-Interfaces: Key Issue to Be Solved for All Solid-State Lithium Battery Technologies. *J. Electrochem. Soc.* **2020**, *167*, 070541. https://doi.org/10.1149/1945-7111/ab7f84.

(6) Kumar, P. P.; Yashonath, S. Ionic Conduction in the Solid State. *J. Chem. Sci* **2006**, *118* (1), 135–154.

(7) Hull, S. Superionics: Crystal Structures and Conduction Processes. *Reports Prog. Phys.* **2004**, *67* (7), 1233–1314. https://doi.org/10.1088/0034-4885/67/7/R05.

(8) Obrovac, M. N.; Chevrier, V. L. Alloy Negative Electrodes for Li-Ion Batteries. *Chem. Rev.* **2014**, *114* (23), 11444–11502. https://doi.org/10.1021/cr500207g.

(9) Pasta, M.; Armstrong, D.; Brown, Z. L.; Bu, J.; Castell, M. R.; Chen, P.; Cocks, A.; Corr,

S. A.; Cussen, E. J.; Darnbrough, E.; Deshpande, V.; Doerrer, C.; Dyer, M. S.; El-Shinawi, H.; Fleck, N.; Grant, P.; Gregory, G. L.; Grovenor, C.; Hardwick, L. J.; S Irvine, J. T.; Jeong Lee, H.; Li, G.; Liberti, E.; McClelland, I.; Monroe, C.; Nellist, P. D.; Shearing, P. R.; Shoko, E.; Song, W.; Spencer Jolly, D.; Thomas, C. I.; Turrell, S. J.; Vestli, M.; Williams, C. K.; Zhou, Y.; Bruce, P. G. 2020 Roadmap on Solid-State Batteries. *J. Phys. Energy* **2020**, *2*, 32008. https://doi.org/10.1088/2515-7655/ab95f4.

(10) Wu, H.; Cui, Y. Designing Nanostructured Si Anodes for High Energy Lithium Ion Batteries. *Nano Today* **2012**, *7*, 414–429. https://doi.org/10.1016/j.nantod.2012.08.004.

(11) Ellis, B. L.; Nazar, L. F. Sodium and Sodium-Ion Energy Storage Batteries. *Curr. Opin. Solid State Mater. Sci.* **2012**, *16* (4), 168–177. https://doi.org/10.1016/j.cossms.2012.04.002.

(12) Kundu, D.; Talaie, E.; Duffort, V.; Nazar, L. F. The Emerging Chemistry of Sodium Ion Batteries for Electrochemical Energy Storage. *Angew. Chemie Int. Ed.* **2015**, No. 150, n/a-n/a. https://doi.org/10.1002/anie.201410376.

(13) Laocharoensuk, R.; Palaniappan, K.; Smith, N. A.; Dickerson, R. M.; Werder, D. J.; Baldwin, J. K.; Hollingsworth, J. A. Flow-Based Solution-Liquid-Solid Nanowire Synthesis. *Nat. Nanotechnol.* **2013**, *8* (9), 660–666. https://doi.org/10.1038/nnano.2013.149.

(14) Watanabe, M.; Thomas, M. L.; Zhang, S.; Ueno, K.; Yasuda, T.; Dokko, K. Application of Ionic Liquids to Energy Storage and Conversion Materials and Devices. *Chem. Rev.* **2017**, acs.chemrev.6b00504. https://doi.org/10.1021/acs.chemrev.6b00504.

(15) Poullikkas, A. A Comparative Overview of Large-Scale Battery Systems for Electricity Storage. *Renew. Sustain. Energy Rev.* **2013**, *27*, 778–788.

https://doi.org/10.1016/j.rser.2013.07.017.

(16) Dunn, B.; Kamath, H.; Tarascon, J.-M. Electrical Energy Storage for the Grid: A Battery of Choices. *Science (80-.).* **2011**, *334* (6058), 928–935. https://doi.org/10.1126/science.1212741.

(17) DiLeo, R. A.; Zhang, Q.; Marschilok, A. C.; Takeuchi, K. J.; Takeuchi, E. S. Composite Anodes for Secondary Magnesium Ion Batteries Prepared via Electrodeposition of Nanostructured Bismuth on Carbon Nanotube Substrates. *ECS Electrochem. Lett.* **2014**, *4* (1), A10–A14. https://doi.org/10.1149/2.0081501eel.

(18) Imanaka, N.; Tamura, S. Development of Multivalent Ion Conducting Solid Electrolytes. *Bull. Chem. Soc. Jpn.* **2011**, *84* (4), 353–362. https://doi.org/10.1246/bcsj.20100178.

(19) Braga, M. H.; Ferreira, J. A.; Stockhausen, V.; Oliveira, J. E.; El-Azab, A.; Dudney, N. J.; Kiggans, J.; Hong, K.; Rondinone, A. J.; Liang, C.; Mitsui, A. A. Novel Li3ClO Based Glasses with Superionic Properties for Lithium Batteries. *J. Mater. Chem. A* **2014**, *2* (15), 5470. https://doi.org/10.1039/c3ta15087a.

(20) Beguin, F.; Frackowiak, E. *Supercapacitors: Materials, Systems and Applications*; John Wiley & Sons, 2013.

(21) Kim, S. W.; Seo, D. H.; Ma, X.; Ceder, G.; Kang, K. Electrode Materials for Rechargeable Sodium-Ion Batteries: Potential Alternatives to Current Lithium-Ion Batteries. *Adv. Energy Mater.* **2012**, *2* (7), 710–721. https://doi.org/10.1002/aenm.201200026.

(22) Bachman, J. C.; Muy, S.; Grimaud, A.; Chang, H.-H.; Pour, N.; Lux, S. F.; Paschos, O.; Maglia, F.; Lupart, S.; Lamp, P.; Giordano, L.; Shao-Horn, Y. Inorganic Solid-State Electrolytes for Lithium Batteries: Mechanisms and Properties Governing Ion Conduction.

Chem. Rev. **2015**, *116* (1), 140–162. https://doi.org/10.1021/ACS.CHEMREV.5B00563.

(23) Dieterich, W. Superionic Conductors. *J. Stat. Phys.* **1985**, *39* (5–6), 583–596. https://doi.org/10.1007/BF01008353.

(24) Maier, J. Ionic Conduction in Space Charge Regions. *Prog. Solid State Chem.* **1995**, *23* (3), 171–263. https://doi.org/10.1016/0079-6786(95)00004-E.

(25) Zhao, W.; Yi, J.; He, P.; Zhou, H. Solid-State Electrolytes for Lithium-Ion Batteries: Fundamentals, Challenges and Perspectives. *Electrochem. Energy Rev.* **2019**, *2* (4), 574–605. https://doi.org/10.1007/s41918-019-00048-0.

(26) Åvall, G.; Mindemark, J.; Brandell, D.; Johansson, P. Sodium-Ion Battery Electrolytes: Modeling and Simulations. *Adv. Energy Mater.* **2018**, *8* (17), 1703036. https://doi.org/10.1002/aenm.201703036.

(27) Van Der Ven, A.; Deng, Z.; Banerjee, S.; Ong, S. P. Rechargeable Alkali-Ion Battery Materials: Theory and Computation. *Chemical Reviews*. American Chemical Society July 22, 2020. https://doi.org/10.1021/acs.chemrev.9b00601.

(28) Zhang, Z.; Shao, Y.; Lotsch, B.; Hu, Y. S.; Li, H.; Janek, J.; Nazar, L. F.; Nan, C. W.; Maier, J.; Armand, M.; Chen, L. New Horizons for Inorganic Solid State Ion Conductors. *Energy and Environmental Science*. Royal Society of Chemistry August 1, 2018, pp 1945–1976. https://doi.org/10.1039/c8ee01053f.

(29) Lu, Y.; Li, L.; Zhang, Q.; Niu, Z.; Chen, J. Electrolyte and Interface Engineering for Solid-State Sodium Batteries. *Joule*. Cell Press September 19, 2018, pp 1747–1770. https://doi.org/10.1016/j.joule.2018.07.028.

(30) Liu, J.; Zhu, H.; Shiraz, M. H. A. Toward 3D Solid-State Batteries via Atomic Layer Deposition Approach. *Front. Energy Res.* **2018**, *6* (MAR), 10.

https://doi.org/10.3389/fenrg.2018.00010.

(31) Weiss, M.; Seidlhofer, B. K.; Geiß, M.; Geis, C.; Busche, M. R.; Becker, M.; Vargas-Barbosa, N. M.; Silvi, L.; Zeier, W. G.; Schröder, D.; Janek, J. Unraveling the Formation Mechanism of Solid-Liquid Electrolyte Interphases on LiPON Thin Films. *ACS Appl. Mater. Interfaces* **2019**, *11* (9), 9539–9547. https://doi.org/10.1021/acsami.8b19973.

(32) Bekaert, E.; Buannic, L.; Lassi, U.; Llordés, A.; Salminen, J. Electrolytes for Li- and Na-Ion Batteries: Concepts, Candidates, and the Role of Nanotechnology. In *Emerging Nanotechnologies in Rechargeable Energy Storage Systems*; Elsevier Inc., 2017; pp 1–43. https://doi.org/10.1016/B978-0-323-42977-1.00001-7.

(33) Hull, S.; Keen, D. A. Pressure-Induced Phase Transitions in AgCl, AgBr, and AgI. *Phys. Rev. B* **1999**, *59* (2), 750–761. https://doi.org/10.1103/PhysRevB.59.750.

(34) Yamamoto, T.; Maesato, M.; Hirao, N.; Kawaguchi, S. I.; Kawaguchi, S.; Ohishi, Y.; Kubota, Y.; Kobayashi, H.; Kitagawa, H. The Room-Temperature Superionic Conductivity of Silver Iodide Nanoparticles under Pressure. *J. Am. Chem. Soc.* **2017**, *139* (4), 1392–1395. https://doi.org/10.1021/jacs.6b11379.

(35) Takahashi, T.; Ikeda, S.; Yamamoto, O. Solid-State Ionics—Solids with High Ionic Conductivity in the Systems Silver Iodide-Silver Oxyacid Salts. *J. Electrochem. Soc.* **1972**, *119* (4), 477. https://doi.org/10.1149/1.2404235.

(36) Huang, H. Y.; Chien, D. J.; Huang, G. G.; Chen, P. Y. Electrochemical Preparation of Photoelectrochemically Active CuI Thin Films from Room Temperature Ionic Liquid. *Electrochim. Acta* **2012**, *65*, 204–209. https://doi.org/10.1016/J.ELECTACTA.2012.01.044.

(37) Vishwanath, R. S.; Kandaiah, S. Electrochemical Preparation of Crystalline γ-CuI Thin

Films through Potential-Controlled Anodization of Copper and Its Photoelectrochemical Investigations. *J. Solid State Electrochem. 2016 207* **2016**, *20* (7), 2093–2102. https://doi.org/10.1007/S10008-016-3218-3.

(38) Allen, P. C.; Lazarus, D. Effect of Pressure on Ionic Conductivity in Rubidium Silver Iodide and Silver Iodide. *Phys. Rev. B* **1978**, *17* (4), 1913–1927. https://doi.org/10.1103/PhysRevB.17.1913.

(39) Kar, P.; Farsinezhad, S.; Zhang, X.; Shankar, K. Anodic Cu2S and CuS Nanorod and Nanowall Arrays: Preparation, Properties and Application in CO2 Photoreduction. *Nanoscale* **2014**, *6* (23), 14305–14318. https://doi.org/10.1039/C4NR05371K.

IV: DESIGN OF A SAMPLE TRANSFER HOLDER TO ENABLE AIR-FREE X-RAY PHOTOELECTRON SPECTROSCOPY[iv]

4.1 Overview

Surface analysis of air-sensitive samples is difficult without controlled-environment sample transfer tubes or expensive vacuum transfer suitcases. Through the use of vacuum sealing and commercial magnets, we demonstrate a concept for a sample holder that can be used to transfer samples from an inert environment directly into an X-ray photoelectron spectrometer. Our results show the efficacy of the holder through analysis of an air-sensitive CuCl powder, where oxidation was not observed when using the sample holder. This method offers a simple, low-cost alternative to enable routine air-free measurements in instrumentation with vacuum-controlled sample introduction chambers. Our aim with this report is to share the design so that this sample holder can be made anywhere where there is access to a basic machine shop.

4.2 Introduction

When dealing with the analysis of material surfaces, it is vital to be able to ensure that the surface being analyzed is as accurate to the *in-operando* surface or product as possible. This can be difficult for lab situations in which there is not a system in place for samples to be transferred into an instrument via vacuum transfer suitcase or where an instrument is not directly attached to an environmentally controlled system such as a glovebox. In order to allow for air-free sample transfer into an X-ray photoelectron spectroscopy (XPS) instrument, we have designed a sample

[iv] This work was published and can be found as Schneider, J. D.; Agocs, D. B.; Prieto, A. L. Design of a Sample Transfer Holder to Enable Air-Free X-Ray Photoelectron Spectroscopy. *Chem. Mater.* **2020**, *32* (19), 8091–8096. https://doi.org/10.1021/ACS.CHEMMATER.0C01895. Collaborating author Dr. Agocs conducted the XPS analysis and contributed to a portion of XPS data analysis, but all holder design, optimization, test system development, and the rest of writing are the work of the dissertation author, Jacob Boissiere.

transfer holder (Figure 4.1) which can maintain an inert sample environment for an extended period of time using a negative pressure seal and magnetic release once inside the instrument entrance chamber and under vacuum.

The surface-sensitive nature of the XPS technique means any changes in surface chemistry due to oxidation or hydration upon exposure to ambient air are detrimental to collecting accurate and impactful data. Such changes have been reported when investigating battery materials,[1–3] nanoparticles,[4–6] bare metal surfaces,[7,8] nitrides,[9,10] and more.[11–14] Due to this, researchers employ a variety of techniques in order to maintain air-free environments. These include vacuum suitcases, vacuum transfer lines, direct attachment of instrumentation to inert environment chambers,[15] commercial transfer vessels, flowing Ar over the sample during transfer,[16] use of glove-bags placed over instrument entrance chambers,[2] or depositing a thin coating such as Al that can be removed via sputtering or measurements can be made through.[10] While all of these techniques are effective, each has its shortcomings.

It is not always possible for a lab, in particular an academic lab or anywhere where the XPS instrument is shared between a variety of users for numerous applications, to have the instrument in direct contact with a glovebox or system where samples are synthesized and prepared. Also, while vacuum transfer suitcases are very effective, they often need to be custom ordered directly from the instrument manufacturer (Thermo or Physical Electronics) or specialty manufacturer (Trans-fer Engineering and Manufacturing Inc.), and can be costly. Additionally, if there is a desire to have multiple samples prepared simultaneously or across various labs, as is often the case in a university setting, the need for several devices arises, and the costs only multiply.

Flowing inert gas throughout sample transfer or the use of a glove-bag system is imperfect and can be inconvenient, despite being more readily available to most users. Lastly, air-free sputter coating may not be accessible for many users (because of the same challenges in sample transfer from a glovebox), and concerns arise over altering the analyte properties both upon deposition of the protective coatings through the sputtering process and during the removal of these coatings in the instrument.

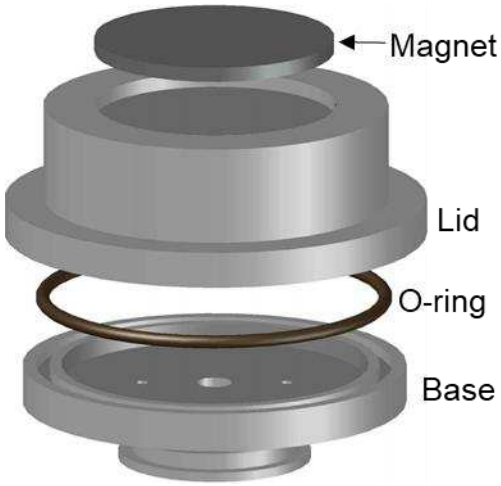

Figure 4.1. Graphic of the air-free XPS sample transfer holder, to scale without sample clips, clip screws, or bleed screw visible. The base and lid are Al, the O-ring is viton, and magnet is a 1.26" neodymium disc magnet that is press-fit into the lid. Additional schematics can be found in Figure 2 and the electronic supplemental information.

Taking all of this into account, we have developed a system that consists of relatively inexpensive, readily sourced materials, can be reproducibly manufactured, is user-friendly, is reusable, and once manufactured, requires no special equipment, significant maintenance, or special training to use. Furthermore, while the design and specifications reported here are specific to our particular XPS instrument specifications (Physical Electronics ESCA 5800), we hope the core concept be-hind the holder's function can be extended to numerous applications and instruments. In theory, most systems that employ a low-pressure antechamber could use the fundamental design principals we report here to make a comparable negative-pressure air-free sample transfer holder. Potential modifications are further discussed in the Troubleshooting and Modification section. This could minimize the barrier for people who need to make this kind of measurement, enabling measurements of air-sensitive samples for a broader participation.

4.3 Materials

The air-free XPS holder was milled on a lathe from 2.25” aluminum 6061-T6511 tight-tolerance round stock (McMaster-Carr) to the specifications detailed in Figure 4.2. Further details on design and specifications can be found in the electronic supplementary information in Figure 4.S1 and an accessible CAD file The main holder O-ring located between the base and lid (standard O-ring size AS568-031), the bleed screw O-ring located between the base and bleed screw (standard O-ring size ISO 3601 A0045A), the bleed screw (US standard #10-32 x 0.5” button head screw), and the sample clip holder screws (US standard #0-80 x 0.125” socket head cap screws) were all purchased from local hardware supply stores. The 1.26” Ni-Cu-Ni triple coated neodymium disc magnets for the holder cap were purchased through amazon.com and are ~0.08” thick. This type of magnet is commercially available through online retailers and craft/home-goods stores. The seller claimed the magnets to be N52 NdFeB, but no verification tests were done nor manufacturing information provided with the purchase. The copper (I) chloride (CuCl anhydrous beads, ≥99.99%) was purchased from Sigma-Aldrich and was ground in an agate mortar and pestle under inert conditions in a N2-filled glovebox. The CuCl powder was adhered to the air-free XPS hold-er via carbon tape (Ted Pella) as shown in Figure 4.S2.

4.4 Procedure

The transfer holder is used to prevent exposure to the atmosphere between an inert glovebox environment and an XPS instrument. In order to do this, the holder is first pumped into the glovebox with the cap and base separated and the bleed screw loosened, which is done to ensure there were no trapped gasses and allow for all surfaces to be exposed for the pumping and purging process. The sample of interest can then be placed on the holder and affixed either by copper clips or using conductive adhesives. For the preliminary results presented here, a two-sided carbon tape

was used. The adhesive was attached to the base of the sample transfer holder prior to pumping and purging into the box in order to remove as much adsorbed oxygen and water as possible. Prior to attaching the sample of interest, the bleed screw is tightened until flush with the base sample surface.

To test for holder efficacy, the sample analyzed consisted of CuCl, freshly ground in an agate mortar and pestle. A reactive Cu(I) species was used for the test due to the clear transition from a Cu(I) to Cu(II) seen in XPS spectra.[17,18] Once the ground CuCl was placed onto the adhesive, the holder cap is placed on the base, ensuring the O-ring is properly seated in the base groove and the lid is seated flush on the O-ring. When aligned properly, the transfer holder is put into the glovebox antechamber. The antechamber is then pumped down slowly, pulling as much trapped gas from the holder as possible. The antechamber is then re-filled with N2, creating a vacuum seal due to the negative pressure within the holder relative to the N2 environment. Re-pressurizing the antechamber with N2 instead of atmospheric air serves a dual purpose: first, it allows the transfer holder to be re-entered into the glovebox where the quality of seal can be evaluated without risking exposure to atmosphere. The seal is tested by attempting to pull apart the base and the lid, which will not readily happen given a good seal. Second, re-pressurizing with

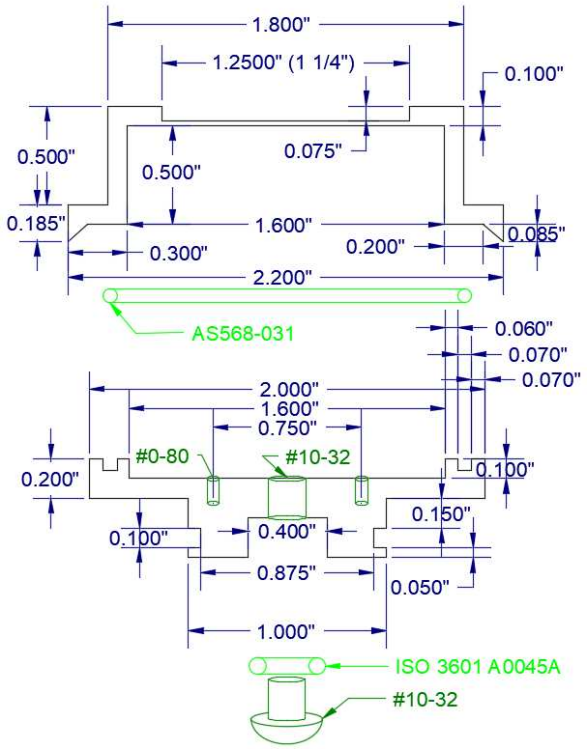

Figure 4.2. Schematic showing dimensions of machined air-free XPS sample transfer holder cap and base. Not shown is the neodymium disc magnet (1.26" diameter), press-fit into the upper cut-out of the sample holder. Listed in green are the O-rings and screws listed in the materials section, as well as the screw-holes tapped into the base. Full schematic with all labeled peripherals can be found in the electronic supplementary information and Figure 4.S1.

N¬2 minimizes the possibility of contamination due to gas getting into the transfer holder while the negative-pressure seal is being established. Once the negative-pressure seal is established and tested, the transfer holder can be removed from the glovebox directly, at which point the sample will remain free from atmospheric contamination and can be stored for extended periods of time or brought directly to the instrument.

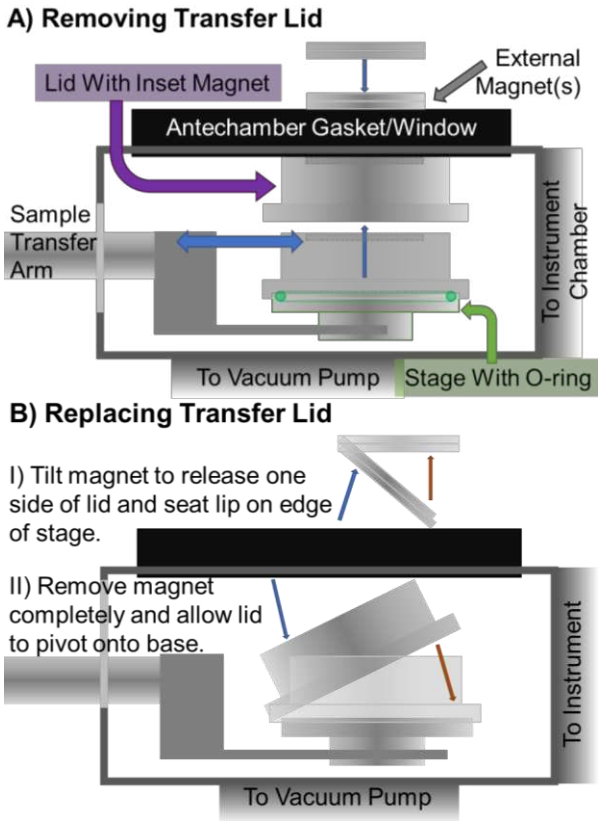

Figure 4.3. Cross sectional representations of the sample transfer holder in the instrument antechamber showing the basic operating principle. A) Following evacuation of the antechamber, magnets are applied to the window, causing the lid to lift off the base and remain suspended. This allows the sample transfer arm to pass under the lid, and the sample to be inserted into the instrument. B) Following analysis and sample removal, the lid can be returned to the base to prevent air exposure upon removal. This is done by I) tilting the external magnet at an angle where one side of the lid falls to the sample stage and the other is held at the window. II) Once the lid is in the correct location, the magnet is lifted completely, allowing the sample to pivot onto the base and seat properly.

To release the seal of the transfer holder for subsequent analysis of the sample, the holder is placed into the entrance chamber of the instrument, which is then pulled down to high-vacuum as is standard for the instrument. As the vacuum of the instrument is higher than the vacuum of the glovebox antechamber, the negative-pressure seal previously established is overcome. The lid is then lifted from the base using magnets external to the sample introduction chamber as seen in Figure 4.3A. This results in the separation of the lid, where it hangs suspended by the magnets, allowing the pristine material

to pass underneath and be introduced into the instrument for analysis as depicted by the blue, two-sided arrow in Figure 4.3A.

For further details relating to the introduction and extraction of a sample using PHI mounts, refer to the electronic supplemental information, relevant instrument operators guide,[19] site-specific standard operating procedures (SOPs), or RBD instruments instructional brochure.[20] The supplemental information also contains optical images of the holder and chamber (Figure 4.S2), and a complete description of the procedure for using the air-free holder along with graphics demonstrating each step (Figure 4.S3).

Upon completion of analysis, resealing the lid is possible by simply returning the sample holder base to the original position and carefully removing the magnets holding the lid in place as shown in Figure 4.3B. Dropping the lid onto the base allows it to reseat, and the vacuum environment in the XPS sample antechamber is used to re-establish the negative pressure seal (now even stronger) when exposed to ambient pressure. The sample can then be transferred back to the glovebox, where it can be opened by breaking the seal by using the bleed screw found on the bottom. Through this process, an air-free environment can be maintained repeatedly for a sample going between inert-atmosphere testing and XPS analysis.

4.5 Safety

Primary safety concerns for using this air-free XPS sample transfer holder are those found when working with vacuums, gloveboxes, and X-ray equipment. This includes being aware of all chemicals present in your workspace, ensuring the sample holder is properly cleaned between all uses (so as to avoid cross-contamination between samples), and having proper training completed through your institution and lab for working with X-ray and glovebox equipment. The primary safety concern more specific to the holder is being aware of pinch-points that occur when working

with magnets. In order to make the sample holder, it is recommended a professional machinist complete the work, but if being completed by an amateur, there are many safety concerns associated with operating machining equipment, and proper training and precautions are required. While not shown in the holder schematics, creating a very slight bevel (rounding) on all corners helps to minimize the possibility of cuts when working with the holder.

4.6 Troubleshooting and Modification

Multiple iterations of the sample holder were designed, built, and tested before coming to this final design. The lower portion of the base (bottom 0.3") cannot be altered significantly due how the sample holder is seated and held in the instrument.[20] Similarly, the dimensions of the base overall are limited due to the instrument entrance chamber. The lip around the base was designed to contain the O-ring and elevate the lid slightly relative to the sample stage surface, assisting in magnetic release of the lid, but was not raised farther to ensure no interference with the incident X-ray beam or any instrument detectors. The lid height was optimized to get the magnet close enough the entrance chamber window that it could be lifted using external magnets, while being short enough to allow the lid to travel far enough to get past the arm used for inserting the sample stage into the instrument (see Figure 4.3). The weight of the lid needed to be light enough to be lifted by the magnets, and the transfer holder overall needed to be light enough to not bend or otherwise damage the pronged arm used to insert the sample into the chamber.

The O-ring groove is located in the base in order to keep the O-ring in place throughout sample moving and manipulation both when entering the chamber and when moving the stage in the instrument. The angled bevel (0.085" depth) was added to the lid to aid in re-seating the lid following analysis, as well as it prevents the lid from shifting when pumping down in the glovebox antechamber, as a higher internal pressure regime is reached in the transfer holder during that

process. Pumping down the antechamber slowly and re-filling quickly was found to create the best negative-pressure seal on the holder. At times the lid can stick to the base and have trouble releasing in the entrance chamber, but the use of additional external magnets can help it to release in those cases. These cases can be minimized by ensuring the O-rings are clean and in good condition, with minimal exposure to solvents or grease, as well as through minimizing the time the sample is left under negative-pressure in the holder.

The bleed screw was designed with an O-ring in the base as it provides a very stable seal with the O-ring being contained on the sides by the base, and establishing a seal between the button-head screw and the base. A different design was successfully tested using a flush, flat-head screw with the base being carefully counter sunk creating a direct seal between the screw and holder base. While both designs work, the tolerances are much tighter for the second option, and therefore machining skill required is lessened and long-term stability is increased through using the O-ring design. Lastly, each holder lid was custom fit to the attached magnet, as the magnets had poor tolerances, and were press-fit into the lid tops in order to prevent the use of any adhesives that could outgas, dry, or otherwise fail through prolonged use in a chemistry lab.

4.6.1 Considerations for holder modification and adaptation to alternate systems.

The hope is that this simple design can be used not necessarily as a blueprint for reproduction, but as a basis for developing similar holders for other XPS instruments and even non-XPS instrumentation. The fundamental negative-pressure sealed lid concept and magnetic release have several necessary or preferred requirements. First the required components for making an analogous system include; 1) low pressure sample entrance chamber (sample must pass from a chamber into the instrument in order to allow separation from lid so it does not interfere with taking measurements), 2) the ability to add a gasket/O-ring to the sample holder stage or lid if

using bonded gasket, 3) the design of a lid with a magnet to accompany the stage. When designing the lid, important considerations must include the lid's ability to clear the sample insertion arm or other apparatus, while still being tall and light enough to interact with an external magnet and remain suspended.

Those are the true fundamentals behind this design, but there are other considerations as well. Generally, there should not be a need to modify the stage at the point where it attaches or interacts with the instrument. Ideally the sample stage would be a flat, solid surface, with the only moving part or potential leak point being a bleed screw. For the instrument, it is beneficial to have sample chamber with window/ability to view, but not necessary (remounting would be less precise). Also, our system is ideal as the sample sits horizontal, so the lid is lifted straight up and set straight down, allowing for re-seating after analysis. Given the bevel-lipped lid design, it is possible to use the holder in an angled sample port (up to ~50° tilt based on benchtop tests) but post-analysis re-sealing would likely be an issue at steep angles. One remedy would be to give the lid a step down around the base instead of or prior to a bevel, which would presumably allow the sample to be tilted to ~90° depending on fit, but this would not allow for re-seating post-analysis. There are cases where this design simply fails to be applied to other instrumentation as reported here. These instances include: most situations where the sample is put directly into an instrument (no antechamber), most fully automated systems that the authors have considered, systems where the ante-chamber is not conducive to through-wall magnetic interactions, and in instances where a sample is not mounted upright (could still work in theory without a magnet and the lid simply falling off, but that would likely be detrimental to the instrument).

4.7 Characterization

X-ray photoelectron spectroscopy measurements were performed using a Physical Electronics ESCA 5800 system equipped with a monochromatic Al Kα source (E=1486.6 eV). Survey scans were performed using a pass energy of 187.85eV and a step size of 1.6 eV/step. High resolution scans were performed using a pass energy of 23.5 eV and a step size of 0.10 eV/step. A neutralizer (15 μA emission, 1.70 V bias, 40.0 V extractor) was employed to mitigate charging effects. Data analysis was performed using Multipak version 9.3.0.3. Background fitting was performed using the iterated Shirley method, and peaks were smoothed using SG5 smoothing.

4.8 Discussion

X-ray photoelectron measurements demonstrate the efficacy of the air-free XPS sample transfer holder. Due to its sensitivity to oxidation upon exposure to atmospheric oxygen, as well as the clear transition between Cu+ and Cu2+ signals in the XPS, CuCl was chosen as the sensor to test the air-free nature of the holder.[17] Initial assessment of CuCl as purchased showed slight presence of Cu2+, so the sample was ground in a N¬2¬ glovebox in order to expose fresh CuCl surface for analysis. To assess the initial purity of the ground CuCl, samples were transferred from the box to the instrument using the transfer holder, and XPS measurements (Figure 4.4A and Figure 4.S4) identified environments due to only Cu+ and Cl- (in addition to C from the carbon tape used to adhere the CuCl powder to the holder) which are shown in Figure 4.S4). This indicates not only the purity of the starting material, but also the ability of the holder to maintain an air-free environment, as no Cu2+ peaks were observed.

To the contrary, a comparable sample of ground CuCl was measured under the same conditions, and transferred in the same amount of time, though without the use of the air-free transfer holder. Though the time this sample spent in air was only about 3 minutes, oxidation is readily observable (Figure 4.4B). An approximately 3-minute time of exposure was used because

that is the time it takes to quickly transfer the sample from the lab glovebox used to the XPS instrument chamber (which, in our case, involves going down one flight of stairs).

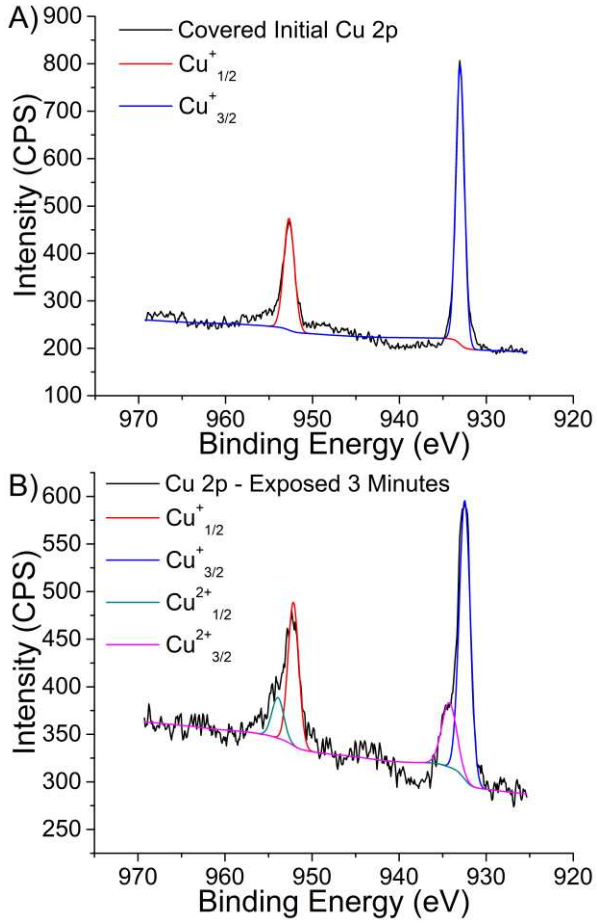

Figure 4.4. High resolution Cu 2p XPS scans with calculated fit depicted for A) CuCl transferred using the designed holder and B) CuCl transferred not using the holder, resulting in approx. 3 minutes of ambient air exposure.

To demonstrate the effectiveness of the holder in maintaining an air-free environment, the covered sample was removed from the instrument and the sealed holder was kept out on a benchtop in atmosphere for 24 hours before being measured again. This process was repeated another 24 hours later (for a total of 48 hours in atmosphere after the initial scan). These spectra also show the lack of a Cu2+ environment (Figure 4.5A). Finally, after maintaining the air-free environment in atmosphere for another 72 hours (120 hours total in atmosphere) the seal was broken, the lid was removed, and the sample was controllably exposed to ambient conditions for 30 minutes. , The multiple-day long experiments were conducted to test the limits of the holder and demonstrate that there isn't just a slow leak of air being hidden by a 3 minute test, but rather a truly robust system, capable of repeated openings, transfers, and analyses, all while maintaining an air-free environment.

Several significant differences in spectra are readily apparent when comparing the unexposed material to the same sample after removing the lid (Figure 4.5A). First and foremost, the appearance of shake up peaks is indicative of the presence of paramagnetic Cu2+, demonstrating that the CuCl readily oxidizes in air. Also, the major signal observed in the Cu 2p scan indexes to Cu2+ instead of the intrinsic Cu+ associated with the native CuCl. Despite the short time of exposure (30 minutes), the majority of the CuCl oxidizes, which is consistent with the reactivity of CuCl in air, and demonstrates the ability of the holder to remain air-free (since the difference in the spectra between exposure to air versus containment in the air free holder are markedly different).

This becomes even more apparent when these peaks are fit (Figure 4.4A and B, and Figure 4.5B). For the covered sample (Figure 4.4A), there are two peaks indicative of the presence of only Cu+. The Cu 2p1/2 peak has a binding energy of 952.7 eV while the Cu 2p3/2 peak is at 933.0 eV, with a peak separation of 19.7 eV. Similarly, for the sample exposed to air for 30 minutes (Figure 4.5B), the same Cu+ environments can be observed, indicating that the CuCl has not fully oxidized in this amount of

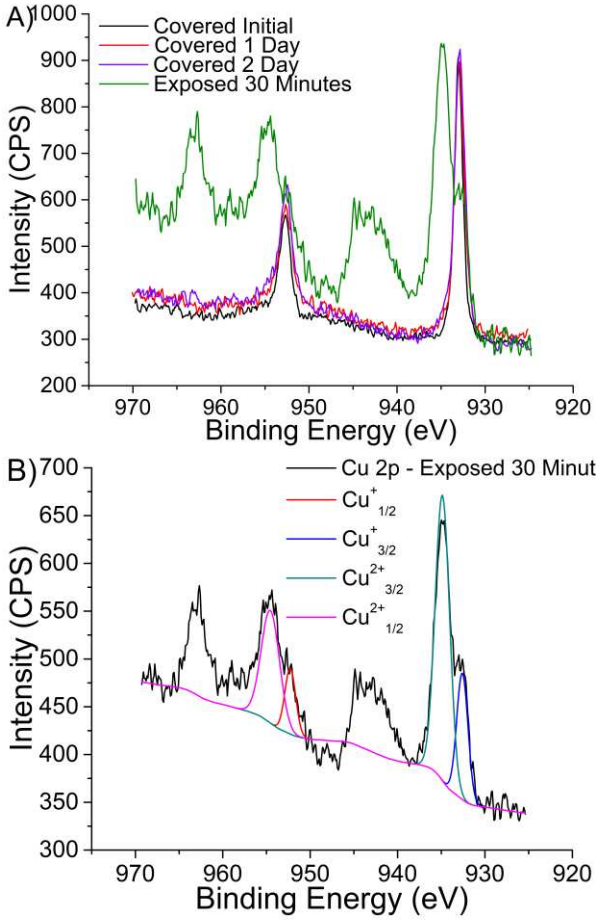

Figure 4.5. A) Cu 2p spectra of the CuCl sample as a function of time in atmosphere in the holder and following air exposure. Despite several days in the holder in air, the CuCl only exhibits peaks due to Cu^{+}. However, after 30 minutes of air exposure, Cu^{2+} peaks and shake-up peaks are readily observable B) Cu 2p spectra of the 30-minute air-exposed CuCl showing the fitting of the Cu^{+} and Cu^{2+} peaks.

time. Here, the Cu+ 2p1/2 peak has a binding energy of 952.3 eV and the Cu+ 2p3/2 peak is at 932.6 eV, with the same peak separation. Additionally, a Cu2+ environment can be observed with Cu2+ 2p1/2 exhibiting a binding energy of 954.6 eV while Cu2+ 2p3/2 is at 934.9 eV with the same separation energy. A comparison of the air-free sample, 3-minute exposed sample, and 30-minute exposed sample qualitatively demonstrating these changes can be found in Figure 4.S5.

Slight changes in the absolute binding energy of the Cu+ peaks are attributed to ambiguity in signal-to-noise ratio of the exposed sample as well as uncertainty in the consistency of carbon signal that spectra were shifted to. Further, due to the paramagnetic nature of Cu2+, shake-up peaks very clearly indicate the presence of the oxidized copper species.

4.9 Conclusions

The XPS data collected on the CuCl samples clearly demonstrate the efficacy of the air-free XPS sample transfer holder. It is shown that the holder is free of air, this air-free environment can be maintained for extended periods of time, and can be used to transfer a sample under inert conditions without contamination by the ambient environment both to-and-from the instrument repeatedly. The final exposure to air results in the rapid oxidation of the CuCl, which demonstrates that there is nothing preventing the oxidation of this species other than the presence of the holder. Through the use of the negative-pressure sealed holder with in-instrument magnetic release, we have presented an opportunity for a sample to be sealed and resealed under vacuum (a condition met in many XPS and inert sample analysis systems). This technique has the potential to avoid the costly infrastructure necessary for inert sample transfer lines or vacuum transfer suitcases, allowing a low-cost alternative for surface analysis of reactive or unstable species.

4.10 Supporting Information

Lid dimensions and 2D representations

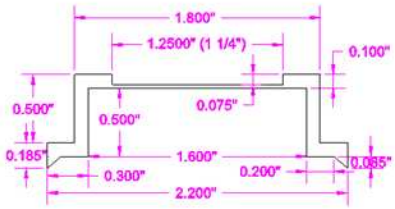

Cap Dimensions - Right angles and bottom edge are given a slight bevel to prevent sharp edges. Magnet gap is actually ~1.26" but custom for each holder in order to press-fit magnet. This is different for each magnet due to low manufacturing tolerances

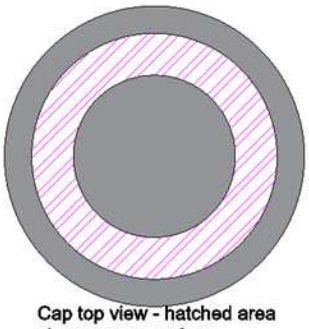

Cap top view - hatched area shows upper surface.

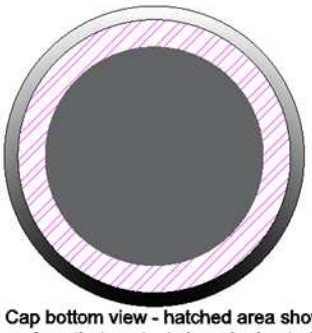

Cap bottom view - hatched area shows surface that contacts base/o-ring to form seal.

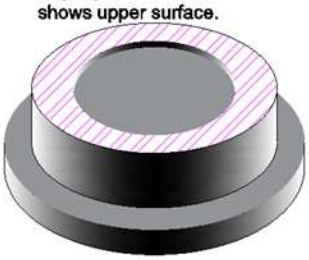

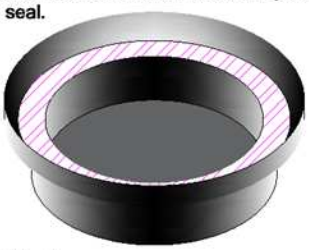

Base dimensions and 2D representations with o-ring and bleed screw

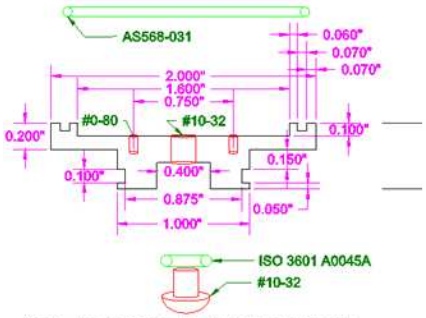

Base dimensions - no beveling on lower central indent and holder groove. Red shows bleed screw and hole (#10-32) as well as two tapped holes for sample clip screws (screws not shown - #0-80) Light green shows main o-ring (upper - AS566-031) and bleed screw o-ring (lower - ISO 2601 A0045A)

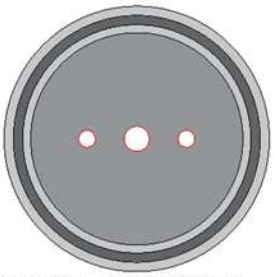

Base top view - empty red circles represent tapped holes for bleed screw and sample holder clip screws (not shown below)

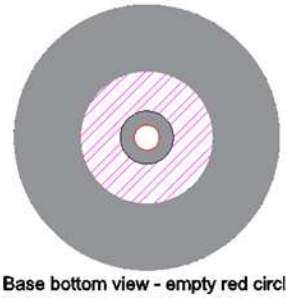

Base bottom view - empty red circles represent tapped hole for bleed screw, lowest face of base is represented as hatched surface for clarity only.

Overall dimensions, peripherals and 3D representation (magnet offset)

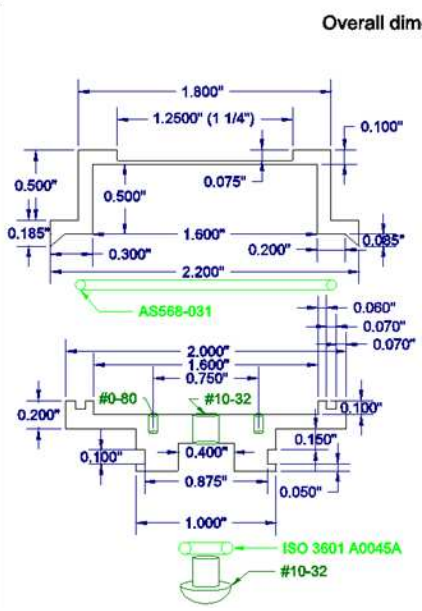

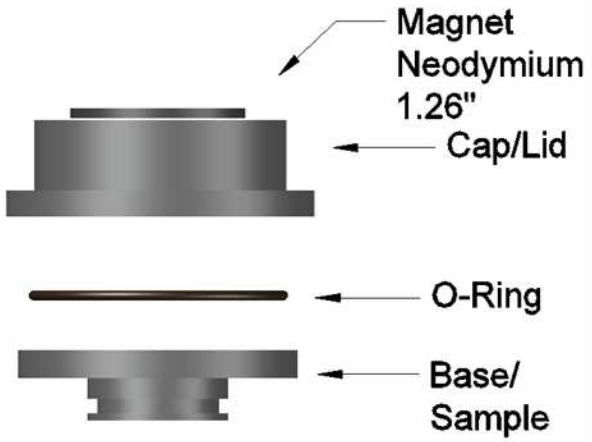

Figure 4.S1 (previous page). This graphic shows all the information contained in the AutoCAD electronically accessible file.

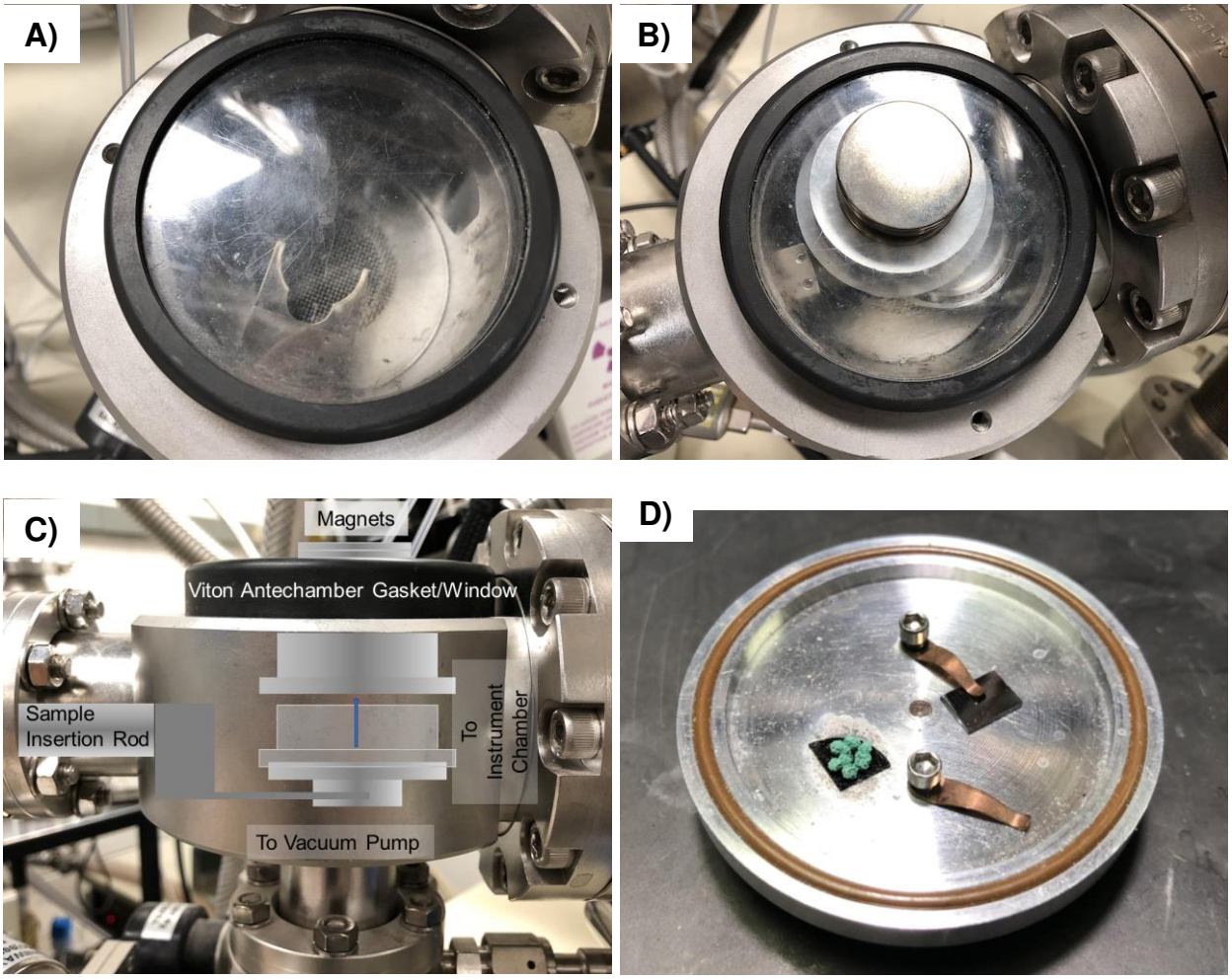

Figure 4.S2. A) Photo of the antechamber taken from above to show the gasket/window, and the sample transfer arm that the holder sits on, taken from above. **B)** Photo of the sample transfer lid lifted off the base and suspended in the instrument antechamber using magnets (the same type as those found in the lid). The holder base and main O-ring are seen on the right of the antechamber, with the insertion arm passing under the lid on the left. **C)** Side view of the antechamber, with a schematic of the holder overlaid representing the operation of the holder. **D)** Photo of the two ways samples are mounted with the transfer holder base, either a film held down using copper clips, or a sample mounted onto a conductive tape. Oxidized CuCl is seen on the left on carbon tape, analogous to how the sample was mounted for this paper.

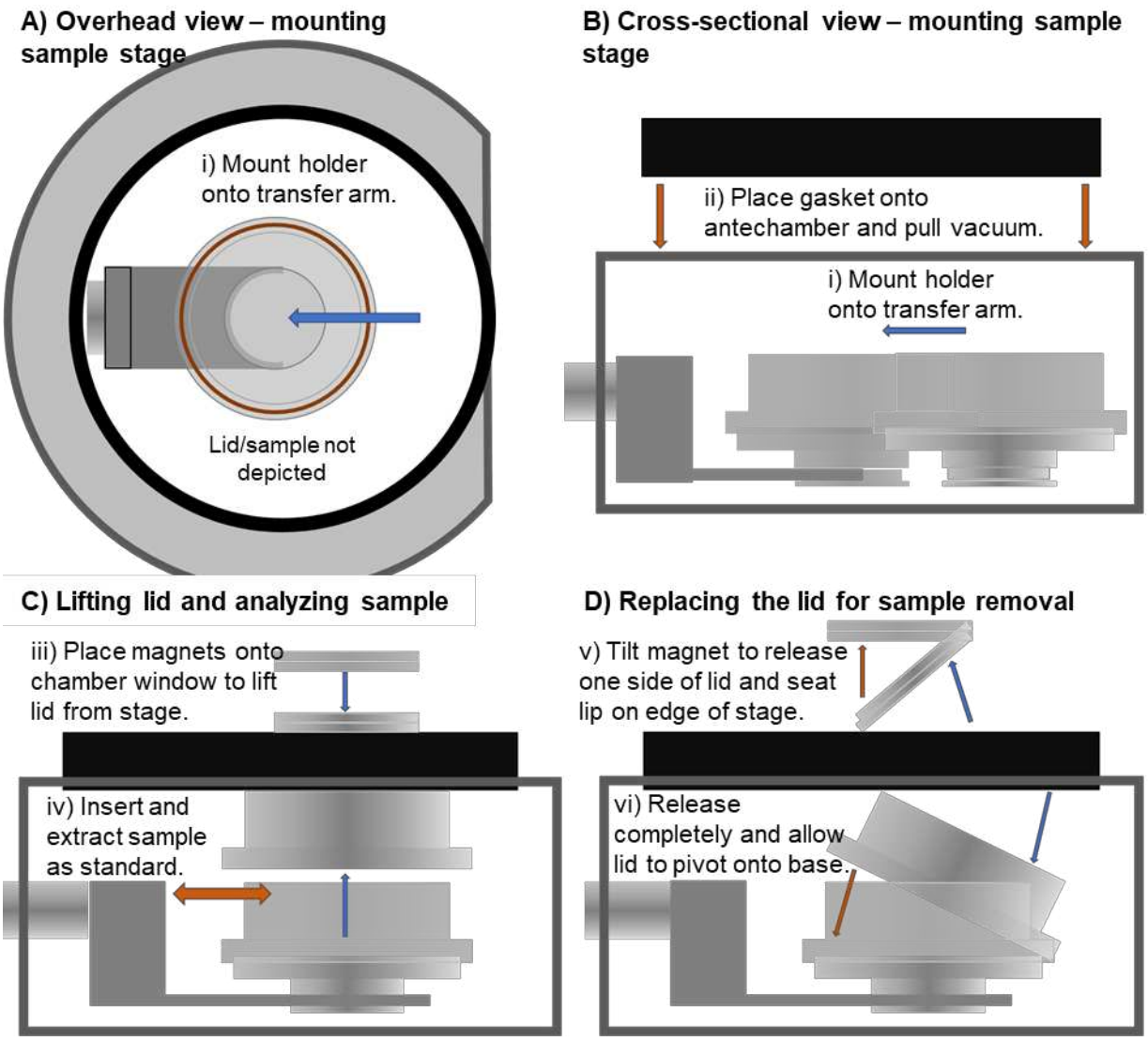

Figure 4.S3. Graphic representations showing the operating principle of the holder and the steps involved in the practical use of the holder in the XPS instrument. **A)** Representation of the sample chamber as viewed from above with the sample transfer arm entering on the left, and a blue arrow showing the base being mounted by sliding the grooved base onto the arm. **B)** Cross-sectional view of the transfer holder base and lid being mounted onto the sample transfer arm in the antechamber (blue arrow). Once the sample is in place the Viton gasket/window is placed onto the antechamber (orange arrows) and the chamber is evacuated. **C)** Once the chamber is evacuated, the magnets can be placed onto the chamber window, lifting the lid from the base and keeping it suspended against the window (blue arrows). This allows the transfer arm to pass under the lid (orange arrow) allowing the sample to be inserted and removed from the instrument. **D)** Following completion of analysis and sample removal, the lid can be replaced by first tilting the magnet (blue arrows) allowing one side of the lid to fall onto the base. The external magnets can be manipulated to ensure the lid is properly positioned with the lip of the lid seated on the edge of the sample stage. Once the lid is correctly oriented, the magnet can be completely removed (orange arrows), allowing the lid to pivot onto the base where the beveled lip ensures proper re-seating.

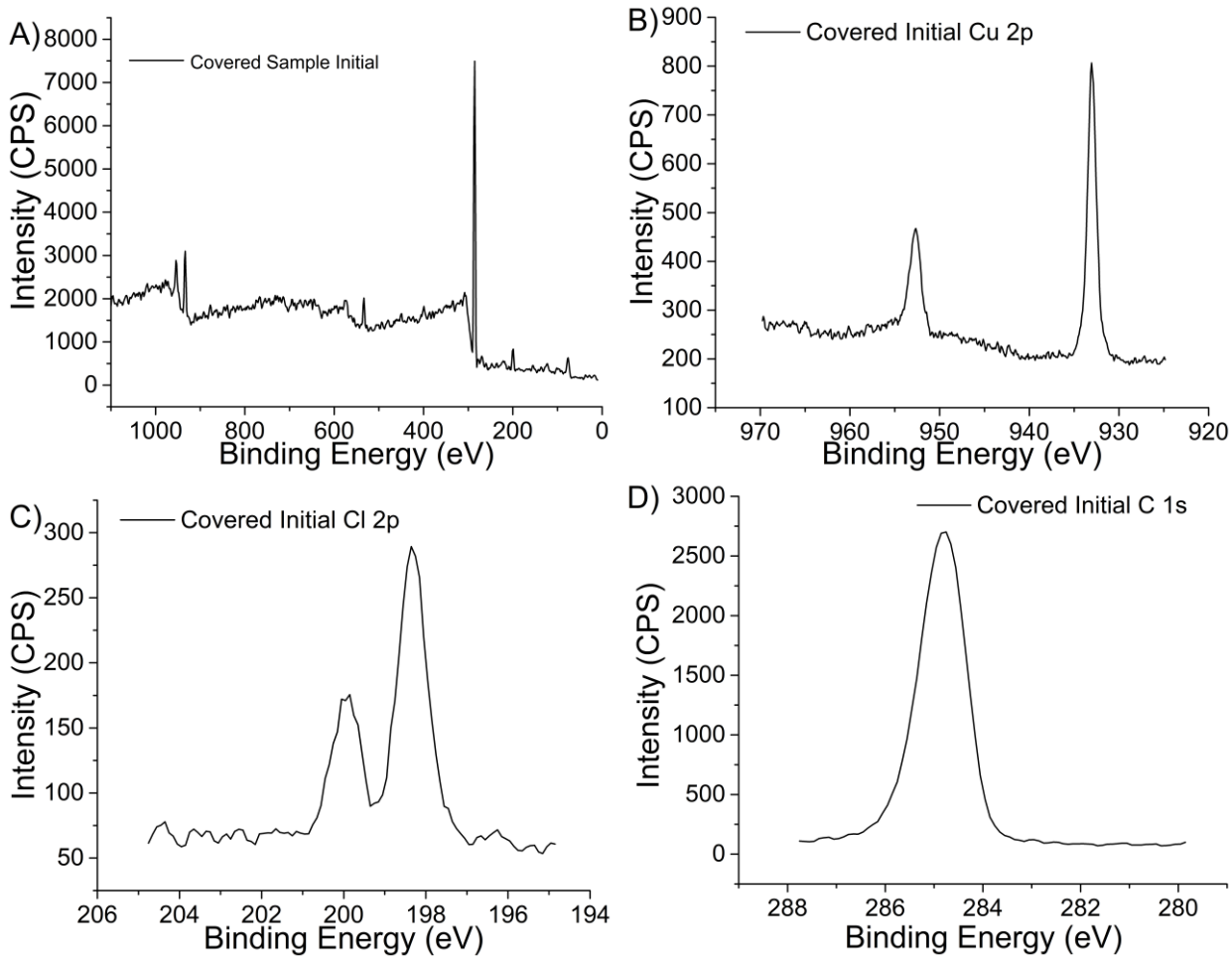

Figure 4.S4. XPS scans of the initial CuCl species transferred to the instrument using the sample transfer holder: **A)** survey scan, **B)** Cu 2p, **C)** Cl 2p, and **D)** C 1s

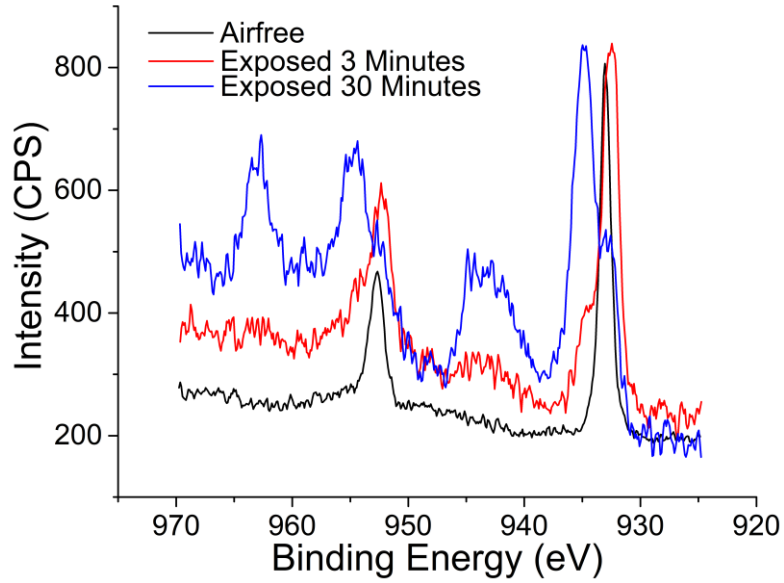

Figure 4.S5. XPS scans of Cu 2p comparing when it is transferred air-free using the sample transfer vessel (black), exposed to ambient air for 3 minutes (red), and exposed for 30 minutes (blue).

REFERENCES

(1) Malmgren, S.; Ciosek, K.; Lindblad, R.; Plogmaker, S.; Kühn, J.; Rensmo, H.; Edström, K.; Hahlin, M. Consequences of Air Exposure on the Lithiated Graphite SEI. Electrochim. Acta 2013, 105, 83–91. https://doi.org/10.1016/J.ELECTACTA.2013.04.118.

(2) Aurbach, D.; Weissman, I.; Schechter, A.; Cohen, H. X-Ray Photoelectron Spectroscopy Studies of Lithium Surfaces Prepared in Several Important Electrolyte Solutions. A Comparison with Previous Studies by Fourier Transform Infrared Spectroscopy. Langmuir 1996, 12 (16), 3991–4007. https://doi.org/10.1021/LA9600762.

(3) Dedryvère, R.; Laruelle, S.; Grugeon, S.; Poizot, P.; Gonbeau, D.; Tarascon, J.-M. Contribution of X-Ray Photoelectron Spectroscopy to the Study of the Electrochemical Reactivity of CoO toward Lithium. Chem. Mater. 2004, 16 (6), 1056–1061. https://doi.org/10.1021/CM0311269.

(4) Agocs, D. B.; Danna, T.; Prieto, A. L. Ambient Surface Stability of Thin Film Nanocrystalline Cu3SbSe4 and Structure–Property Relationships. ACS Appl. Energy Mater. 2019, 2 (3), 1903–1910. https://doi.org/10.1021/acsaem.8b02019.

(5) Riha, S. C.; Johnson, D. C.; Prieto, A. L. Cu2Se Nanoparticles with Tunable Electronic Properties Due to a Controlled Solid-State Phase Transition Driven by Copper Oxidation and Cationic Conduction. J. Am. Chem. Soc. 2011, 133 (5), 1383–1390. https://doi.org/10.1021/ja106254h.

(6) Afanasiev, P.; Lorentz, C. Oxidation of Nanodispersed MoS2 in Ambient Air: The Products and the Mechanistic Steps. J. Phys. Chem. C 2019, 123 (12), 7486–7494. https://doi.org/10.1021/acs.jpcc.9b01682.

(7) Suzuki, S.; Yanagihara, K.; Hirokawa, K. XPS Study of Oxides Formed on the Surface of High-Purity Iron Exposed to Air. Surf. Interface Anal. 2000, 30 (1), 372–376. https://doi.org/10.1002/1096-9918(200008)30:1<372::AID-SIA721>3.0.CO;2-R.

(8) Kalazhokov, Z. K.; Karamurzov, B. S.; Kochur, A. G.; Misakova, L. B.; Kardanova, Z. V.; Kalazhokov, K. K. Calculation of the Pure Surface Composition of the Binary Alloy According to XPS Data Obtained after the Alloy Surface Contact with Air. J. Struct. Chem. 2015, 56 (3), 576–581. https://doi.org/10.1134/S0022476615030269.

(9) Greczynski, G.; Hultman, L. Self-Consistent Modelling of X-Ray Photoelectron Spectra from Air-Exposed Polycrystalline TiN Thin Films. Appl. Surf. Sci. 2016, 387, 294–300. https://doi.org/10.1016/J.APSUSC.2016.06.012.

(10) Greczynski, G.; Petrov, I.; Greene, J. E.; Hultman, L. Al Capping Layers for Nondestructive X-Ray Photoelectron Spectroscopy Analyses of Transition-Metal Nitride Thin Films. J. Vac. Sci. Technol. A Vacuum, Surfaces, Film. 2015, 33 (5), 05E101. https://doi.org/10.1116/1.4916239.

(11) Castner, D. G.; And, K. H.; Grainger, D. W. X-Ray Photoelectron Spectroscopy Sulfur 2p Study of Organic Thiol and Disulfide Binding Interactions with Gold Surfaces. Langmuir 1996, 12 (21), 5083–5086. https://doi.org/10.1021/LA960465W.

(12) Harper, J. M. E.; Charai, A.; Stolt, L.; d'Heurle, F. M.; Fryer, P. M. Room-Temperature Oxidation of Silicon Catalyzed by Cu3Si. Appl. Phys. Lett. 1990, 56 (25), 2519. https://doi.org/10.1063/1.103260.

(13) Stolt, L. Formation of Cu3Si and Its Catalytic Effect on Silicon Oxidation at Room Temperature. J. Vac. Sci. Technol. A Vacuum, Surfaces, Film. 1991, 9 (3), 1501. https://doi.org/10.1116/1.577653.

(14) Liu, C. S.; Chen, L. J. Catalytic Oxidation of (001)Si in the Presence of Cu3Si at Room Temperature. J. Appl. Phys. 1993, 74 (5), 3611–3613. https://doi.org/10.1063/1.354499.

(15) Rutkowski, M. M.; McNicholas, K. M.; Zeng, Z.; Brillson, L. J. Design of an Ultrahigh Vacuum Transfer Mechanism to Interconnect an Oxide Molecular Beam Epitaxy Growth Chamber and an X-Ray Photoemission Spectroscopy Analysis System. Rev. Sci. Instrum. 2013, 84 (6), 065105. https://doi.org/10.1063/1.4804195.

(16) Kuiry, S. C.; Seal, S.; Fei, W.; Ramsdell, J.; H. Desai, V.; Li, Y.; Babu, S. V.; Wood, B. Effect of PH and H2O2 on Ta Chemical Mechanical Planarization. J. Electrochem. Soc. 2003, 150 (1), C36. https://doi.org/10.1149/1.1528202.

(17) Biesinger, M. C. Advanced Analysis of Copper X-Ray Photoelectron Spectra. Surf. Interface Anal. 2017, 49 (13), 1325–1334. https://doi.org/10.1002/sia.6239.

(18) Moulder, J. F.; Stickle, W. F.; Sobol, P. E.; Bomben, K. D. Handbook of X-Ray Photoelectron Spectroscopy: A Reference Book of Standard Spectra for Identification and Interpretation of XPS Data; Chastain, J., King, R. C. J., Eds.; Physical Electronics, Inc., 1992.

(19) Physical Electronics, I. PHI 5800 MultiTechnique ESCA Operator's Guide: Part N. 647268 Rev. A https://www.phi.com/assets/documents/manuals/5800-operators-guide.pdf (accessed Apr 27, 2020).

(20) Randy. Loading PHI specimen mounts | RBD TechSpot https://www.rbdinstruments.com/blog/loading-phi-specimen-mounts/ (accessed Apr 27, 2020).